1-1-2006

High temperature creep behaviour niobium bearing ferritic stainless steels

Victoria Cain
Cape Peninsula University of Technology

HIGH TEMPERATURE CREEP BEHAVIOUR OF NIOBIUM BEARING FERRITIC STAINLESS STEELS

March 2005

A thesis submitted to the Faculty of Engineering in fulfilment of the requirements for the degree of Master of Technology in Mechanical Engineering

Prepared by:

VICTORIA CAIN

Supervised by:

Professor Rob Knutsen (Centre for Materials Engineering,

University of Cape Town)

&

Mr Ian Noble-Jack (Department of Mechanical

Engineering, Cape Peninsula University of Technology)

DECLARATION

The contents of this dissertation represent my own work and the opinions contained herein are my own and not necessarily those of the Cape Peninsula University of Technology.

Signature: V. Ca- Date: March 2005

A thesis submitted in fulfillment of the requirements for the MAGISTER TECHNOLOGIAE (Mechanical Engineering) in the Faculty of Engineering at the Cape Peninsula University of Technology.

Cape Town, South Africa March 2005

ACKNOWLEDGEMENTS

Firstly I would like to thank my supervisors, Prof Rob Knutsen (Centre for Materials Engineering, UCT) and Mr Ian Noble-Jack (Mechanical Engineering Department, CPUT) for their guidance.

I am immensely grateful to Prof Knutsen for the endless support, encouragement and advice he has given me over the last three years. You have become my mentor and you are truly an inspiration to all aspiring academics and educators alike. Thank-you for having faith in me, this would not have been possible without you.

A special thank-you to the Centre of Materials Engineering, including staff and students for making me feel so welcome during my time spent there. I am particularly indebted to Andrew Cousins for always being eager to assist me even though it sometimes meant endangering his own safety! I am proud to have been given the opportunity to be part of this wonderful team of dedicated people.

Thank-you to the Cape Peninsula University of Technology, especially the Research and Development Department for awarding me Research Seed Funding that greatly assisted throughout this project. Also thanks to the Department of Mechanical Engineering, Head of Department, Mr. Tap van der Schyff for his support in granting me study leave in order to complete my project.

Thank-you also to the Mechanical Engineering Departments workshop staff at both CPUT and UCT. Particularly to Ghalick Janodien (CPUT) and Glenn Newins (UCT).

I would also like to acknowledge Columbus Stainless Pty (Ltd) for providing me with such an interesting project and for their support throughout its undertaking.

Thank-you to my best friend and partner Thomas for always supporting me in all that I do. Particularly for never complaining whilst escorting me to switch off late night experiments! I am very lucky to have you in my life.

Finally a special thank-you to my parents, who without their constant love, support and never ceasing encouragement I would not be the person I am today. Thank-you for always believing in me, when I hardly believed in myself.

ABSTRACT

The objective of this project was to monitor the high temperature creep behaviour of 441 stainless steel. Two different alloys of 441 were investigated; the main difference between them being the Niobium content. Particularly important to the project was how the Niobium content and grain size affected the creep resistance of the material.

Creep tests were performed using purpose built constant load creep test rigs. Initially the rigs were not suitable for the testing procedures pertaining to this project. This was due to persistent problems being experienced with regards the reliability and reproducibility of the rigs. After various modifications were made the results produced from the rigs were consistent.

Creep test data was used in order to determine the mechanism of creep that is operative within the material (at a predetermined temperature) under a predetermined load. Particular attention was paid to the resulting stress exponents, in order to identify the operative creep mechanism. The identification of the operative creep mechanisms was also aided by microscopical analysis. This analysis was also necessary to monitor how the grain size had altered at various annealing temperatures.

Heat treatment was used as a method to alter the high temperature strength and microstructure of the material. Heat treatments were performed at various temperatures in order to determine the ideal temperature to promote optimum creep resistance of 441. All heat treatments were performed in a purpose designed and built high temperature salt bath furnace. The commissioning of the salt bath formed part of the objectives for this project.

Sag testing was also conducted, using purpose built sag test rigs. It was necessary to design and manufacture a sag test rig that could be comparable to the industry accepted method of sag testing known as the two-point beam method, as this method is believed to produce inconsistent results.

Conclusions have been drawn from the results of the data and from previous research on the subject matter.

TABLE OF CONTENTS

LIST OF FIGURES

LIST OF TABLES

CHAPTER 1

Introduction

1.1 Background to the project

This project was to investigate a particular grade of stainless steel for the end use of catalytic converter housings, which forms part of the exhaust system of a motorcar. The average life span of a catalytic converter varies between 5 to 7 years, supposedly the average time an initial owner keeps a vehicle[1].

It was in 1928 that the first recorded use of stainless steel in the automotive industry was noted, which was for the Ford Model A radiator cover and hubcaps[2]. Various grades of stainless steels are common in this industry; generally the average amount of stainless steel used during the manufacturing of a motorcar is 23 kg[3].

Stainless steel is popular in this application due to its extensive properties such as[4]:

- High resistance to aqueous corrosion
- Resistance to creep
- Relative light weight to strength ratio
- Good high temperature strength properties
- Excellent fabrication properties
- Durable aesthetic appeal

Automotive exhaust components such as the catalytic converter need a material that has a particularly high creep resistance and high temperature strength, taking note that catalytic converters can be exposed to temperatures in excess of 800 °C[5] in service and are in operation for prolonged periods.

Type 441 (DIN 1.4509) stainless steel, which is a ferritic grade of stainless steel is specially produced by Columbus Stainless (Pty) LTD for use in automotive components[6]. It is especially made use of for the front end of an exhaust system due to its superior mechanical strength at elevated temperatures[7]. This property makes it particularly preferable for the fabrication of catalytic converters. Although ferritic stainless steels have less high temperature strength than austenitic steels and their oxidation and creep resistance is not as good, it is the more chosen grade due to it being more cost effective. The reason for the higher cost of austenitic grades is because they are composed of Chromium (18%), Nickel (8-12%) and various other alloying elements, whereas the ferritic

grades contain Chromium (approximately 12-18%) and other alloying elements but no Nickel[4]. It is the Nickel content in the austenitic grades that makes them expensive.

The ferritic grade that is investigated in this project, 441, is dual stabilised with Titanium and Niobium. The Titanium helps to prevent sensitisation (intergranular corrosion after welding) and the Niobium renders high temperature creep resistance [8 & 9].

Columbus Stainless (Pty) Ltd is a producer of 441 in South Africa. This company is particularly interested in this material's creep characteristics in temperatures in the vicinity of 850 °C. It is therefore necessary to test at this temperature in order to try best to simulate the service conditions of the material in this particular application (housings of catalytic converters).

Owing to the fact that there are certain requirements that manufacturers of catalytic converters need to work to with regards creep resistance it is necessary that Columbus Stainless Pty (Ltd) produces 441 to render the maximum reliability and performance of the steel. To do this various heat treatments need to be investigated, such as annealing.

For Columbus Stainless Pty (Ltd) to optimise this grade of stainless steel it is necessary for them to understand fully the effect the thermo-mechanical processes have on the steel and whether or not these processes can in fact be altered to guarantee the ultimate in results and promote a certain degree of consistency with regards to quality. Research has indicated that for optimum creep resistance an increase in Niobium, a high final annealing temperature and a large grain size is preferred[10]. Therefore in order to check materials creep resistance, creep tests using purpose built rigs must be performed.

A simpler, low cost alternative to a creep test that can also be used is the sag test (using purpose built sag test rigs). The two-point beam method is the industry-accepted test used in order to compare the varying sag/creep resistance of alloys of a particular grade of material[11]. There is, however, debate surrounding the accuracy of the results achieved using this method.

1.2 Aims of the project

The purpose of the research was to investigate the high temperature creep (and) sag resistance of 441 using purpose built test rigs.

Different alloys of 441 will be investigated; this will assist in determining the effect Niobium has on the creep resistance of the material.

Material has been supplied in the cold rolled condition and various annealing matrices will be investigated to determine what effect this may have on the overall creep resistance.

Broadly the aims of the project can be noted as follows:

- To develop two fully functional constant load creep test rigs.
- To manufacture a high temperature salt bath.
- To determine the mechanism of creep that is operative within the material during service operation (in the vicinity of 850 °C), paying particular attention to the stress exponents.
- To determine whether it is the amount of Niobium in solution (dislocation creep) that affects the creep/sag resistance of the material or whether it is the grain size (diffusion creep).
- To determine what effect varying the final annealing time and temperature will have on the creep resistance of the said material.
- To optimise the creep/sag resistance of stainless steel 441.
- To develop a more accurate form of sag testing.

1.3 Constraints of the project

A salt bath furnace was purchased for high temperature annealing treatments, although due to design errors, the salt bath furnace took longer to manufacture and commission than was expected.

The creep rigs had various modifications made to them to make them more suitable for testing, the commissioning of the rigs took longer than expected due to these modifications.

It was also proved that the creep rigs were extremely sensitive to set-up. There was also an unforeseen problem with the data acquisition system that needed to be addressed. This held up testing considerably as it was not possible to start testing until the creep rigs were fully commissioned and producing reproducible results.

CHAPTER 2

Literature Review

2.1 Development of stainless steel

A definition of stainless steel quoted by The South African Stainless Steel Development Association (SASSDA) is as follows:

"Stainless steel is a generic term for a group of corrosion resistant steels containing a minimum of 11 % of Chromium. Varying additions of Nickel, Molybdenum, Titanium, Niobium and other elements may be present." [12]

The actual 'discovery' of stainless steel is difficult to account to one individual. In fact a number of people appeared to discover the material almost simultaneously. In Britain, in 1912, Harry Brearly of the Brown Firth Research Laboratories, found through a fortunate accident that adding Chromium to low Carbon steel gave it stain resistance[13]. He had been investigating ways to reduce corrosion in gun barrels, when it was noticed that a discarded sample was not rusting[14].

It was through this discovery that the first commercial cast of stainless steel was produced on the 20th of August 1913[13]. It was almost at the same time that Haynes, in the USA, who was at the time investigating Cobalt-Chromium and Cobalt-Chromium-Tungsten alloys noted their exceptional corrosion resistance; although there had to be at least 10 % Cr in the alloy and 5% cobalt. In a paper published in 1914 by Strauss and Maurer (under The Krupp Research Department) in Germany they make reference to the rust resisting properties of steel that contains sufficient Chromium and Nickel. In fact it was Strauss and Maurer (via the Krupp Research Institute) who were credited with the discovery of Austenitic stainless steel[13]. France was also involved in stainless steel development. It was in 1917 that work was carried out by Chevenard at the Imphy Laboratory on steels containing 15-20 % Chromium[14].

Nevertheless, it is believed that the above work would not have been possible had in not been for the foundation research that was conducted by Guillet, Portevin and Giesen[13]. In 1904 they started research on a wide range of chromium steels, including what is known today as ferritic, martensitic and austenitic stainless steels. They were accounted for realising their mechanical properties and microstructures. It was through the persistence of work such as Harry Brearly in England (martensitic stainless steel), Frederick Becket and Christian Dantsizen in the United States (ferritic stainless steel) and Eduard Maurer and Benno Strauss in Germany (austenitic stainless steel) that the industrial usefulness of

stainless steels was acknowledged. The name stainless, however, is believed to have been coined by Ernest Stuart who was a manager at a cutlery company. He came up with the name while attempting to describe a range of stainless steel cutlery knives[13].

During the 1940s research on composition, heat treatment and alloying elements led to the development of precipitation-hardenable (PH) stainless steels. Then during World War II, Nickel shortages led to the development of high-manganese austenitic stainless steels. Duplex stainless steels were discovered in the 1930's, but their commercial development did not occur until the 1960's[15].

Stainless steels are synonymous with having a high resistance to corrosion, this is predominately due to the Chromium content of the steel. In general the corrosion resistance of stainless steels improves as the Chromium content increases. When the Chromium is combined with Oxygen it results in a Chromium containing oxide that forms a passive protective film on the surface of the steel. The layer is too thin to be visible, meaning that the metal retains its shiny appearance. It is this film that prevents the Iron in the steel from oxidising or what is known to the layperson as rusting. This film is quickly self-repairing so in the event of the surface of the steel being damaged i.e. cut or scratched, more oxide quickly forms and protects the exposed surface. In spite of this and contrary to belief, stainless steels are not indestructible. The passive state can be broken down under certain conditions and corrosion can result. It is for this reason that it is essential therefore to select the correct type and grade of stainless steel for a particular application. When selecting a type and grade it is also important to consider the mechanical and physical properties that it possesses, as the way in which it performs in service is largely due to the composition and prior thermal treatment of the material.

There are numerous different kinds of alloys that can be recognized as belonging to the stainless steel group[16]. Over the years since the first introduction of stainless steel various grades have been developed and are still being developed. These new grades are produced by alloying the basic composition of stainless steel (Iron, Carbon and Chromium) with other elements such as Nickel, Molybdenum, Titanium, Niobium, Silicon, Tantalum, Tungsten, Vanadium, Aluminium, Manganese, Cobalt and Copper. By adding these elements specific properties of the material can be obtained i.e. their structure and mechanical properties can be enhanced.

Stainless steels are the favoured choice of material in a wide variety of industries due to their many mechanical and physical properties, which range from:

- Excellent corrosion resistance: Some grades will resist scaling and maintain high strength at very high temperatures (while resisting scaling), while others show exceptional toughness at cryogenic temperatures.
- Ease of fabrication: The majority of stainless steels can be cut, welded, formed, machined and fabricated.
- Strength: The cold work hardening properties of many stainless steels can be used in design to reduce material thicknesses and reduce weight and costs.
- They are heat treatable, which results in very high strength components.
- Aesthetic appeal: Stainless steel is available in many surface finishes. It is easily maintained and gives a high quality appearance.
- Hygienic properties: The "cleanability" of stainless steel makes it the first choice in hospitals, kitchens, food and pharmaceutical facilities.
- Life cycle characteristics: It is a durable, low maintenance material and is often the least expensive choice in a life cycle cost comparison.
- High strength vs. mass[4 & 12].

2.2 Stainless steel types

The three main types of stainless steels available today are namely austenitic, ferritic and martensitic. These grades were all well known within twenty years of Harry Brearly's accidental discovery.

The crystal structure of a metal is dependent on its chemical composition and these crystal structures are defined by given names. The crystal structures of the main types of stainless steels are martensite (martensitic), ferrite (ferritic) and austenite (austenitic). It is the names of these crystal structures that are used to classify these main types of stainless steels.

The different types of stainless steels are due to the materials differing chemical compositions: when Nickel, for instance is added to the material the austenite structure of Iron is stabilized and these steels become non-magnetic. For higher hardness and strength, Carbon is added.

The American Iron and Steel Institute (AISI) uses three numbers to identify the standard grades of stainless steel. Austentic grades are designated by numbers in the 200 and 300 series, while ferritic and martensitic grades are designated by numbers in the 400 series.

Austenitic and ferritic grades account for approximately 95 % of stainless steel applications[17].

The following paragraphs deal with the each of the three main types of stainless steels individually.

2.2.1 Austenitic stainless steels

Austenitic stainless steels are the most well known of the stainless steel family (generally the 300 series). They account for more than 70 % of production. They contain a maximum of 0.15 % Carbon, a minimum of 16 % Chromium and sufficient Nickel and/or Manganese to retain an austenitic structure at all temperatures from the cryogenic region to the melting point of the alloy. These non-magnetic alloys are generally more expensive than the other grades due to their Nickel content, which is responsible for enhancing their superior corrosion resistance to the other grades. Some of their properties are as follows:

- Excellent corrosion resistance
- Excellent formability and weldabiltiy
- Moderate strength

- Excellent high temperature properties
- Resistance to creep

They are used in a variety of applications ranging from cutlery to medical equipment to food and beverage processing to marine hardware. Their resistance to attack by acids, alkalis and other chemicals has led to a wide use in the chemical and process plant industries.

The following is as defined by the AISI:
300 Series—austenitic iron-chromium-nickel alloys

- Type 301: Highly ductile, for formed products.
- Type 304: The most common; austenitic (contains Nickel).
- Type 316: For food and medical uses; contains Nickel and Molybdenum (this type has virtually the same mechanical, physical and fabrication characteristics as 304, but with better corrosion resistance).

"Super" austenitic grades have enhanced pitting and crevice corrosion resistance compared with the ordinary austenitic types. This is due to further additions of Chromium, Molybdenum and Nitrogen[12].

The material is commonly available in various forms such as plate, coil, strip, sheet, bar, pipe and tube[12].

2.2.2 Martensitic stainless steels

Martensitic stainless steels were the first stainless steels that were commercially developed (they were predominantly used as cutlery) and they have a relatively high Carbon content. They are not as corrosion resistant as the other two classes, but are extremely strong and highly machineable, and can be hardened by heat treatment. The basic composition of this magnetic alloy is typically 12 % to 18 % Chromium with higher carbon content than the ferritic types. Some grades include additional alloying elements in small quantities.

Some of their properties are as follows:

- Moderate corrosion resistance
- A high strength and hardness factor
- Good wear resistance

They do, however, have poor weldability properties.

There applications range from cutlery to surgical instruments to springs and fasteners.

The material is commonly available in various forms such as bar and strip[12].

2.2.3 *Ferritic stainless steels*

Ferritic stainless steels are corrosion resistant, although they are less corrosion resistant than the austenitic grades, but have superior corrosion resistance to martensitic stainless steels. They contain between 10.5 % and 27 % chromium and very little or often no Nickel content at all. They usually have a low Carbon content. Compositions can include Molybdenum, Titanium and Niobium. The balance of the composition is made up of Iron and Chromium. Some of their properties are as follows:

- They are magnetic
- Good ductility
- Good to moderate resistance to corrosion and oxidation
- Are generally resistant to stress corrosion cracking
- Good strength
- Low hardness
- High temperature strength

However, their weldability is poor and formability is not as good as the austenitics.

Due to the low or lack of Nickel content of this grade, ferritic stainless steel has allowed stainless steel to become more affordable. It is for this reason that this grade is known as the lower cost stainless steel and is generally used in the more mildly corrosive environments, often being used in trim work and somewhat less demanding applications. Ferritic stainless steels are used widely in the automotive industry.

The following is as defined by the AISI:
400 Series—ferritic and martensitic alloys

- Type 408: Heat-resistant; poor corrosion resistance; 11 % Chromium, 8 % Nickel.
- Type 409: Cheapest type; used for automobile exhaust tubing and trim.
- Type 410: Martensitic (high-strength iron/chromium).
- Type 420: "Cutlery Grade" martensitic; similar to Brearly's original "rustless steel".
- Type 430: Decorative. Used for automotive trim; cutlery and catering equipment.
- Type 444: Hot water tanks.

- Type 441 (DIN 1.4509): Due to constant demands on the properties of stainless steel various alloys were developed for varying applications. As demands became greater it became necessary to develop a stainless steel that could withstand higher temperatures, i.e. to increase the hot strength of the material. Niobium was added to the mix of the 18% Chromium, ferritic alloy. This grade then became known as 441. Columbus Stainless (Pty) Ltd specially produces this grade for use in automotive components. Its superior mechanical strength at elevated temperatures (up to 850 °C) makes it the ideal material for the front end (close to the engine) of an exhaust system[18]. The high temperature strength in fact exceeds that of type 409 and 439[19]. It also shows a marked increase in corrosion and oxidation resistance to type 409, which could be explained due to its higher percentage Cr content (17 %) whereas the 409 has a 11 % Cr content[19]. Type 441 is also used in the fabrication of heat exchanger tubes.

The material is commonly available in various forms such as sheet, coil and welded tube[12].

Table 2.1 shows various properties of 441.

Table 2.1: Properties of stainless steel type 441[6]

Property	Nominal
Tensile strength	496 MPa
Yield strength	320 MPa
Elongation	28 %
Hardness	155 Hv

2.2.3.1 Stabilisation of ferritic stainless steels

Traditional ferritic stainless steels have previously been stabilised with only Titanium, which results in a single stabilised steel. But, the resulting properties for use in exhaust systems were found not to be adequate. Research has shown that by dual stabilising the stainless steel using both Titanium and Niobium the properties are greatly enhanced. These properties range from improved surface quality, improved formability and weldability, higher temperature strength (superior creep resistance), superior thermal fatigue resistance, better high temperature oxidation and aqueous corrosion resistance[3].

2.2.3.2 High temperature applications of ferritic stainless steels

Ferritic stainless steels are often preferred for high temperature applications due to them being cheaper than the austenitic alloys. Although austenitic stainless steels do exhibit better thermal fatigue resistance and mechanical properties at higher temperatures, than the ferritic grades. Some ferritic grades also have good high temperature corrosion properties. In fact the class of ferritic stainless steels are inherently not strong at elevated temperatures, but with the addition of Niobium and with the appropriate heat treatments this can be altered. Research has been conducted into improving the performance of 8 % to 14 % Chromium ferritic stainless steels. It is said that these steels will fill the need for demanding applications such as for advanced power plants[20].

The most common high temperature applications include automobile exhaust components, steam turbine rotors, boiler tubing, heater elements and components for nuclear reactors and petroleum refineries.

2.2.4 Niobium in stainless steels

Research has shown that small amounts of Niobium affect the high temperature strength of this steel significantly [7, 9, 11 & 20].

Niobium is a chemical element in the periodic table that has the symbol Nb. It is a rare, soft, grey, ductile transition metal, that is found in niobite and is used as an alloying element. Niobium was discovered in a variety of Columbite (now called Niobite) and was at first named after this mineral. It is also sometimes referred to as Columbium (Cb).

Niobium has a number of uses: it is included in some stainless steels and is an alloy of other nonferrous metals. Other uses include:

- Arc welding rods for some stabilised grades of stainless steel.
- Due to its bluish color, Niobium has become popular for body piercing jewelery (where it is usually used as an alloy).
- Appreciable amounts of Niobium are used in Nickel, Cobalt, and iron-base superalloys for such applications as jet engine components, rocket subassemblies, and heat-resisting and combustion equipment.

Brazil and Canada are the major producers of Niobium mineral concentrates and extensive ore reserves are also in Nigeria, Democratic Republic of Congo, and in Russia[17].

Ferritic stainless steels are alloyed with Niobium to increase the material's high temperature strength.

One of the most effective methods of improving the high temperature strength of ferritic stainless steel is to increase the solid solution content of Niobium to as much as possible[9]. It has been found that creep strength is related to the amount of Niobium in solution[11].

2.2.5 Stainless steel and the catalytic converter

The automotive industry has benefitted greatly since the advent of stainless steel. From the early days of 1928 when the Ford Model A sported a stainless radiator cover and hubcaps to today's demand for the material. It is said that in the automotive industry nearly 70 applications of stainless steel can be seen[2].

The majority of a motorcar's exhaust system is today manufactured from stainless steel. These components range from mufflers, to manifolds to resonators to housings of catalytic converters to heat shields, brackets and pipes[3]. The hot front section of motorcar exhaust systems requires steel that has a high scaling resistance and elevated temperature and creep strength. The material should also be able to resist high oscillating stresses due to vibration. As well as the mentioned properties, steels for exhaust systems should also have good forming and welding properties[21].

The majority of a motorcars exhaust system has in the past been fabricated from ferritic stainless steel type 409[22]. This is a cheaper Titanium stabilised 12 % Chromium stainless steel. But, metal temperatures of some of the components (within the exhaust system) are expected to exceed 815 °C, which is the useful temperature limit of type 409[23]. This material was therefore found to lack the necessary oxidation resistance and hot strength capability, particularly for some engines with higher than average exhaust temperatures[2]. An example of where particularly high temperature exhaust gases are experienced is in the case of light-truck exhaust systems. Initially a move was made whereby type 439 was used instead of type 409, which would result in an increase in 6 % Chromium, raising the Chromium content to 18 %. This alloy proved better at handling the oxidation encountered at the high temperatures and enhanced the resistance to surface rust staining which type 409 was prone to. However, as temperatures soared even higher for exhaust gases it became necessary to increase the materials hot strength (creep resistance and thermal fatigue strength) capabilities, this was done by adding Niobium to the 18 % Chromium alloy, thereby creating type 441[2]. These steels have adequate heat resistance in the temperature range of 815-982 °C[23]. It is important to note at this stage

that catalytic converters can reach temperatures of up to 800°C in service[5]; this is due to the temperature of the exhaust gases. Type 441 also raises the progressive oxidation scaling resistance to the 900 to 980 °C range. In South Africa the company Arwin Meritor who are leading producers of catalytic converter housings prefer either type 441 or 409 (DIN 1.4512) for the fabrication of the housings of catalytic converters[24]. High temperature application of ferritic Chromium steels is usually restricted to conditions with very low stresses[20]. This could also explain its use in the case of the housing of catalytic converters, as the majority of the stress exerted on the housing would be due to its own weight and the weight of the honeycomb structure inside the housing.

The catalytic converter was developed in the 1970's to help to reduce the emissions from motorcar exhausts. It is installed in the exhaust line, between the exhaust manifold and the muffler. Table 2.2 gives an outlined history of the catalytic converter's development[25]. Since the 1980's the use of these devices has been necessitated in many countries, such as developed countries like the United States, Western Europe and Japan because of legislation (relating to clean air laws)[15].

Table 2.2: Catalytic converter introduction[25]

Year	Action
1974	Cars with catalytic converters introduced in the USA
1985	Catalytic converters introduced in Europe
1980's	Legislation passed requiring catalytic converters in the USA
1993	Legislation passed requiring catalytic converters in Europe

The South African government has proposed that all new petrol vehicles will have to be fitted with catalytic converters by 2008[26]. It has been stated that their introduction will reduce toxic vehicle emissions by up to 90 %.

According to statistics by 2001, 275 million of the world's 500 million cars were fitted with catalytic converters and 85 % of all new cars worldwide are fitted with catalytic converters[15].

The device uses a catalyst (which is in the form of Platinum, Rhodium and or Palladium) to convert three harmful compounds that occur in automobiles exhaust fumes into harmless compounds, the compounds are as follows:

- Hydrocarbons, which produce smog are converted to carbon dioxide gas.
- Carbon monoxide, which is highly poisonous to all living creatures, is converted to water vapour.

- Nitrogen oxides, which leads to smog and acid rain is converted to nitrogen gas.

A catalytic converter typically consists of a ceramic honeycomb structure or ceramic beads (although most motorcars today use the ceramic honeycomb structure). This structure is housed, in a muffler-like stainless steel housing. The catalyst is coated onto the ceramic honeycomb structure.

Figure 2.1: Honeycomb structure[27]

On assembly, the housing is welded together and in turn attached to the exhaust pipe. The most common catalytic converter is located between the engine and muffler on a motorcar. Most carmakers position the converter under the front passenger seat, far enough from the engine to keep the temperature of the device down to levels that are not harmful[27], i.e. allow the housing to deteriorate due to excessive heat exposure.

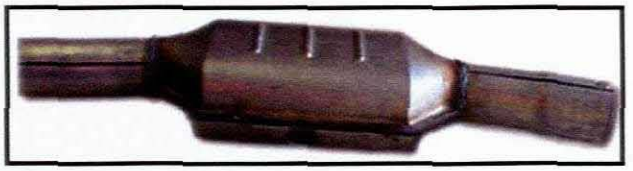

Figure 2.2: Catalytic converter housing[27]

Exhaust gases should reach temperatures above 700 °C in order to gain optimal performance from the catalytic converter. The temperature to which the catalytic converter housing can be exposed is in the region of 500-800 °C; this value depends on the make and model of the motorcar. It is therefore imperative that the material has excellent high temperature properties such as resistance to creep, thermal fatigue and oxidation resistance.

South Africa is the leading source of the platinum, which is used to 'clean' the exhaust gases and is rapidly becoming a significant manufacturing center for catalytic converters

used by motorcar manufacturers around the world. In fact the manufacture of catalytic converters has steadily been moving from countries like the US and Europe to cheaper production locations like South Africa[28]. Annual production of catalytic converters in South Africa doubled in less than five years, from nearly five million converters in 1998 to approximately ten million units in 2002[29].

2.3 High temperature creep in metallic materials

2.3.1 Introduction

Creep is the plastic deformation of a material that is subjected to a stress below its yield stress. It is defined as the time-dependent strain/deformation of a material under a stress or load over a period of time[30]. In some cases this load can be self weight. Creep is therefore obviously undesirable as it can result in the change of geometry of components, and can and sometimes does end in fracture.

There are three basic parameters for creep to occur:

- stress (σ)
- temperature (T)
- time (t)

These parameters can be expressed using the following formula:

$$\dot{\varepsilon} = f, (t, \sigma, T)$$

Where $\dot{\varepsilon}$ is the creep strain rate

Another factor that can influence creep is the materials particular microstructural characteristics (i.e. the internal structure of the material), which could relate to grain size, dislocations and vacancies in the material, and precipitates.

The strength of most materials will decrease if the temperature, to which the material is exposed to, increases above a certain range of temperature, where the material could be susceptible to brittle fracture. Due to this exposure to high temperatures the material may begin to elongate or deform. This elongation or deformation may continue for a substantial time before fracture occurs. The temperature above which this slow deformation can be seen differs, depending on the material[31]. It is for this reason that the temperature of service of a component needs to be considered during a design process, in other words should creep be considered to occur. Creep becomes a limiting factor when a material is operating at a high homologous temperature (the ratio of a material's absolute temperature, T to its melting temperature, T_m). In metals, creep becomes a limiting factor at 0.4 T_m. This is known as the regime of high-temperature creep, which is also sometimes known as Andrade creep. It was so named in honour of an early pioneer in the study of this subject (1910; 1914). Creep is a factor that should therefore be

seriously considered when designing components and choosing of materials that have long-term exposure to high temperatures[32].
Figure 2.3 shows a characteristic creep graph with creep strain rate versus time. The other variables would be temperature and load (in this case load would be constant).

Due to the fact that creep is undesirable there are various methods that can be used for the development of creep resistance in materials:

- Choose a metal that has a high melting point.
- *Creep resistance is greater in a matrix of low stacking fault energy.* This is because the dislocations are dissociated, and therefore it is more difficult for them to cross-slip and climb, to avoid obstacles.
- Solid solution strengthening is a popular method, such as alloying with Niobium.
- Encourage the formation of precipitates[33].

Some of these methods will be discussed in more detail at the end of the chapter.

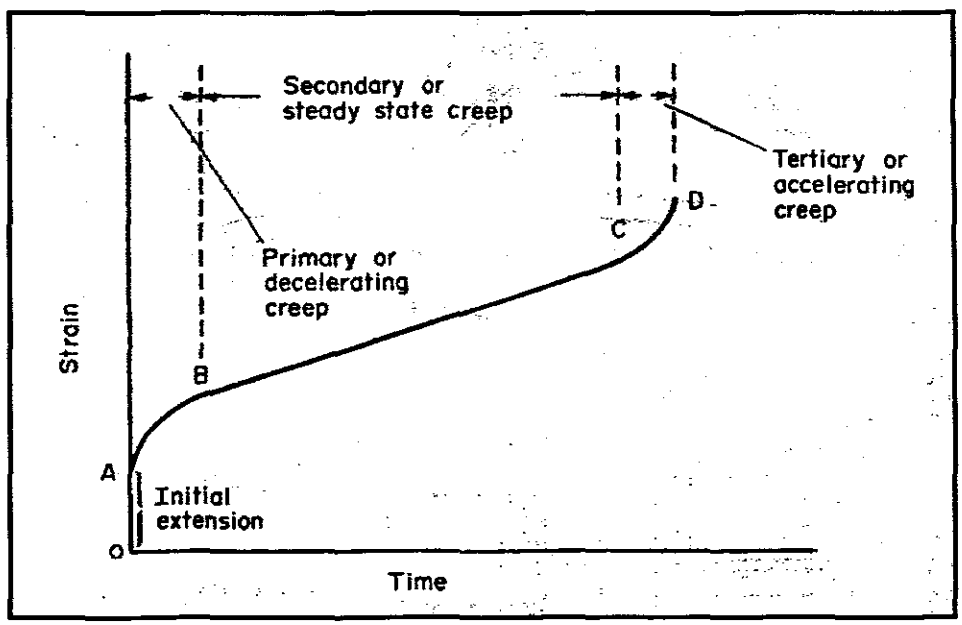

Figure 2.3: Characteristic creep curve, showing the various stages of creep[34]

There are three distinct stages of creep:

- Primary (transient)
- Secondary (steady-state)
- Tertiary

The three stages of creep can be seen in the above graph. Each one of these stages can be investigated to determine the strain/creep rate pertaining to each stage. Ideally a

creep test should show a plot as in figure 2.3[34], which demonstrates on application of load a decreasing creep rate with time. As the creep rate levels a state is reached which is known as the secondary creep stage (steady state creep). This stage translates to a minimum creep rate, which continues with little change over a significant range of strain. Tertiary creep is prominent once the material develops voids and or cracks, which results in the material having an increase in creep rate. Tertiary creep can and generally does result in fracture.

The important part of the curve to designers and engineers is the steady state section (which is invariably the straight section), this is because steady state creep usually takes up most of the time in a creep test and components generally spend most of their service life in this section. Also steady state creep rate is given by the slope of the straight line (when the slope is constant). Knowing the creep rate or the strain rate allows designers and engineers to estimate how much time it takes for a component to reach a certain amount of deformation.

Creep curves, however, do not always look like the characteristic creep curve. They can look different depending on materials properties and also the temperature and applied stress to which the material is exposed to during the creep test[35].

The high temperature strength of materials and their deformation behaviour at elevated temperatures are affected by several factors. Therefore, before creep mechanisms and the mechanics of creep can be explained it is necessary to understand the basic concepts of material principles with regards to deformation. The following paragraphs will deal with these factors.

2.3.2 Introduction to material deformation behaviour

When a material is exposed to an applied stress it reacts either elastically or plastically. Elastic behaviour is the strain of a material that is not permanent and allows the material to return to its original geometry when the applied stress is removed. Plastic behaviour, however, describes a material that has been strained and does not return to original geometry when the stress is removed[36].

The point where a material's behaviour changes from elastic to plastic is known as its yield stress.

After continued tensile stress on a specimen in the plastic range necking of the specimen will occur. Necking is a decrease in a localised region of the specimen instead of over its entire length. This is the point where it has reached its Ultimate Tensile Strength (UTS)[37].

If deformation continues due to plastic deformation, the specimen eventually pulls apart through a ductile fracture process. In this process voids start to form which further weaken the material and increase the local stress which eventually leads to fracture[37].

2.3.2.1 Defects

The crystal lattice of a material is not perfect, but contains defects[35]. There are three main types of defects:

- Point
- Linear
- Planar

Point defects can be classified as:

- Substitutional impurities: which are foreign atoms in a crystal lattice
- Interstitials: which are foreign atoms in the spaces between atoms (such as C, O and N)
- Vacancies: where there is a vacant lattice site in the crystal lattice, resulting in a hole.

Linear defects can be classified as:

- Line defects: which are linear bands of lattice imperfections.
- Dislocations: linear band of atoms that joins an area in a crystal that has slipped relative to the rest of the crystal.

Planar defects can be classified as:

- Grains boundaries: Most metals are polycrystalline, meaning that they are composed of small grains, each of which is an individual crystal[38]. These grains are separated by grain boundaries. The grains are known as planar defects[39]. A grain boundary separates grains whose lattice has different orientations. These boundaries are primarily made up of vacancies[37]. Grain boundaries are the agents of intergranular deformation[35]. Grain boundaries can move in their plane (sliding) or normal to it (migration)[37]. Sliding occurs under an applied shear stress. Migration of grain boundaries can also occur under stress and produce strain.

2.3.3.2 Dislocation motion

It is the movement of these dislocations through the crystal lattice that causes a material to plastically deform under an applied stress. A material will favour dislocation motion in particular crystallographically controlled directions. There are two types of dislocations: edge dislocations and screw dislocations.

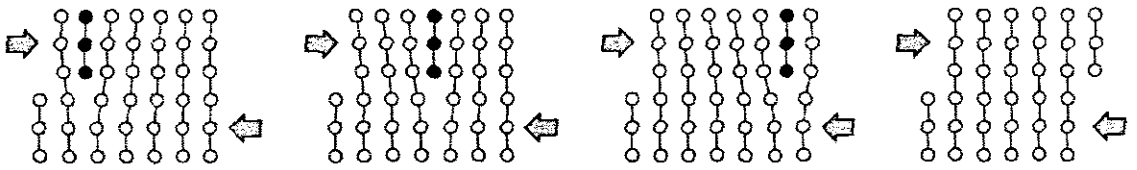

Figure 2.4: Glide of an edge dislocation

The result of an edge dislocation moving through an entire crystal is that the upper portion of the crystal slips a distance relative to the lower portion of the crystal. This results in an extra half plane of atoms being introduced into the crystal lattice, as shown in figure 2.4. The direction and magnitude of the amount of slip is known as the Burgers vector, b.

The plane in which a dislocation moves through the lattice is known as the slip plane or the glide plane and the direction in which it moves is called the slip direction. The combination of the two is known as a slip system.

An edge dislocation is restricted to a single glide plane whereas a screw dislocation is not and can cross slip into another glide plane, which then allows the dislocation to move around an obstacle[40].

The Critical Resolved Shear Stress (CRSS), also known as the Peierls stress, is the stress needed to cause this dislocation motion.

Once the CRSS has been reached dislocation movement may still be impeded by obstacles within the crystal lattice. Yet it is possible for the dislocations to overcome these obstacles[37]. The dislocations may move out of their glide planes by cross slip, the mobility of the dislocations increases under high temperatures. This is because climb and cross-slip are both diffusional processes, which means that they are thermally activated. Since the mobility of atoms increases with high temperature, diffusion controlled processes become more noticeable at higher temperatures[31].

Dislocations may further dissociate into one or more partial dislocations. This can result in the atoms between them being no longer stacked in the correct sequence, which results in a stacking fault.

Stacking faults by themselves are simple two-dimensional defects. They carry certain stacking fault energy[41]. Creep resistance is greater in a matrix of low stacking fault energy[42]. Ferritic stainless steels do, however, have a high stacking fault energy[43].

In most crystals and under most circumstances there is no such thing as a straight dislocation. Real dislocations contain kinks and jogs. Kinks and jogs are generally formed during glide when dislocations interact. A kink is a step in the dislocation line in the slip plane, whereas a jog is a step in the dislocation line onto another slip plane. A kink lying in a slip plane provides no impediment to glide, a jog, on the other hand does[40].

2.3.2.3 Diffusion

Diffusion occurs when a defect migrates through a crystal lattice. This process occurs because of the presence of vacancies within the crystal lattice[44]. The process is thermally activated and generally becomes significant in metals at high temperatures (generally greater than 0.4 times the melting temperature). Self-diffusion is defined as being the transport of matter in a pure metal (ie the movement or diffusion of Cu atoms in the Cu lattice).

At high temperatures there is sufficient thermal energy for diffusion to progress through the bulk of the lattice (bulk or volume diffussion) whereas at lower temperatures diffusion occurs along paths offering less resistance such as grain boundaries (grain boundary diffusion[38]).

2.3.3 Creep mechanisms

At low stresses most systems respond in a linear manner to creep and the creep rate is given by creep rate proportional to stress. At intermediate stresses, power law creep is observed, which means that the creep rate is proportional to stress to a power. At higher stresses the creep rate increases even more rapidly and is known as the region of power law breakdown[31].

The continuous plastic flow of a material during creep can result in large deformations and significant modifications to the microstructure of the material. Creep involves dislocation motion and diffusion of vacancies. This deformation of a material is a result of these defects moving through the crystal lattice of the material. The defects start to move

through the material when there is enough thermal energy provided, which is provided by high temperatures.

There are varying mechanisms of creep that occur during the creeping of a material. It is these creep mechanisms that have caused constant debate amongst researchers in the past and still today. A broad explanation of each one of these mechanisms and information pertaining to them will be presented in the following paragraphs.

It is possible to identify two primary creep mechanisms that occur, namely diffusional and dislocation creep. The mechanism, that is operative, can be differentiated by the microstructure of the material, and the temperature and the stress to which the material is exposed[45]. It is generally accepted that diffusional creep is prevalent at high temperatures and low stresses whereas dislocation creep is prevalent at lower temperatures and higher stresses.

For a given material, a deformation mechanism map can be drawn (figure 2.5) that can give a general idea of what creep mechanism is dominant at a particular stress and temperature. Ashby originally devised these maps. The maps are based on applications of constitutive equations describing the stress, temperature, grain size and stacking fault energy dependence of creep rates due to individual mechanisms[46].

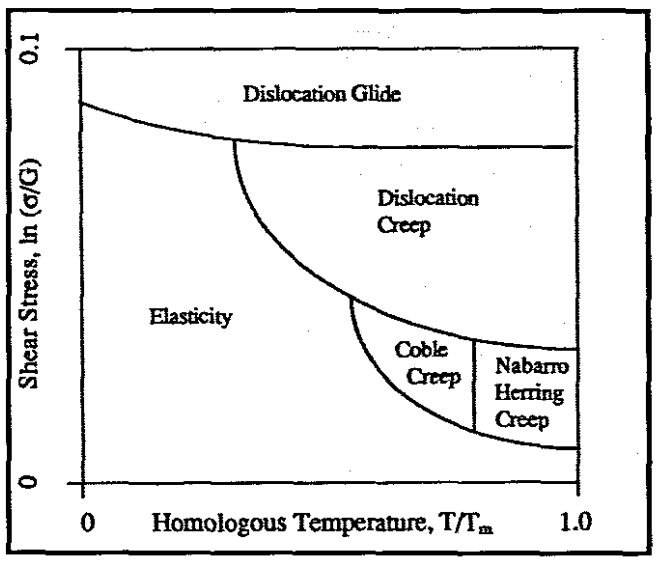

Figure 2.5: Example of a primary deformation map[42]

Each material will have a dissimilar deformation map; however, to construct one of these maps it is necessary to have a large amount of data. Furthermore changes in a materials microstructure can affect the map quite significantly[42].

2.3.3.1 Diffusional creep mechanisms

Diffusional creep is the movement of vacancies (point defects) in a crystal lattice[30].

The first type of diffusional creep is known as Nabarro-Herring creep after Nabarro and Herring. Nabarro, a leading expert in creep, was the first to propose self-diffusion as a mechanism of creep deformation[47]. He noted that vacancies generally diffuse across the bulk of a material, which results in an elongation of the grains in the direction of the tensile axis. The deformation of the material is due to the flow of atoms and vacancies that causes them to rearrange themselves along the direction of the applied load. Herring later did more research into this theory and extended it into the high temperature region. The creep mechanism then became known as Nabarro-Herring creep[35]. This form of creep generally occurs at high temperatures and low stresses[48].

Nevertheless, during their research they neglected diffusion along the grain boundaries. Coble suggested that diffusion along the grain boundaries could control the creep rate, and proposed this theory due to the fact that diffusion is easier along grain boundaries (grain boundary diffusion). This is because vacancies are more common in the grain boundary than in the bulk of the lattice[49]. This theory then extended the original Nabarro Herring theory to the creep mechanism known as Coble creep. But, Coble creep should be more prominent at lower temperatures where grain boundaries provide an easier path for diffusion to take place which means that there is therefore less thermal energy needed for the movement of these defects[44].

Grain boundary sliding is another factor that needs to be considered during creep. In order to maintain continuity within the creeping material the grains must rearrange themselves and they can do this only by sliding past each other. This process occurs during creep because the grain boundaries, which are imperfectly bonded, are weaker than the ordered crystalline structure of the grains. During diffusion creep, each grain becomes elongated along the tensile axis; it is therefore necessary that the grains slide over each other with the sliding occurring as a rearrangement process. This rearrangement process is known as Lifshitz sliding[50]. There is yet another type of grain boundary sliding known as Rachinger sliding is quite different. In Lifshitz sliding the grains retain their relative positions in the matrix and there is no increase in the number of grains lying along the tensile axis. On the other hand, a situation can also arise where grains slide past one another with no grain elongation, which results in an increased number of grains along the tensile axis of the material. This rearrangement process is known as Rachinger sliding[50]. An example of Lifshitz grain boundary sliding is shown in

figure 2.6. In this case, precipitate-free zones are formed at the ends of the grains in a Mg-Zr alloy as a result of a diffusion process that leads to grain elongation.

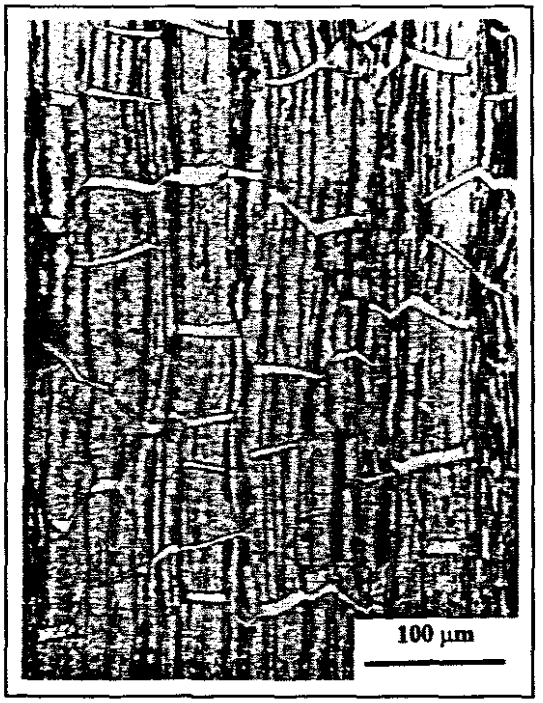

Figure 2.6: Micrograph of Mg-0.55 % Zr after diffusion creep[50]

2.3.3.2 Dislocation creep mechanisms

Dislocation creep is the movement of dislocations in a crystal lattice. This movement is caused by the glide and climb of these dislocations. This mechanism of creep is often not fully understood; however, it can be described in broad terms.

As a dislocation moves on its slip plane it may come across an obstacle (which could be a precipitate) within the lattice. At this point the dislocation movement can become blocked. In order to move away from this obstacle the dislocation will climb until it reaches a new slip plane. The dislocation is able to climb due to the action of thermal energy (when the influence of diffusion becomes significant) and a high enough stress to overcome the obstacles. The dislocation then again begins to glide within the new slip plane until it once again may encounter another obstacle and become blocked. At this stage the cycle of climb and glide continues. The rate of creep is therefore determined by the rate at which these dislocations move through the crystal lattice.

Dislocation creep is a mechanism observed for many materials, it is also often referred to as power law creep. Although at stresses high enough the power-law breakdown is generally observed, this is also evident when the stress exponent increases above the region of 3~6, which is the accepted value region for dislocation creep. This observation

is visible by the fact that a log strain vs. log stress plot is no longer linear over a wide range of applied stresses, as the power law equation usually does not hold true at high stresses. Creep rate increases exponentially with stress, which results in the log strain-log stress plot no longer being a straight line which then indicates power law breakdown.

2.3.3.3 *Harper-Dorn creep*

Harper-Dorn creep was first reported in 1957 by Harper and Dorn. The two researchers tested tensile specimens of both single and polycrystalline Aluminium (99.99% purity) at very low stresses (less than 0.1 MPa) and at high temperatures near the melting point[51]. It was concluded that this mechanism of creep appeared to be independent of grain size[52].

Harper-Dorn creep is only observed if the initial dislocation density is not too high. It is generally accepted that the mechanism of Harper-Dorn creep is the climb of edge dislocations[53] that occurs at high temperatures and very low stresses[50 & 51].

2.3.3.4 *Identifying creep mechanisms*

Amongst the more obvious methods of attempting to identify creep mechanisms, such as the stress and temperature levels that tests are run at, there are a number of other methods to aid in identification. The controlling process of creep can generally be found by noting the stress exponent, n[54]. This stress exponent generally increases with falling temperature and increasing stress[55]. The identification of the process can further be aided by careful observation of the materials microstructure prior to and after creep testing[46].

The identification of the presence of denuded zones at grain boundaries, normal to the tensile stress during deformation can be indicative of Nabarro-Herring diffusional creep[56].

Generally the creep rate is proportional to the applied stress on the specimen raised to a power (which is known as the stress exponent, n). In determining this exponent experiments are conducted at constant temperature, but varying stress. Deformation data is then presented as plots of log of creep strain rate versus log of stress. A straight-line relationship is generally observed.

This straight line indicates the presence of secondary creep stage or the steady state stage of creep. It is this stage that allows for n to be determined. The straight line suggests that,

$$\dot{\varepsilon} = A\,\sigma^{n}$$

$$\log_e \dot{\varepsilon} = \log_e A + n \log_e \sigma$$

The gradient of this straight line yields the stress exponent. The above expression is often referred to as Norton's law and is a basis for a power law relationship, which is widely used to describe high temperature creep behaviour[44].

The resulting stress exponents can then be interpreted in terms of different deformation mechanisms or creep mechanisms.

Table 2.3 gives approximate values of stress exponents for the various creep mechanisms. Although this cannot be construed as a sure deduction, but rather as a tool of identification.

Table 2.3: Various creep mechanisms indicating relevant stress exponents

Creep mechanism	Stress exponent, n
Diffusion creep	1
Harper-Dorn creep	1
Dislocation creep	3~6
Dislocation glide	3
Dislocation climb	4.5~6-5
Grain boundary sliding	1~3

As can be seen from table 2.3 different stress exponents are a result of different creep mechanisms.

Values of n in the vicinity of five have been recorded for most pure metals (class 2 metals), although n values varying from about 3 to as high as 40 have also been reported for various alloys (class 1 metals). Dislocation processes are associated with stress exponents of three or more, whereas n values of one would be expected for diffusional creep processes and Harper-Dorn creep[57]. Stress exponents above 10 can be suggestive of the power law breakdown regime[58].

Most theories of creep are regarded as being successful once the correct stress exponent for the steady state creep rate has been predicted[59].

Another method of distinguishing between two different creep mechanisms is discussed below.

Diffusion creep requires some form of grain boundary accommodating process due to the grain boundary sliding that occurs. Whereas Harper-Dorn creep has no grain boundary sliding. However, it can be difficult to distinguish between the two with regards to stress exponents as they both have a stress exponent equal to one. Due to this Langdon proposed a method to help to distinguish between these two creep mechanisms. The method consists of inscribing marker lines (AA and BB) onto the surface of specimens prior to creep testing[60]. If diffusion creep occurs the marker lines will be offset (due to grain boundary sliding). Conversely, if Harper-Dorn creep is the acting creep mechanism the marker lines will retain their original location.

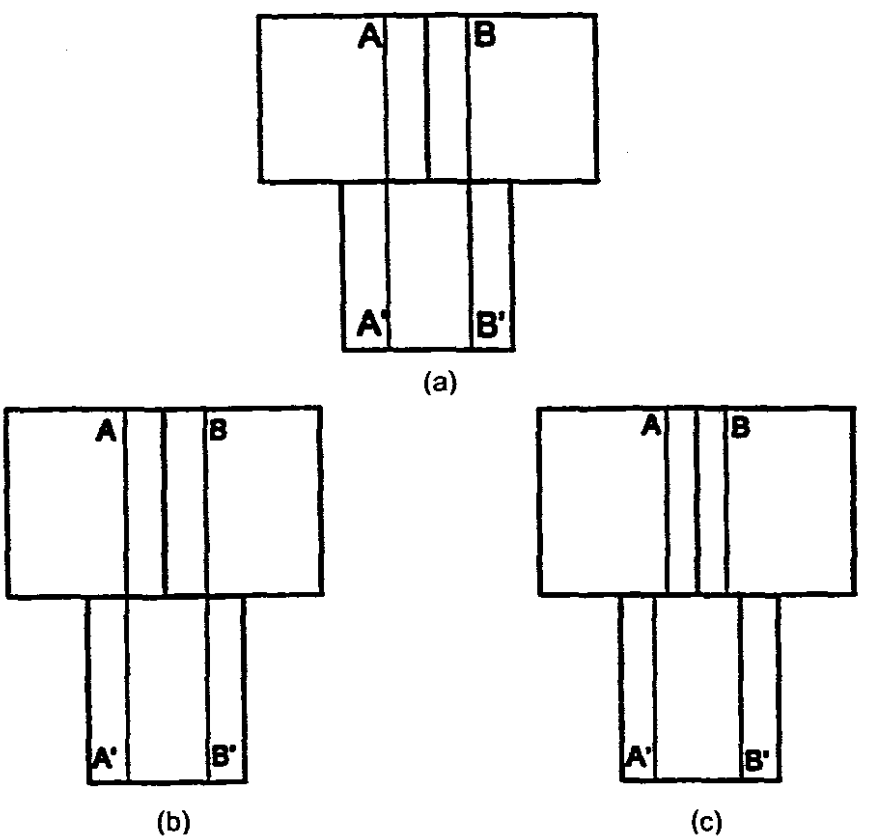

Figure 2.7: (a) Shows marker lines AA and AB prior to testing, (b) Shows deformation by Harper-Dorn creep, (c) shows deformation by diffusional creep

2.3.3.5 Dispute over the existence of various creep mechanisms

Diffusional creep:

Various researchers have questioned the theory of diffusional creep and the parameters necessary for it to occur. These researchers include Ruano and Wilshire[61 & 62].

The doubt has arisen from the fact that denuded zones (the presence of these denuded zones has been argued to be direct evidence of diffusion creep being present) have been observed where a stress exponent of 4~6 (dislocation creep) has resulted[61]. However, for diffusion creep to be active a stress exponent of one must result.

Nabarro has acknowledged these objections and has said that the theory of diffusional creep, although fairly well established, still has many details to be resolved[47].

Harper-Dorn creep:

Although this mechanism of high temperature deformation is well established, according to some researchers the experimental evidence is not convincing. Experiments performed by Blum and Maier questioned the existence of Harper-Dorn creep as a unique mechanism of viscous creep[63]. The reason for this uncertainty is that they found in their investigation that the resulting stress exponent was in the region of 3.2~5.1[63]. But, the stress exponent for Harper-Dorn creep should be unity.

Yet, Nabarro has disputed this claim[53], arguing Blum and Maier's suggestion that the mechanism of Harper-Dorn creep does not exist rests on an incomplete application of the conditions under which Harper-Dorn creep is expected to be the dominant mechanism[53].

2.2.4 The Effects of material microstructure on creep

There are three main strengthening mechanisms in materials that can influence a materials creep resistance[33]. These mechanisms will now be discussed.

2.2.4.1 Grain size

It is possible to decrease the diffusion pathways by having a large grain size; by having less grain boundary per volume an increase in creep resistance may be observed[33]. Grain size can therefore affect the strength of a metal quite significantly[10]. It is for this reason that in diffusion creep, particularly in Coble creep grain size is of great relevance.

High temperature annealing can increase the grain size of a material[10 & 37], which can lead to improved creep resistance.

2.2.4.2 Precipitates

Engineering materials can be strengthened by precipitates that accumulate on grain boundaries or within grains. They can contribute to slowing down the creep process, by preventing diffusion and dislocation through the crystal lattice[47]. A precipitate can be defined as a product of decomposition of the matrix solid solution, which is introduced by properly chosen or supplementary heat treatments. This precipitate consists of a substance that has a different solid phase of composition than the rest of the lattice and forms because an alloy material is not soluble in the parent lattice. Most commercial creep resistant alloys derive their strength from a uniform dispersion of precipitates[64], as the precipitate becomes an obstacle in the path of dislocations.

For Niobium bearing ferritic stainless steels, Niobium, when in solid solution is responsible for improving the high temperature strength of this material, and its resistance to thermal fatigue. This is often the result of the precipitation of NbC carbides on dislocations[65]. These precipitates often also consist of a Laves phase (Fe_2Nb)[66].

The Laves phase, which is a hexagonally structured intermetallic compound, is a type of phase formed when atoms of two or more metals combine in a fixed ratio to produce a crystal different in structure from the individual metals. It can be identified through x-ray diffraction techniques[10].

This Laves phase precipitate appears to have an effect of increasing the creep resistance of ferritic stainless steel; however, it only forms at high temperatures[67]. Therefore the use of intermetallic compounds, such as a Laves phase is a popular method to enhance elevated temperature creep strength of ferritic stainless steels[64].

2.2.4.3 Solid solution strengthening

This is when an alloy is added to a base metal to make it stronger. An example of solid solution strengthening is when Zinc is added to Copper to produce Brass.

In the case of Niobium bearing ferritic stainless steels it has been found that when the Niobium content is less than 0.2 % mass, Niobium is not in solid solution, but is in the form of precipitates. When the Niobium addition exceeds 0.2 % mass the amount of Niobium in solid solution increases as the Niobium addition content increases. This can lead one to believe that the strengthening effects at high temperature by the Niobium additions (and in the case of this research Molybdenum additions as well) should derive from solid solution strengthening[68].

2.4 Creep Testing

2.4.1 General concepts

A creep test measures deformation of a material under predetermined conditions of temperature and stress over a specific period of time. Creep tests are performed using purpose built creep test rigs.

Tensile testing is the universally accepted method to study creep[13]. This is a broad description, though, as the technique used for creep testing is quite different from the standard tensile test. This is because a creep test includes the prolonged application of a constant load to the specimen, the monitoring of steady temperatures within close limits of the specimens during the test and the measurement of the deflection (often extremely small) of the specimen at specified intervals over a specified time period. This monitoring of the deflection must be done in such a way as to not interrupt or disturb the test itself[69].

Creep testing, however, is usually a lengthy process. Test time periods can range from 100 hours to 10000 hours or even longer. The reason for the extended time tests is because it is important to try to relate the results to the normal life span of a component concerned[13], i.e. to reproduce service conditions and lifetimes of components. On the other hand, depending on the load on the specimen, tests that are meant to run for example 100 hours may run for less time due to the specimen failing before the 100 hour time limit has been reached.

Creep testing is also an expensive process. Purpose built rigs are expensive and often difficult and tedious to operate. Accurate measurement of deformations is often complicated. Due to the fact that small changes of stress and temperature can result in large changes of strain, tolerances on the variables have to be small. i.e. reproducibility must be achieved within results/data[70].

The type of testing for creep varies depending on subject specifics. There are tests that measure creep, stress-rupture and stress relaxation properties of a material.

Most common forms of creep tests are constant load creep tests where the load is kept constant for the duration of a test. Therefore, as the specimen elongates and the cross sectional area decreases the stress increases. However, the initial stress that was applied to the specimen is the stress that is documented[71].

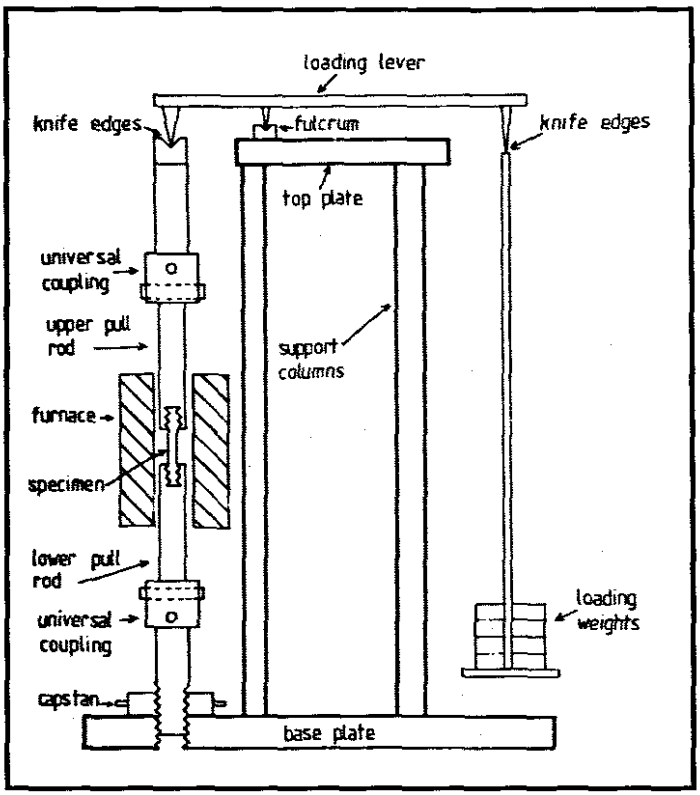

Figure 2.8: Schematic of constant load creep rig[44]

It is also sometimes necessary to obtain creep data under constant stress conditions. This is slightly more involved than constant load creep testing as it requires a method whereby the applied load must be adjusted as the specimen elongates in order to maintain a constant stress on the specimen. This is done by making use of specially designed cams.

Two types of creep tests can usually be performed on similar rigs, depending on what data is required. The stress rupture test allows the specimen to deform until it actually fractures or fails. The test is run under a constant stress and temperature. The displacement of the specimen is not monitored; it is just the time to failure that is documented.

The stress-relaxation test is on the other hand, a test that has the load continually decreasing instead of remaining constant as in a constant load creep test. The load is reduced at specific intervals in order to maintain a constant strain on the specimen[71].

It is essential that accurate test procedures be in place to determine the creep rates of materials. For this reason a series of national and international standards have been produced with regards to creep testing. Creep testing with reference to this project was

done according to ASTM standard E139-00[72]. A summary of the standard is presented in Section 2.4.2.

2.4.2 ASTM Standard E139-00

Testing machine

The load on the specimen should be applied as axially as possible.

It is important that the machine is not prone to external noises that could cause shock to the system whilst running a test.

Heating apparatus:

Temperature is controlled by a tubular furnace that encompasses the specimen. The heating apparatus is designed to maintain a constant temperature throughout the length of the furnace and should control temperature variation to within the limits given in table 2.4.

Table 2.4: Temperature variation limits for furnace

Up to and including 1000 °C	± 2 °C
Above 1000 °C	± 3 °C

Temperature measuring apparatus:

Temperatures should be measured with thermocouples. It is important to select the correct type of thermocouple. Depending on the gauge length of the specimen more than one thermocouple may be used to monitor the temperature during the test. Thermocouples should be calibrated regularly.

Extensometer system:

The strain measuring equipment should be accurate and sensitive according to the degree of accuracy required from the creep test results.

The extensometer should be attached to opposite sides of the specimen in order to avoid nonaxiality of loading.

Where possible the extensometer system should be directly attached to the specimen and not to any load carrying parts of the equipment, which could lead to extensions that are not accurate. It is preferable to attach it to the guage length notches.

Care should be taken that the extensometer is sufficiently secured to the specimen so that it does not slip off the specimen during a test.

Room temperature control:

The temperature of the room should be kept constant, so as not to influence temperature readings.

Timing apparatus:

It is necessary that sufficient method of measuring the elapsed time from the start of a test be put in place[72].

2.5 Sag testing

2.5.1 General concepts

The sag test was developed as a more cost effective method of comparing alloys creep resistances against one another[11]. The two-point beam arrangement is commonly known within the industry as the benchmark testing method for sag testing.

2.5.2 Industry standard: Two-point beam method

This method is known in the industry as the two-point beam arrangement and is a widely accepted form of sag testing. The specimens are placed onto a rig, which allow the specimens to lie across two supports. Once the specimens have been placed onto this rig it is placed into a furnace for a specific time at a specific temperature and the specimens are allowed to sag or creep under their own load for this time frame. The amount by which the specimen has sagged is determined by monitoring how much the specimen has deflected from a particular position before the test relative to that after the test.

Although this method appears fairly simplistic, it is a convenient and economical means of comparing the creep resistances of different alloys.

Figure 2.9: Two-point beam sag test rig

The rig in figure 2.9 was manufactured from T310 stainless steel as per Douthett[11].

The sag test specimens are strips of material 25.4 mm (I inch) wide and 292.1 mm (11 ½ inches) long with a 12.7 mm (½ inch), 90 ° locating bend at one end[11].

Literature regarding the sag testing technique is difficult to locate; however, it was found that this method of comparing materials creep properties is an accepted industry benchmark test to compare alloys as a form of quality control measure.

2.6 Heat treatment

Ferritic stainless steels, as with most engineering metals and alloys may be heat treated to impart the desired mechanical properties through microstructural changes[73]. Annealing is one such heat treatment process and is performed using a purpose built high temperature salt bath.

Annealing may be carried out:

- To relieve internal stresses induced by some previous treatment (i.e. cold rolling)
- To promote grain growth
- To rearrange dislocations into a lower energy configuration (recovery).
- To create new, strain free grains (recrystallisation).
- To promote solid solution (i.e. solution heat treatment).

By using the appropriate annealing treatment creep strength can be increased for a ferritic stainless steel with increasing Niobium content[10].

Heat treatment is applied to forgings, cold-worked sheets and wire and castings. The operation consists of:

- Heating the steel to a certain temperature,
- 'Soaking' at this temperature for a time sufficient to allow the necessary changes to occur,
- Cooling at a predetermined rate (which could involve quenching in oil or water or air cooling).

A salt bath furnace is often used when it is vitally necessary that a specimen experiences constant heat all over the specimen and for when rapid heat-up rate is required. It is constant and uniform, whereas using an ordinary box furnace could result in the specimen experiencing different temperatures across it due to temperature variations within the furnace. This is especially evident in the case of specimens that are long and rectangular in shape.

CHAPTER 3

Constant load creep test rigs

This project utilises (amongst other equipment) two constant load creep test rigs that were designed and built in house[43]. Creep tests are performed on these two purpose built rigs. They are lever-arm type, constant load creep test rigs. The design of the rigs is similar to any commercially available constant load creep test rig. For the purpose of clarity these rigs will be referred to as Rig 1 and Rig 2.

The creep test rigs used in this project consist of the following components: (Refer to figure 1):

- Load frame
- Base plates (between which the load is applied)
- Adjustable lever arm (through which the load is applied to the specimen). The ratio on these particular rigs may be adjusted to 1:3, 1:5 and 1:10; this allows loads of between 10 kg and 1000 kg to be applied to the specimen.
- A weight pan to control the load.
- A screw jack to allow vertical positioning of the lower pull rod to allow various lengths of specimens to be tested.
- A vertical electric tube furnace that has a maximum operating temperature of 1200 °C. The furnace has three heat zones, which are monitored by one thermocouple each (i.e. there are three monitoring thermocouples within the furnace).
- Load cell (sensor) used to monitor the load on the specimen
- Extensometer system.
- LVDT (linear variable displacement transformer) to continually monitor the elongation of the specimen.
- 2 type K thermocouples monitoring the temperature of the specimen (one at the top and one at the bottom). The thermocouple is applied directly onto the specimen.
- Data acquisition system, which monitors temperature, load, displacement and time. This system allows the user to log load, extension and specimen temperature against time.

3.1 Test rig

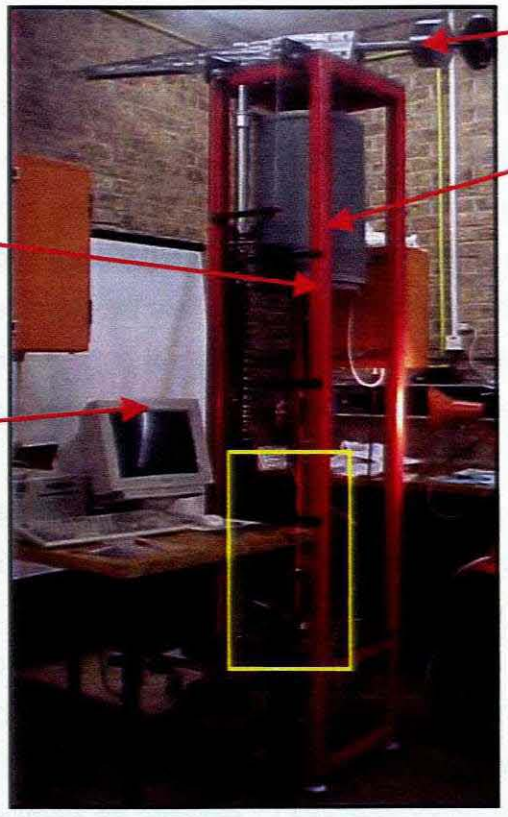

Figure 3.1: Constant load creep test rig

Detail of figure 3.1

Detail of figure 3.1

3.1.1 Basic components

The basic components of the creep test rig consist of the load frame and the base plates. The frame is constructed from welded box section mild steel tube (50 x 50 x 4.5). There are two base plates, an upper and a lower one. The load is applied between these two plates onto the specimen.

3.1.2 Load application parts

The load on the specimen is applied via a lever through the various pull rods. The lever consists of two steel plates (3CR12) that have been bolted together with spacers between

them. Two ball bearings allow the lever to move freely. A counter weight is threaded onto the end of the lever; this allows the load to be adjusted.

The specimen is held between two grips inside of the furnace (these grips form part of the extensometer system). The load that is applied to the specimen is made up of the lower pull rod, extensometer and thermocouples. Weights are then added into the weight pan in order to increase the load to the necessary weight; these weights then apply the constant load to the specimen. The load that is placed into the weight pan is transmitted to the specimen via the lever (manufactured from 3CR12) in proportion with the lever ratio. The load that is being applied to the specimen is monitored by a load cell. This load cell is positioned above the furnace and is kept cool by a built in cooling system.

3.1.3 Heating system

The three heat zone furnace was custom designed and manufactured by Custom Furnaces. There is a temperature controller monitoring the top, middle and bottom of the furnace core (three zone temperature furnace). The temperature inside of the furnace is maintained at a constant level by the temperature controllers (RKC SA 200). The specimen temperature is monitored with two type K thermocouples that are kept as close to the specimen as possible. One thermocouple monitors the bottom half of the guage length temperature and the other the top half. The temperature is kept constant to within ± 2 °C of the set temperature during the test[72]. After the set temperature is reached, a 30 minute period is given in order to allow the system to attain thermal equilibrium.

3.1.4 Extensometer system

The extensometer system is made up of four rods that extend into the furnace and attach directly onto the notches of the specimen gauge length. The relative displacement of the rods is measured outside the furnace by an LVDT.

Figure 3.2: Extensometer system

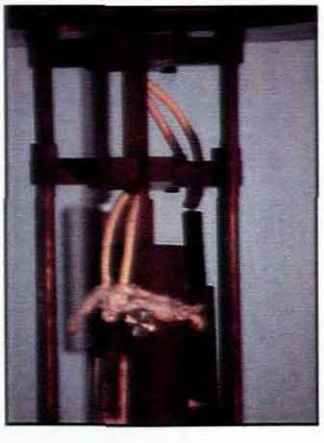

Figure 3.3: Thermocouple monitoring temperature of specimen (at bottom)

Parts of the components of the extensometer system are exposed to high temperatures (as they are encompassed by the furnace). Therefore these components have been manufactured from materials that can withstand high temperatures such as:

- 316 stainless steel (upper and lower pull rods, and pull rod connectors)
- Haynes 230 alloy (hot pull rods and threaded specimen grips)
- Inconel 601 alloy (extensometer clamps and rods)

3.1.5 Sensors

The sensors used for capturing the necessary data consist of a load cell, LVDT and two type K thermocouples. The K type is necessary due to the high temperature that the tests are run at.

It is imperative that calibration of the various sensors is good. Due to the sensitivity of the rigs, it is vital that readings are exact. It can be suggested that calibration of the load cells and LVDT's is done on a regular basis, after a series of tests, in order to ensure sensors have not drifted. Calibration methods for the LVDT's and the load cells can be observed in appendices (Appendix E).

3.1.6 Data acquisition system

Data is logged to a suitable data logging system via a data acquisition card.

Due to problems with the design that rendered the rigs unsuitable for testing, various modifications to the rigs were recommended and are discussed further in section 3.2.

3.2 Modifications

3.2.1 Ceramic brick inserts

The furnace was initially insulated at the top and bottom end by ceramic fibre blanket. It was recommended that the top end rather be insulated by specially cast refractory brick inserts. A mould was made to suit and the inserts cast. Cape Refractory Industries produced the inserts.

Figure 3.4: Ceramic brick insert

Figure 3.5: Placement of insert

3.2.2 Lower pull rod

The lower pull rod was modified from a single rod (see figure 3.6) into two thinner rods that sit side-by-side and are joined by braces at the top and bottom (see figure 3.7).

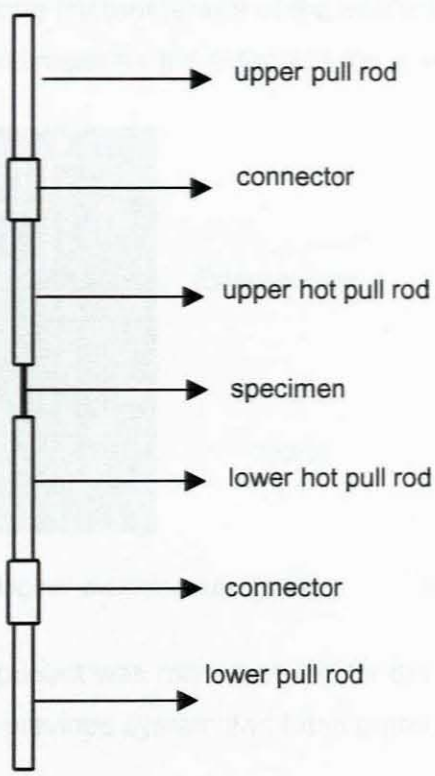

Figure 3.6: Schematic of original load train

Figure 3.7: Schematic of new load train

By making this modification it will ensure that the centre of the weight of the extensometer system is directly in line with the axis of loading. This will also allow the test to be set up with minimal weight hanging from the specimen.

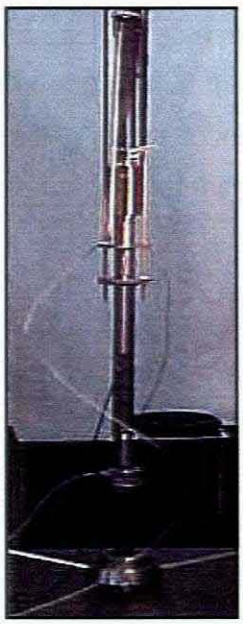

Figure 3.8: Original lower pull rod (single rod)

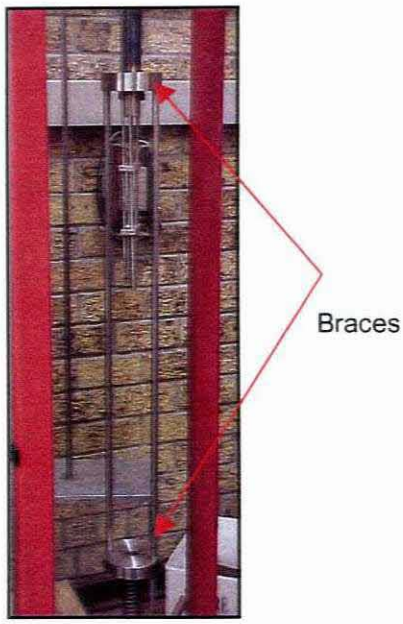

Figure 3.9: New lower pull rod (two rods)

3.3.3 Extensometer

Due to the lower pull rod being modified it was therefore necessary to replace the existing extensometer plates that house the LVDT with similar plates that will allow the LVDT to be positioned along the tensile axis of the load train. Allowances were made in the lower and upper pull rod braces for the extensometer arms to pass through.

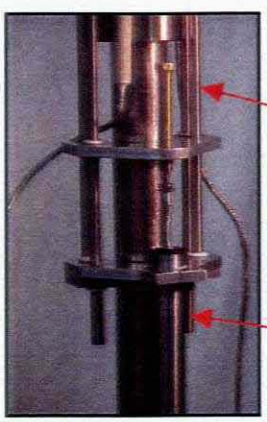

Figure 3.10: Original extensometer plates

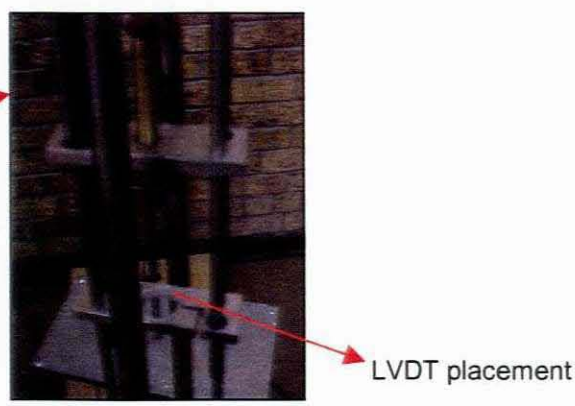

Figure 3.11: New extensometer plates

A small component was manufactured for the moving part of the extension section of the LVDT as the previous system had been prone to slippage.

3.3.4 Thermocouples

Due to the modification of the lower pull rod it was necessary to also modify the thermocouple arrangement. The modification included a stainless steel extension being fitted to the end of the ceramic outer covering to enable the thermocouple to sit up against the top brace. Problems were, however, experienced with the thermocouples due to the high temperature that they were subjected to. And it was found that the ceramic sheaths and beading at the monitoring end were prone to degradation. Preliminary testing was therefore run without the thermocouples until a better arrangement could be devised.

Figure 3.12: Fitment of thermocouples

3.3 Creep testing with regards to the sensitivity of the rigs

Experimental work was consistently carried out on the project, although there were many set backs regarding equipment instability, particularly with regards to the constant load creep test rigs.

Results from each of the rigs were consistently monitored and found to be inaccurate; this was initially thought to be due to certain aspects of the design of the rigs that were not suitable for the testing procedure. It was also thought that there was an influence on the results due to the way in which the test was set up. However, after various attempts to rectify the set up procedure, the problems persisted and it was deemed necessary to further investigate.

The main problem was that the rigs were not recording reproducible results. Also both rigs consistently gave different results to each other. Originally two rigs were manufactured in order to ease time constraints.

The following paragraphs highlight the various problems encountered with the rigs and the various attempts to solve them. A section is included which illustrates the solutions that have been reached to strive to eliminate any further problems and to produce the best possible results using the above-mentioned equipment.

Due to the fact that there are two creep rigs it was firstly necessary to ascertain whether both rigs were producing the same data under the same conditions of load and temperature.

3.3.1 Furnaces

It was during initial test runs that problems were encountered with the furnaces. A particular problem that became apparent was that the temperature monitoring thermocouples could easily become dislodged from their initial positions due to the continuous vertical movement of the furnace. Therefore great care is necessary when handling the furnaces to prevent this.

Problems were also encountered with the data acquisition card (Eagle Technologies PCI 703S). All readings were completely inaccurate. The card was therefore repaired by an Eagle Technology technician; the fault with the board being reported as the input channels being electrically cluttered (or noisy).

3.3.2 Load cell placement and usage

The original creep rig set up included a load cell (Gefran TU KIC; 100 kg), which was placed in the rig set up below the furnace. This load cell was used to monitor the load on the specimen. It was at first considered to eliminate the load cell completely from the creep rig set-up because if the weight of the lower hot pull rod and extensometer system is known, then the force on the sample before testing is also known. Also if the mass of the weights placed on the weight pan are measured before applying the load and then the lever ratio is applied, the load on the sample can be calculated without using the load cell.

Various tests were run on samples to monitor the load that the specimen was experiencing during the test and also the displacement. After tests were run data produced by the two rigs was not the same and therefore could not be verified. This was despite tests being set up identically.

Eventually it was deemed necessary to include the load cell into the creep rig set-up as it was concluded that each rig, although identical to look at, must be slightly different in its make-up. Load cells (Gefran TU KIC; 100 kg) were installed in the upper base plate of the rig, which is above the furnace. They were installed here to allow, firstly, continuous load monitoring, and secondly, to avoid the complication of the load train if installed below the furnace.

During initial testing a load cell drift was detected, this drift appeared to be closely related to a rise in temperature. After checking the surface temperature of the load cells it was found that they were reaching temperatures in excess of 60 °C, which is the maximum operating temperature of this type of load cell. To counteract this problem a cooling system for the load cells was installed.

This was achieved by wrapping Ø 80 mm copper pipe around each of the upper pull rods (just below the load cell). The system was kept in place by a hose clamp underneath it. The copper pipe was in turn attached to a hose, which was in turn connected to a water tap. Once the tap was turned on water passed through the hose. Through a system of piping the water was then passed from the cooling system of Rig 1 to the cooling system of Rig 2, where it passes through the system, finally the water passes through a hose to a drain. Using this system the upper pull rod is kept cool, which in turn keeps the load cell cool (± 20 °C). It can be recommended, for future work, that a system be devised where the water used for the cooling system can be recirculated.

Figure 3.13: Load cell placement

Figure 3.14: Cooling system

Although the cooling system did keep the load cells cool, they continued to give out readings that were misreading and consistently different from each other.

It was attempted to test the load cells accuracy by hanging known weights from the specimen. The results are shown in Appendix A.

Unitemp (agents for Gefran) performed various checks on the load cells in situ. Unitemp performed these checks and it was found that one of the load cells could not be calibrated and was completely unworkable (Rig 2). This load cell was therefore replaced.

3.3.3 Thermocouples

Due to various modifications performed to the creep rigs (as discussed above) it was necessary to modify the thermocouple arrangement. Two thermocouples monitor the temperature of the specimen, one at the top and one at the bottom of the gauge length. This is per ASTM standards for creep testing (E 139-00). Original thermocouples were protected by a ceramic sheath and manufactured especially for the set-up. Problems

were, however, experienced with the ceramic sheaths breaking up due to the high temperature that the thermocouples endure. This adaptation also proved not to be ideal as due to the ceramic sheaths the thermocouples were bulky; this caused a problem as the furnace has little available space inside. It must be noted that it is vital that when the thermocouples are attached, they are attached somewhere that will not influence the specimen being able to extend freely.

Unitemp then made up new thermocouples to specific dimensions (3 mm diameter, length 450 mm thermocouple with a 1.5 m length cable). The thermocouples were manufactured and then bent to fit on site. The ceramic sheath was left off therefore alleviating the problem regarding the space restrictions. Ni80/Cr20 (Goodfellows Metals) wire is used to keep the thermocouples in position during testing.

3.3.4 Control unit

The control unit's purpose is for logging the information from the sensors to a suitable data acquisition system. Voltage outputs from sensors are transmitted to the control unit, where these readings are adjusted to give values of load, extension and temperature.

Values are transmitted to the computer via an analogue to digital card (Eagle Technologies PCI 703S) where they may be logged. The sensors include a load cell, 2 thermocouples and an LVDT (per rig). The software logs data at user defined intervals. Each rig has 4 available channels: one for load, one for the LVDT and the remaining two, for the thermocouples.

The control unit proved problematic due to inaccurate readings and difficulties where consistently found in zeroing the load cells. Over time the control unit seemed to degenerate and display readings that appeared to be more and more inaccurate. It is imperative that the control unit displays and transmits results that are accurate in order to produce accurate data.

At this stage, although considerable effort was directed towards improving the basic test hardware, the persistent inconsistency in creep data suggested that the electronic control and monitoring system was inadequate. This situation prompted a rebuild of the electronic interfaces associated with the control and data acquisition systems for both creep rigs. The modifications, which were performed by Mr. Alon Bas of Intelec Systems, are briefly summarised below.

It was determined that there was an earth potential difference between the rigs and the transducer power supplies after erroneous readings were obtained once the initial system was set up. There also appeared to be an earth potential difference between the rigs and the thermocouples. This was noted as there appeared to be shorts between the thermocouple sheaths and the hot or cold junction, thereby shorting the rig structure to different mains earth potentials via the furnace earth points. At one stage, the potential differences were so poor that the input multiplexors of two APC50 main boards were blown. To solve these problems, the following was performed:

The electronics used to power and amplify the sensors (load cells, LVDT's and thermocouples) were removed (except for the power supply) and replaced with a APC50 Pro Therm_TC data acquisition board from Intelec Systems.

It was found necessary to earth the board and add extra protection to the board (using Bipolar transorbs).

The metallic structure of each rig was connected to a common earth point along with extra earthing to the sheath of each thermocouple. This was deemed necessary as well, since the thermocouples were developing shorts to the sheath, thus eliminating the isolation from ground. Furthermore the common earth point was connected to the ground point of the APC 50 main board.

Custom software was provided by Intelec Systems to allow the rigs to be calibrated and creep data to be logged.

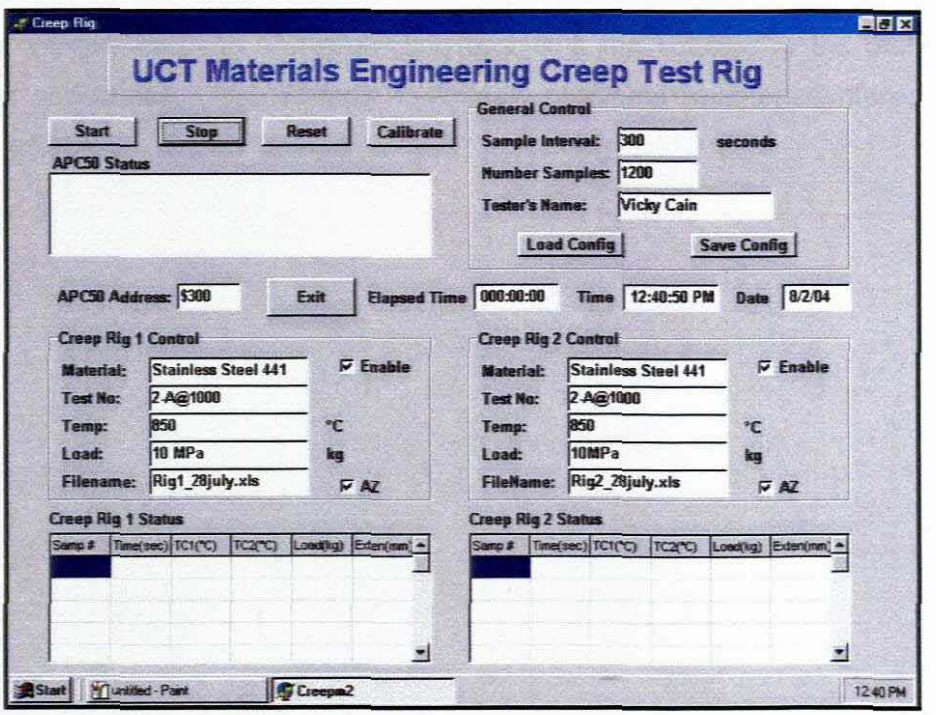

Figure 3.15: Creep data acquisition system interface

Data from the data acquisition programme can then be exported to a suitable spreadsheet programme (MsExcel in this case) where it can be analysed.

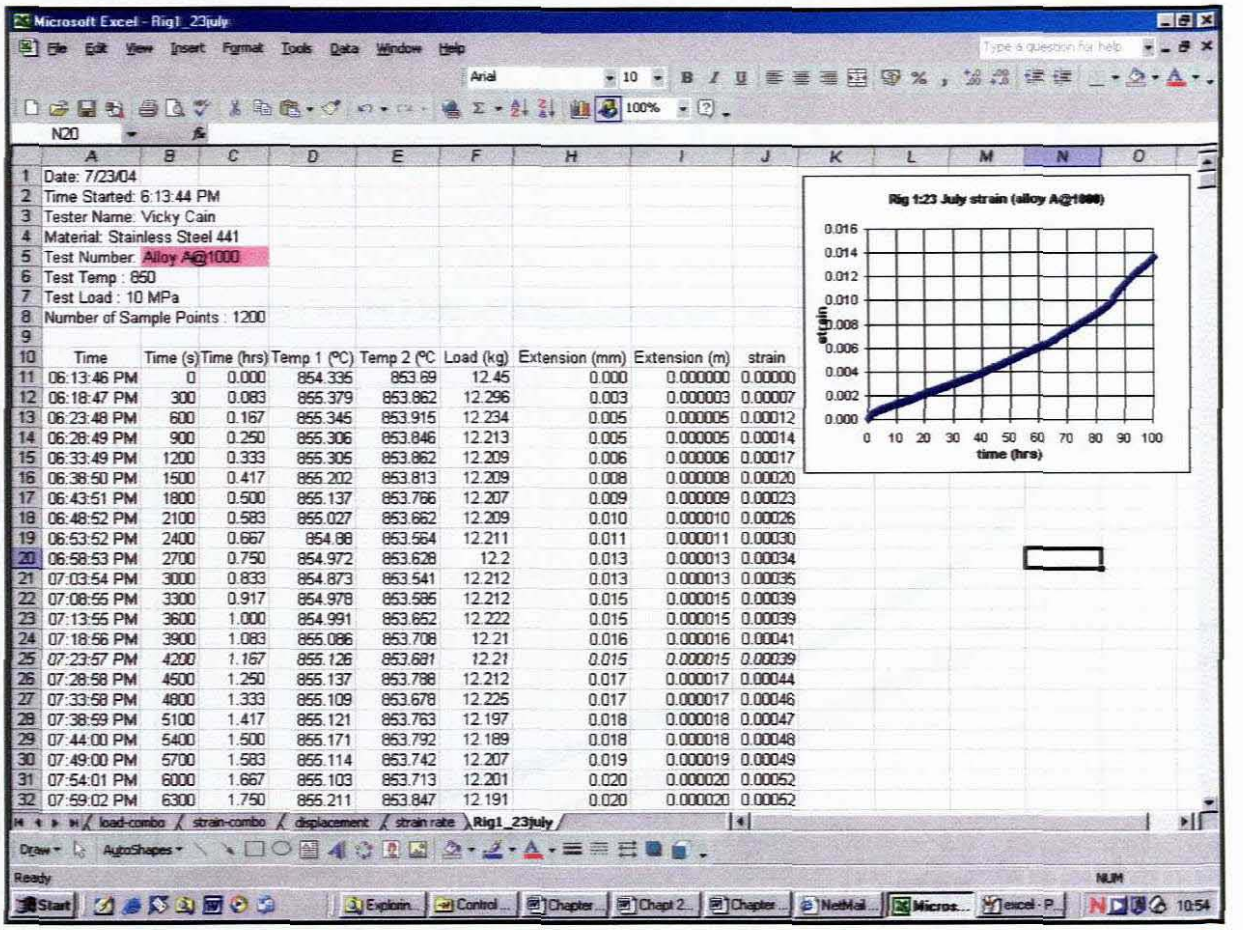

	A	B	C	D	E	F	H	I	J
1	Date: 7/23/04								
2	Time Started: 6:13:44 PM								
3	Tester Name: Vicky Cain								
4	Material: Stainless Steel 441								
5	Test Number: Alloy A@1000								
6	Test Temp : 850								
7	Test Load : 10 MPa								
8	Number of Sample Points : 1200								
9									
10	Time	Time (s)	Time (hrs)	Temp 1 (°C)	Temp 2 (°C	Load (kg)	Extension (mm)	Extension (m)	strain
11	06:13:46 PM	0	0.000	854.335	853.69	12.45	0.000	0.000000	0.00000
12	06:18:47 PM	300	0.083	855.379	853.862	12.296	0.003	0.000003	0.00007
13	06:23:48 PM	600	0.167	855.345	853.915	12.234	0.005	0.000005	0.00012
14	06:28:49 PM	900	0.250	855.306	853.846	12.213	0.005	0.000005	0.00014
15	06:33:49 PM	1200	0.333	855.305	853.862	12.209	0.006	0.000006	0.00017
16	06:38:50 PM	1500	0.417	855.202	853.813	12.209	0.008	0.000008	0.00020
17	06:43:51 PM	1800	0.500	855.137	853.766	12.207	0.009	0.000009	0.00023
18	06:48:52 PM	2100	0.583	855.027	853.662	12.209	0.010	0.000010	0.00026
19	06:53:52 PM	2400	0.667	854.88	853.564	12.211	0.011	0.000011	0.00030
20	06:58:53 PM	2700	0.750	854.972	853.628	12.2	0.013	0.000013	0.00034
21	07:03:54 PM	3000	0.833	854.873	853.541	12.212	0.013	0.000013	0.00035
22	07:08:55 PM	3300	0.917	854.978	853.585	12.212	0.015	0.000015	0.00039
23	07:13:55 PM	3600	1.000	854.991	853.652	12.222	0.015	0.000015	0.00039
24	07:18:56 PM	3900	1.083	855.086	853.708	12.21	0.016	0.000016	0.00041
25	07:23:57 PM	4200	1.167	855.126	853.681	12.21	0.015	0.000015	0.00039
26	07:28:58 PM	4500	1.250	855.137	853.788	12.212	0.017	0.000017	0.00044
27	07:33:58 PM	4800	1.333	855.109	853.678	12.225	0.017	0.000017	0.00046
28	07:38:59 PM	5100	1.417	855.121	853.763	12.197	0.018	0.000018	0.00047
29	07:44:00 PM	5400	1.500	855.171	853.792	12.189	0.018	0.000018	0.00048
30	07:49:00 PM	5700	1.583	855.114	853.742	12.207	0.019	0.000019	0.00049
31	07:54:01 PM	6000	1.667	855.103	853.713	12.201	0.020	0.000020	0.00052
32	07:59:02 PM	6300	1.750	855.211	853.847	12.191	0.020	0.000020	0.00052

Figure 3.16: Data as it appears in a spreadsheet form.

Due to the various earthing and grounding problems the solution to the problem took longer than anticipated. Also various preliminary problems were encountered with the software package.

3.3.5 Initial results after changes

An example of one of the test results is as follows. These tests were run at 850 °C under a stress of 10 MPa (which equates to a load of 12,3 kg being exerted on the specimen). The test specimens were manufactured from 441 and had been annealed at 1000 °C for 200 s.

The graphs show the consistency of the two rigs after completion of all the modifications.

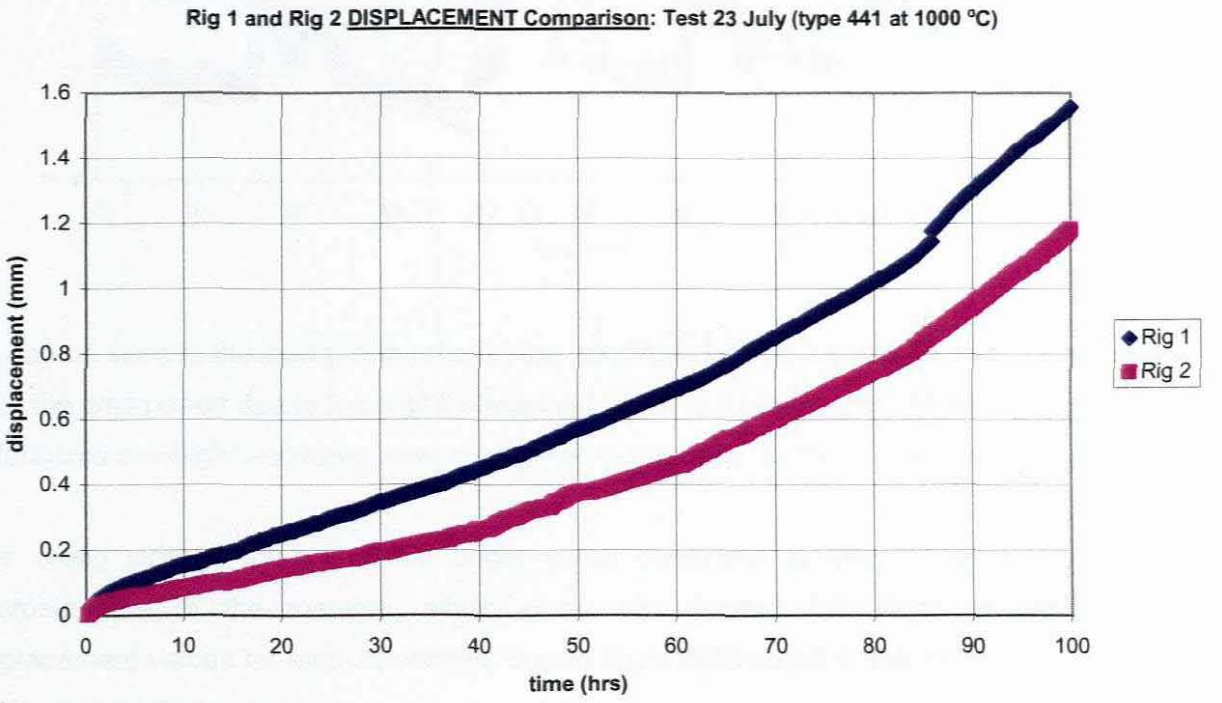

The above graph shows how much the specimens have displaced over a 100 hour period.

Rig 1 and Rig 2 LOAD Comparison: Test 23 July (type 441 at 1000 °C)

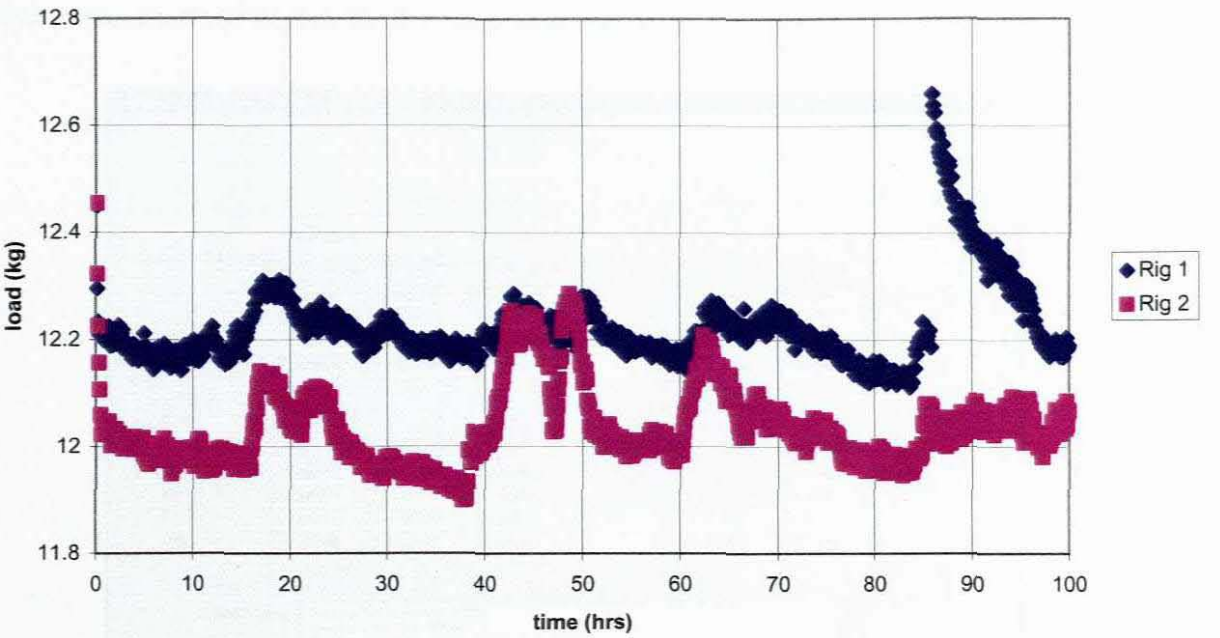

As can be seen in the load graph (above) the specimen on Rig 2 could be displacing less over the time period due to the slightly less load that it is experiencing. Nevertheless, the differences are slight and have been considered acceptable for the present test approach.

The creep strength of a material under given conditions is also influenced by the microstructure of the material, which could also explain the slight difference in displacement values for each specimen, due to slight differences in the microstructure of each one of the specimens.

Creep is also extremely sensitive to minor variations in the physical state of material. Identical metals may show very different creep behaviour. It is also generally accepted that there may be considerable variations between specimens. This could be due to the fact that the specimens may have been taken from different parts of the same sheet.

3.3.6 Test approach

Below is the interface screen for the calibration set-up of the rigs.

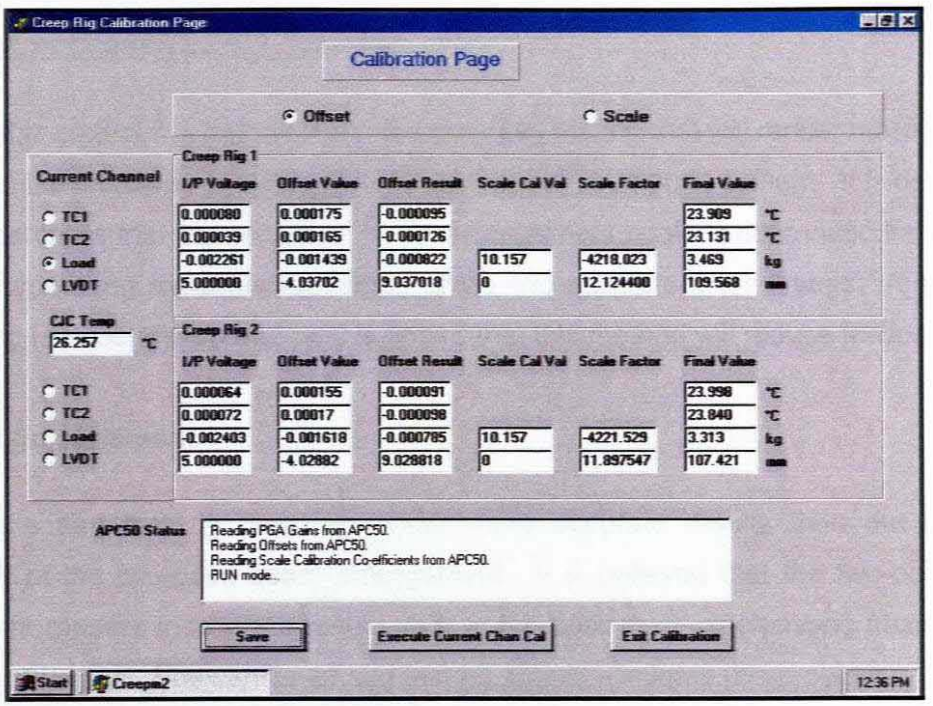

Figure 3.17: Calibration system interface

Before a test is performed, the measurement sensors must be calibrated. Refer to appendix E for notes on calibration methods.

It has been found through relentless testing that the constant load creep test rigs are extremely sensitive. It is imperative that tests are set up extremely cautiously and that components of the rigs are handled with the utmost care. A creep test set-up procedure has been devised during this research work; it is strongly recommended that users follow this procedure meticulously.

Refer to appendices for constant load creep test rig set-up (Appendix F) and constant load creep test rig end procedure (Appendix G).

CHAPTER 4

Sag testing

4.1 A new approach to sag testing

As part of this project it is necessary to design a sag test rig that will render more accurate results than the industrial benchmark of the two-point beam arrangement. It is debated by some researchers that the two-point beam arrangement could render inaccurate results due to the specimen experiencing friction at the two supports when it sags. A cantilever style test rig is to be researched as it is hoped that this method will reduce friction.

4.1.1 Design statement

To design a sag test rig that will render more accurate results than the industrial benchmark of the two-point beam arrangement. It is believed that the two-point beam arrangement renders inaccurate results due to the specimen experiencing friction at the beams when it sags. The cantilever sag test rig should eliminate this problem.

4.1.2 Cantilever sag test rig requirements

There are certain requirements that must be met by the cantilever test rig design.

The cantilever sag test rig design requirements are as follows:

- be cost effective.
- be able to be used for testing of a wide range of materials having different sag characteristics.
- Be of a manageable weight (i.e. where it can be picked up with relative ease).
- Allow for measurements of deflections to be made without adding heavily to the cost.
- Be manufactured from a material that can withstand high temperatures.

4.1.3 Sag test rig design constraints

There are certain factors that constrain the design of the sag test rig.

The rig should:

- Be able to be manufactured within a reasonable timeframe and with relative ease.

- Be cost effective (bearing in mind sag testing is a more economical method of testing than creep testing).
- Be manufactured from a high quality material so as to be used for many tests.
- The material to manufacture the rig must be chosen with care, as it is necessary that it is able to withstand high temperatures and have corrosion and oxidation resistance.
- Should be of a manageable size so as to fit into the average laboratory furnace.
- Be able to be picked up by the average person (i.e. not be too heavy). Should be within the limits of 5 kg to 10 kg.

4.1.4 Sag test rig design concepts

Initial designs were based on the concept of the sag test rig that was found on 'Haynes International' website[74]. But, as can be seen in figure 4.1 this particular rig appears to have specimens welded to it. This was decided against as not only could this change the metallurgical properties of the specimen at the point of attachment, but could also prove to be problematic when it is necessary to remove the specimens after a test. Removing them could damage the specimen and also the rig itself.

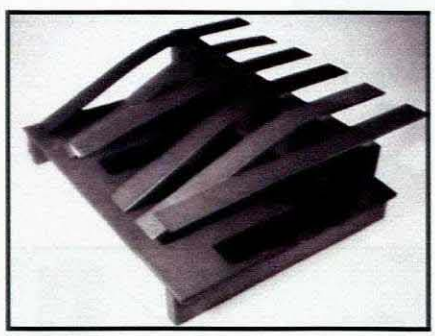

Figure 4.1: Cantilever style sag test rig[74]

The next design that was considered was to have the specimens held into place by a form of clamp that would be aided by a series of bolts.

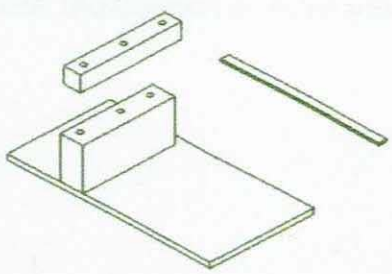

Figure 4.2: Concept design 1

This was also decided against, as it was believed that due to the high temperature that the rig would be experiencing it could prove problematic to undo and tighten the bolts repeatedly.

The next concept (concept design 2) planned to merely have the specimen held in place by another plate. A test rig was manufactured from mild steel, with the purpose being to monitor the specimen behaviour under high temperature. A test was performed at 850 °C. After 24 hours it could be seen that the specimen had in fact not only deflected where anticipated, but also between the two plates. This can be seen in figure 4.5. It was decided that sagging in this area would have a detrimental effect to the deflection values needed and this idea was rejected.

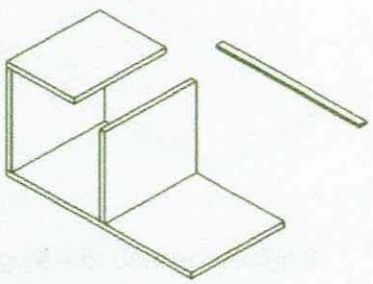

Figure 4.3: Concept design 2

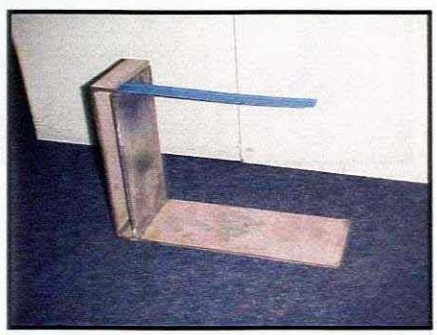

Figure 4.4: Test rig

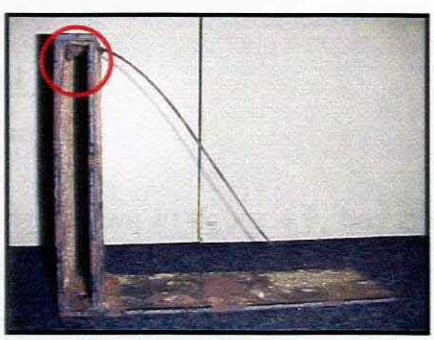

Figure 4.5: Test rig and specimen after high temperature exposure. Note: Displacement in circled area.

The design was modified to incorporate a slot at the top of the rig in which the specimens are retained without additional applied force. This slot system would not be held together by bolts, since the space between the two plates is very small, the specimen would simply rest in between the two plates.

It was also considered necessary to have holes drilled through the specimen and for pins to pass through the slot to keep them in place. Keyways were instead machined into the bottom part of the slot for alignment of the specimens.

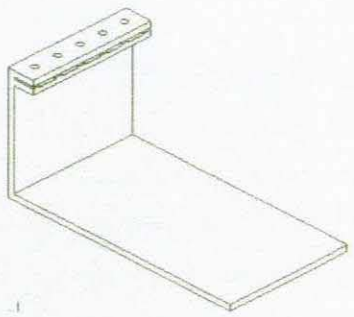

Figure 4.6: Concept design 3

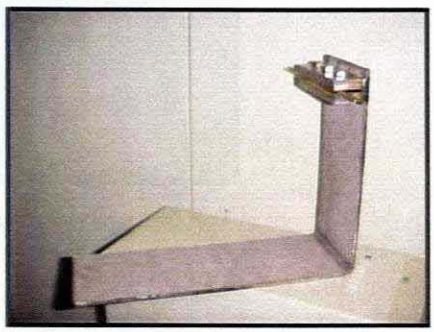

Figure 4.7: Test rig

This idea seemed to be the most appropriate, although small modifications were made to the design before the final rig was manufactured. The specifications of the final rig are as follows:

4.2 Cantilever sag test rig

4.2.1 General description

The cantilever sag test rig, shown in figure 4.8, has been designed to conform to the requirements and criteria set out as above. A set of technical drawings of the rig has been included in Appendix B.

The final design has the following features:

- The weight of the rig is 7.5 kg.
- All plate is 10 mm thick.
- There is no welding; the rig has been instead bolted together, using allen cap screws.
- Specimens are aligned by a slot system in the bottom part of the retainer piece.

- The material to manufacture the rig from was chosen, on recommendation as stainless steel 316. This material was chosen due to its ability to be able to withstand high temperatures and its corrosion and oxidation resistance.
- Two supports were added to give the rig extra stability.

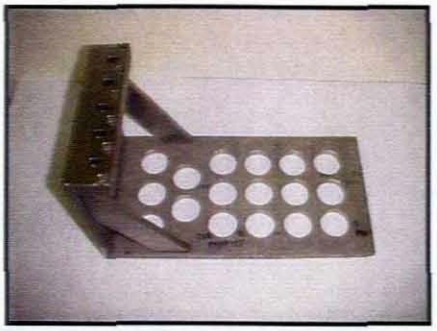

Figure 4.8: Cantilever sag test rig

There were 26 holes of diameter 40 mm drilled into the two plates forming the body of the rig; this was done to reduce the weight of the rig in order to make it more manageable. 10mm plate was used to provide rigidity, although this led to a heavy rig (10kg), significantly heavier than the two-point beam rig (5 kg). Due to the cumbersome weight problem holes were drilled uniformly in the rig (this rendered the rig to eventually weigh 7,2 kg).

These holes have been left out of the technical drawing. It can be recommended that future rigs be manufactured from 8 mm plate instead of 10 mm in order to reduce the overall weight of the rig.

4.3 Comparison of sag test rigs

The results of the sag testing for each rig were used for the purpose of comparing the accuracy of the rigs against each other. Additional material was supplied from Columbus Stainless (Pty) LTD. It was supplied in the cold rolled condition as sheet with an approximate gauge thickness of 1.5 mm.

All sag testing was performed in a box furnace, the set-up of which is described in Section 4.4.

4.4 Box furnace: Sag testing

Previously sag testing had been performed using the two-point beam arrangement in a box furnace at the Centre for Materials Engineering at UCT. Due to circumstances and conveniences it was decided to perform sag testing at the Cape Peninsula University of Technology in the Department of Mechanical Engineering in a larger box furnace. The only difference being that this furnace is considerably larger than the UCT one (table 4.1).

Table 4.1: Comparison of the sizes of the two furnaces

CPUT FURNACE			UCT FURNACE		
L	B	H	L	B	H
0.6	0.375	0.355	0.375	0.2	0.15

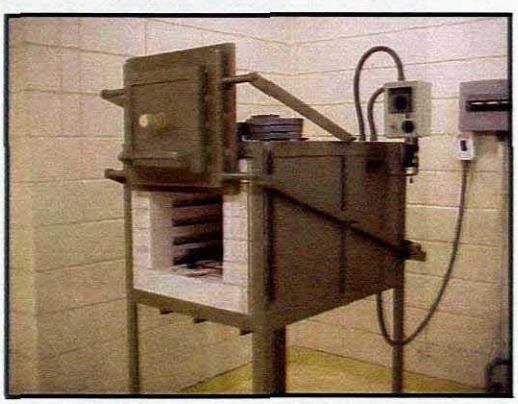

Figure 4.9: Box furnace (CPUT)

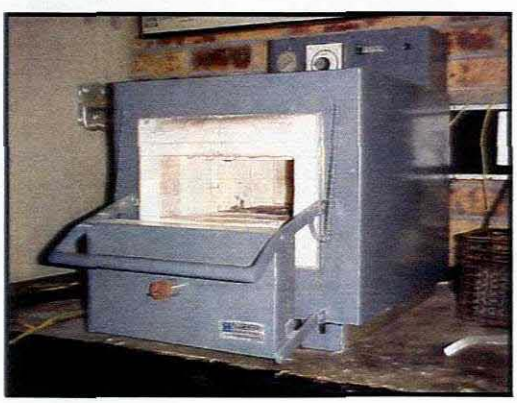

Figure 4.10: Box furnace (UCT)

It was recommended that to improve the reliability of the tests, sag testing could be performed in a furnace fitted with a circulating fan to promote an isothermal temperature inside the furnace. The furnace that was to be utilised did not have a fan. Therefore this option was researched, but on the advice of Kiln Contracts was decided against. They advised that due to the furnace being used for melting purposes, which results in regular

tranches of high temperature (another research field within the department) the fitting of a fan would be impractical. There would also be an unjustified high cost that would be involved for such a large furnace. The cost would be somewhat high due to the material that the fan would have to be manufactured from in order to withstand the high temperatures. It was, however, agreed that due to the fact that the furnace at CPUT is relatively large, temperature variations may not be as pronounced. It was advised that the best method to even out temperature variations would be to add more elements to the furnace. Originally the furnace had only elements on the bottom and side surfaces. Therefore more elements were added to the top surface of the furnace.

Figure 4.11: New elements on top surface

Temperature variations of the furnace were checked before and after the modifications using temperature monitoring thermocouples linked to a digital read-out, indicating temperature.

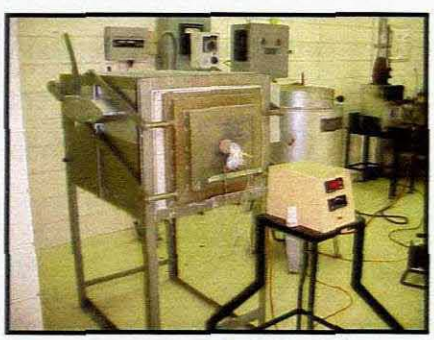

Figure 4.12: Temperature monitoring set-up

Figure 4.13: Temperature monitoring thermocouples

The temperature of the furnace at specific points was then recorded.

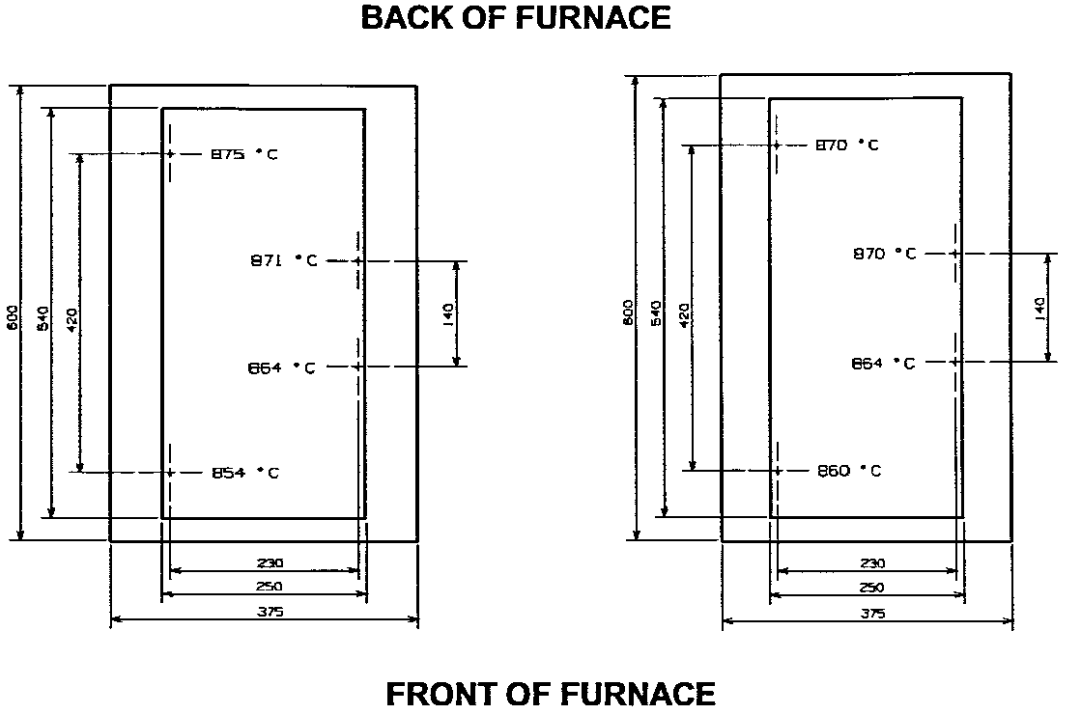

Figure 4.14: Schematic view of furnace showing change in temperature distribution due to added elements. The view on the left is the before and on the right the after.

This experiment was performed with the temperature controller of the furnace set at 850 °C. As can be seen from figure 4.14 the addition of more elements into the furnace did produce an improvement in temperature uniformity.

Another modification that was made to the furnace to suit the testing procedure was that the furnace was fitted with a more accurate temperature controller, a Gefran 600 digital controller.

CHAPTER 5

Experimental methods

5.1 Material

The material, 441, is supplied in the cold rolled condition as sheet with an approximate gauge thickness of 1.5 mm.

Two alloys of 441 have been supplied for this project. The difference between the two alloys is that one contains more Niobium than the other. For reference purposes these alloys will be referred to as alloy A and alloy B, were alloy B (0.74 wt %) has more percentage Niobium than alloy A (0.46 wt %).

Table 5.1 shows the chemical compositions for both alloy A and alloy B.

Table 5.1: Alloy chemical compositions

Element	Alloy A	Alloy B
	(wt%)	*(wt%)*
C	**0.0190**	**0.0130**
Mn	**0.5600**	**0.4700**
Co	0.0400	0.0300
Cr	**17.9600**	**17.6300**
B	0.0011	0.0002
H	7.4300	3.4200
V	0.1400	0.1300
Pb	0.0000	0.0000
S	0.0004	0.0004
Si	**0.5000**	**0.5400**
Ti	**0.1990**	**0.1790**
Ni	**0.1900**	**0.3300**
N	0.0208	0.0194
Al	0.0060	0.0050
P	0.0260	0.0240
Cu	0.0700	0.1700
Mo	0.0200	0.0100
Nb	**0.4670**	**0.7350**
O	0.0099	0.0087
Sn	0.0070	0.0080

5.2 Heat treatment: Salt bath furnace

A salt bath furnace was used for the heat treatment procedures. A salt bath furnace is often used when it is necessary that a specimen experience a specific temperature for a short duration. It is constant and uniform, whereas using an ordinary box furnace could result in the specimen experiencing different temperatures across its length.

It was necessary for the Centre for Materials Engineering at the University of Cape Town to acquire another salt bath furnace for the heat treatments. The salt bath furnace that was originally going to be used for the treatments could only reach a maximum operating temperature of 850 °C. This project required considerably higher temperatures than this.

A salt bath furnace was therefore custom designed to meet certain requirements and was built by a local company. There were, however, various modifications to the original design and the design needed to be reworked. Due to these modifications the commissioning of the salt bath took considerably longer than anticipated.

Figure 5.1: Salt bath furnace

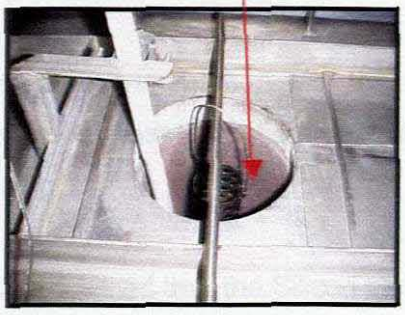

Figure 5.2: Crucible with basket suspended

Figure 5.3: Temperature monitoring thermocouple

Various procedures need to be followed when working with salt baths furnaces. In particular it is vitally necessary that users exercise great care and are aware of the safety procedures.

The annealing salt that is used within the bath is GS 750 and is supplied by Houghton Durferrit. This salts main ingredient is Barium Chloride[75]; it has a working range of 900-1100 °C and melts at 750 °C.

Decarburisation is prevented by avoiding a reaction between the salt bath furnace and the specimen being heat treated. This is achieved by adding an additive to the salt, as the salt baths do tend to enrich themselves with traces of oxygen compounds. Research by Houghton Durferrit has found that only a small amount of this compound is enough to cause severe decarburisation. These contaminations can be reduced by adding R2 which will render the salt bath inert, which means that it neither carburises nor decarburises irrespective of the Carbon content of the steel being treated. The additive, R2, is termed an inertor, which contains barium. This inertor is used to inert the barium containing annealing salt, GS 750.

The process for adding the inertor is as follows:

- Allow annealing salt to melt
- Finely sprinkle R2 into the bath
- Check the bath using the foil method. This is a method whereby 1 % Carbon steel foil, is immersed into the bath, removed after a short period of time and then quenched. An immersion time for 1000 °C is ± 15 minutes.
- After quenching the foil is bent between the fingers, if it splinters (has become brittle) the bath is suitable, if it does not splinter more R2 must be added and the foil test repeated[76].

During experimentation with the salt bath furnace it was noted that the silicon carbide crucible appeared to be beginning to blister. A concern was raised that it could be leaking.

It was deemed that the Silicon carbide crucible was highly inappropriate. This was mainly due to the high temperature range and also the corrosive environment that the salt created. The crucible was therefore replaced with an Inconel crucible instead. It was constructed from seamless pipe and a base was welded onto the bottom of the pipe after it had been machined with a step seal to improve the strength of the joint. The weld was

dye tested to ensure there were no leaks. The Inconel crucible is tolerant up to a temperature of 1050 °C.

It was noticed once the Silicon carbide crucible had been removed that it had in fact split down the side. Fortunately the pot was removed prior to it leaking.

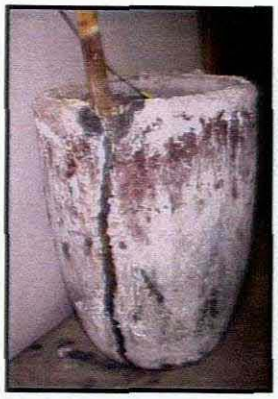

Figure 5.4: Silicon carbide crucible

Figure 5.5: Broken up thermocouple

It was also noted that the thermocouple had in fact degraded quite badly and the ceramic covering had broken up.

Figure 5.6: Salt bath furnace. Note: new thermocouple arrangement

Figure 5.7: Temperature monitoring thermocouple. Note: bath is in operation

After heat treating specimens were oil quenched, in Isodur 220. It was found that after quenching there was a residue on the specimens. After a standard 100 hour sag test specimens appeared to oxidise dramatically. At first it was thought that the temperature that was indicated on the controller was in fact misreading. Due to this a concern was raised that perhaps the temperature inside the furnace was in fact greater than it should have been, which could result in this excessive oxidisation.

Figure 5.8: Uncleaned specimens after 100 hour sag test resting on two point beam sag test rig

Tests were run to check the temperature of the inside of the furnace using thermocouples yet the temperature read within the range of 850 °C. Another test was also run in another furnace to eliminate the question of the furnace having a temperature misreading problem. The result was that the temperature was not affecting this problem.

After research it was found that salt bath heat treatments do invariably result in difficulties with cleaning specimens, therefore on recommendation from industry (Sanderson Speciality Steels and Bohler Steel) specimens were washed in hot water and soap. They were then rubbed slightly with water paper and wiped clean with Acetone. This method was found to be the most suitable method of cleaning specimens after a salt bath furnace heat treatment.

5.3 Creep testing

5.3.1 Heat treatment

Creep test specimens were heat treated at varying annealing temperatures, while the annealing time remained the same (200 s). This matrix follows the work of previous researchers with regards to this project [10, 43 and 77].

Table 5.2: Annealing treatments for creep test specimens

Time (s)	Temperature (°C)
200	950
200	1000
200	1050

Since two alloys were used in this investigation, heat treatments (and consequently creep tests) were performed twice (on both sets of alloys).

In order to obtain maximum creep resistance it is necessary to determine the optimum heat treatment. The optimum heat treatment may render the material with the optimum microstructure for improved creep resistance. This could be related to a number of factors such as grain size, solid solution strengthening and or precipitate distribution.

5.3.2 Specimens

Specimens were machined accordingly (see figure 5.9 for dimensions).

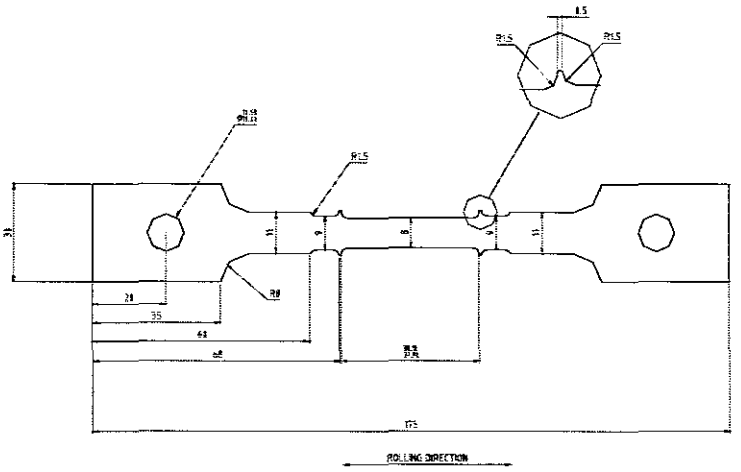

Figure 5.9: Creep test specimen. Note: notches for attachment of extensometer

5.3.3 Testing procedure

Creep tests are to be performed at a temperature of 850 °C for a period of 100 hours at fixed loads for each test. Table 5.3 indicates the matrix of prior annealing temperatures and stress conditions for alloys A and B.

Table 5.3: Creep test matrix

Alloy	Annealing temp (° C)	Stress (MPa)
A	950	5; 10; 15
	1000	5; 10; 15
	1050	5; 10; 15
B	950	5; 10; 15
	1000	5; 10; 15
	1050	5; 10; 15

The stress values are low in order to simulate what the material experiences in service. This project will endeavour to identify what creep mechanisms are prevalent under a low load (simulating the applied load in service operation) by evaluating the stress exponent from the combination of tests presented in Table 5.3.

All creep testing was performed using purpose built creep test rigs as described in chapter 3.

5.4 Microscopy

It was necessary to perform a certain amount of microscopy; this was deemed necessary in order to determine the grain size of each alloy after heat treatment, which could indicate the effect of grain size on the creep resistance of the material.

A sample of each alloy at the various heat treatments was mounted in a resin mount. This was done using a Struers Labo Press-3 mounting machine. The specimens were then polished using a Struers RotoPol 22 automatic polisher to a 0.25 micron finish. Each specimen was then checked in turn for surface scratches using a Reichert MeF3A polarised light microscope.

After this procedure samples were chemically etched. Etching is done in order to reveal the grain structure and any other microstructrual characteristics that could pertain to the study.

A solution of the following was used for the etchant:

10 ml Nitric acid (HNO_3)
20 ml Hydrochloric acid (HCl)
30 ml water (H_2O)

Specimens were etched for between two and three minutes.

5.4.1 Grain size measurement

Grain size was measured from etched specimens, using lineal analysis, according to ASTM standard E112-88[78]. The magnification in the light microscope was set such that grain boundaries could be easily observed, whilst maintaining sufficiently large fields of view to capture the overall grain size distribution.

5.5 Sag testing

5.5.1 Heat treatment

Before sag testing specimens were heat treated at 1000 °C for 200 seconds.

Table 5.4: Sag test matrix

Time (s)	200 s	Temperature (°C)	
		1000 °C	
		(TPB x 5) x 2 (TPB x 4) x 2	(C x 5) x 2 (C x 4) x 2

TPB identifies the two-point beam method of sag testing and C represents the cantilever method of sag testing.

Owing to the fact that the purpose of the sag testing was to compare the two-point beam method to the cantilever method it was decided to adhere to one temperature for heat treatments (i.e. all specimens would be annealed to the same temperature for the same time period).

Each sag test rig holds five specimens. However, due to a shortage of material two tests of each method were performed with five specimens and two tests of each method were performed with four specimens (see Table 5.4).

5.5.2 Specimens

The material was machined into the specimens for the two sag test rigs. Specimens are slightly different to accommodate the two rigs; however, every effort has been made to keep the dimensions similar for comparison reasons. The main similarities are that both specimens are 25.4 millimetres wide (1 inch) and 1.5 mm thick (this is governed by the thickness of the sheet).

The two-point beam sag test rig specimens are strips of material 25.4 mm (I inch) wide and 292.1 mm (11 ½ inches) long with a 12.7 mm (½ inch), 90 ° locating bend at one end. Therefore the span that deflects is 290.6 mm (292.1 - 1.5). This follows the same dimensions as previous work [10,44 and 77].

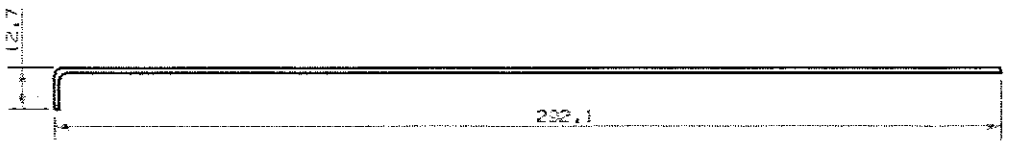

Figure 5.10: Two-point beam sag test specimen

The cantilever sag test rig specimens are strips of material 25.4 mm (I inch) wide and 185.3 mm long. Therefore the span that deflects is 145.3 (185.3 – 40). The 40 mm is the amount that the specimen is fixed by inside of the clamp of the sag test rig.

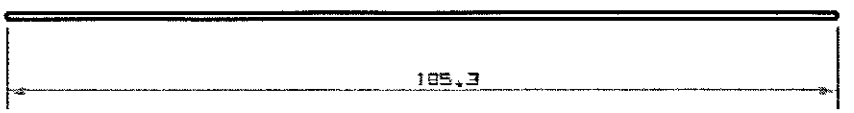

Figure 5.11: Cantilever sag test specimen

Refer to Appendix C for equations regarding chosen length of cantilever sag test specimen.

For the two-point beam specimens, firstly they were heat treated and then the locating bend put in as it was found that if the bend was put in prior to heat treatment the material would crack, this was deemed to be due to cold work hardening. The annealing softened the material thereby preventing the cracking.

In order to determine the deflection of the specimens a dial-gauge set-up was introduced. The dial gauge renders an accuracy of ± 0.01 mm for measurements of deflection. The

dial gauge works on a method whereby the deflection of the specimen is measured before the testing and then again after the testing. The difference then between these two values is taken as the amount the specimen had deflected under the given conditions.

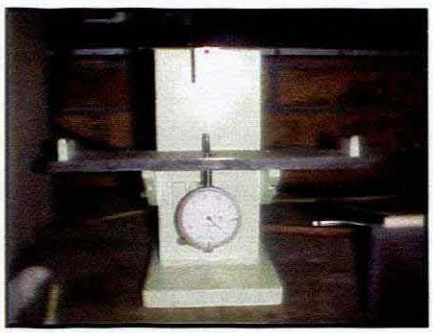

Figure 5.12: Dial guage set-up

The measurement of deflection for the cantilever testing was performed using a height gauge on a flat surface. The height gauge works on a method whereby the deflection of the specimen is measured before the testing and then again after the testing. The difference between these two values is taken as the amount the specimen has deflected under the given conditions.

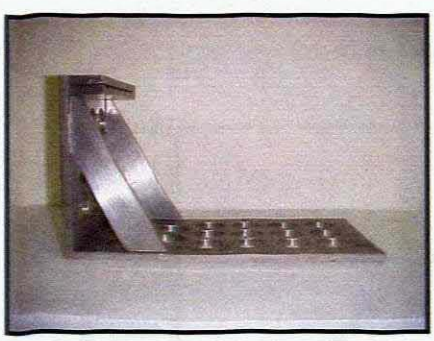

Figure 5.13: Cantilever sag test rig

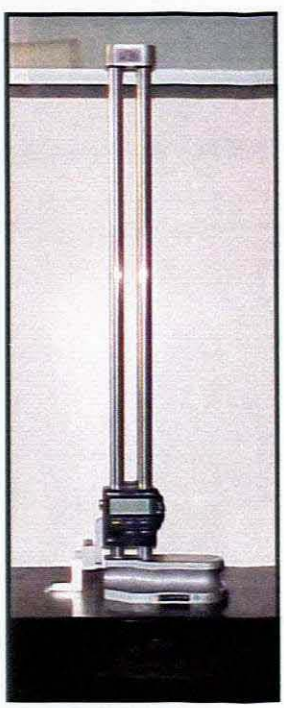

Figure 5.14: Height gauge

All sag testing was performed in a box furnace as described in chapter 4. Sag testing was performed for both sag test rigs at a temperature of 850 °C for 100 hours.

CHAPTER 6

Experimental results

6.1 Creep testing

Creep testing was performed in order to gain a better understanding of the high temperature creep behaviour of 441. It was also necessary in order to better understand what role Niobium had in aiding the material's creep resistance. As discussed previously two alloys of 441 (alloy A and alloy B) have been investigated.

6.1.1 Creep test results

The creep test results of the two different alloys that were heat treated at three varying temperatures under specific loads are presented. Each graph shows the difference in creep strain at the different annealing temperatures. Graphs may have different time scales i.e. from under 25 hours to 200 hours, this would depend on whether or not the specimen had fractured or if a more prominent steady state creep range was attempted to be displayed.

6.1.1.1 Creep test results: Alloy A

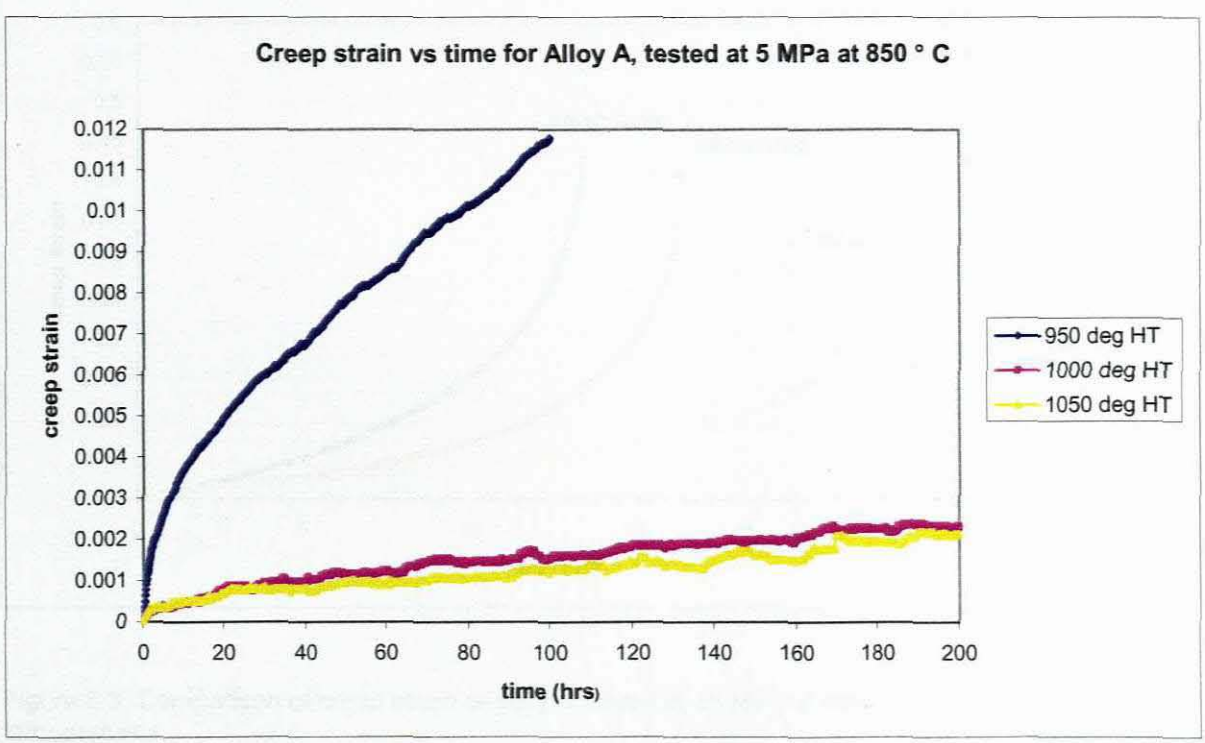

Figure 6.1: Comparison of creep strain of alloy A tested at 5 MPa at three different annealing temperatures

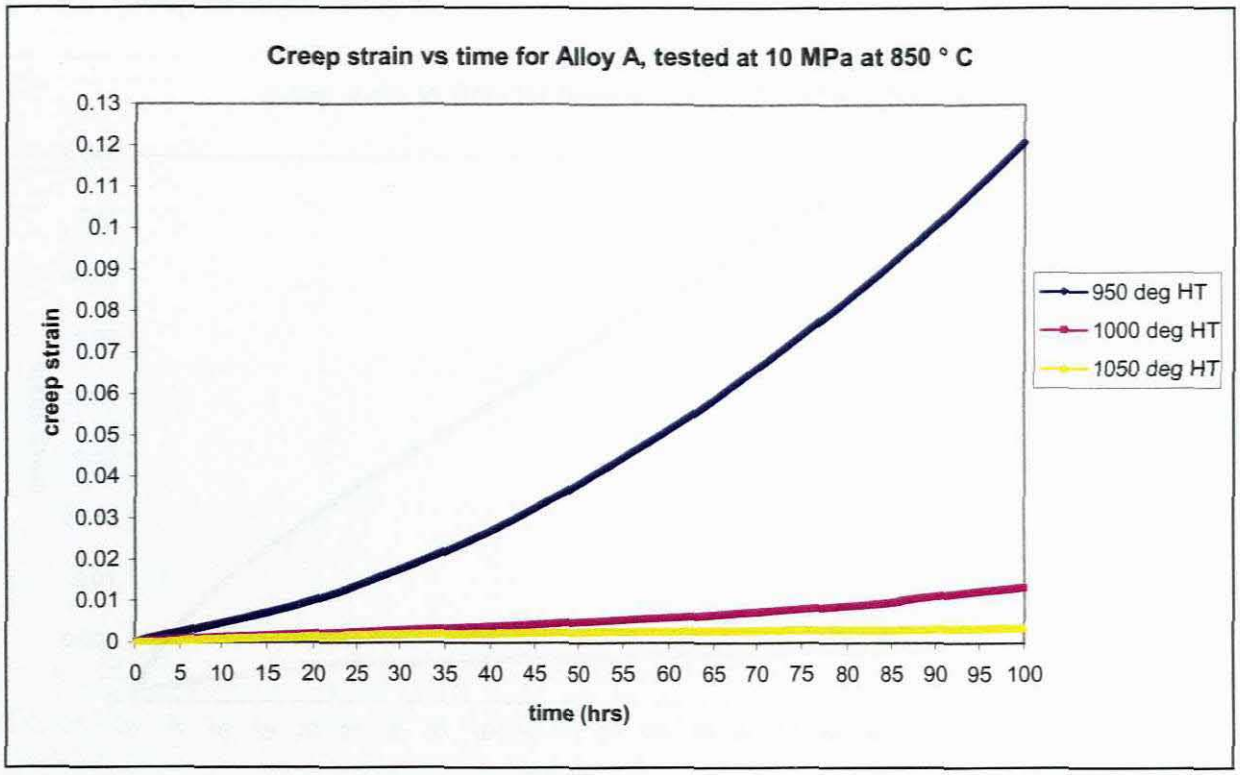

Figure 6.2: Comparison of creep strain of alloy A tested at 10 MPa at three different annealing temperatures.

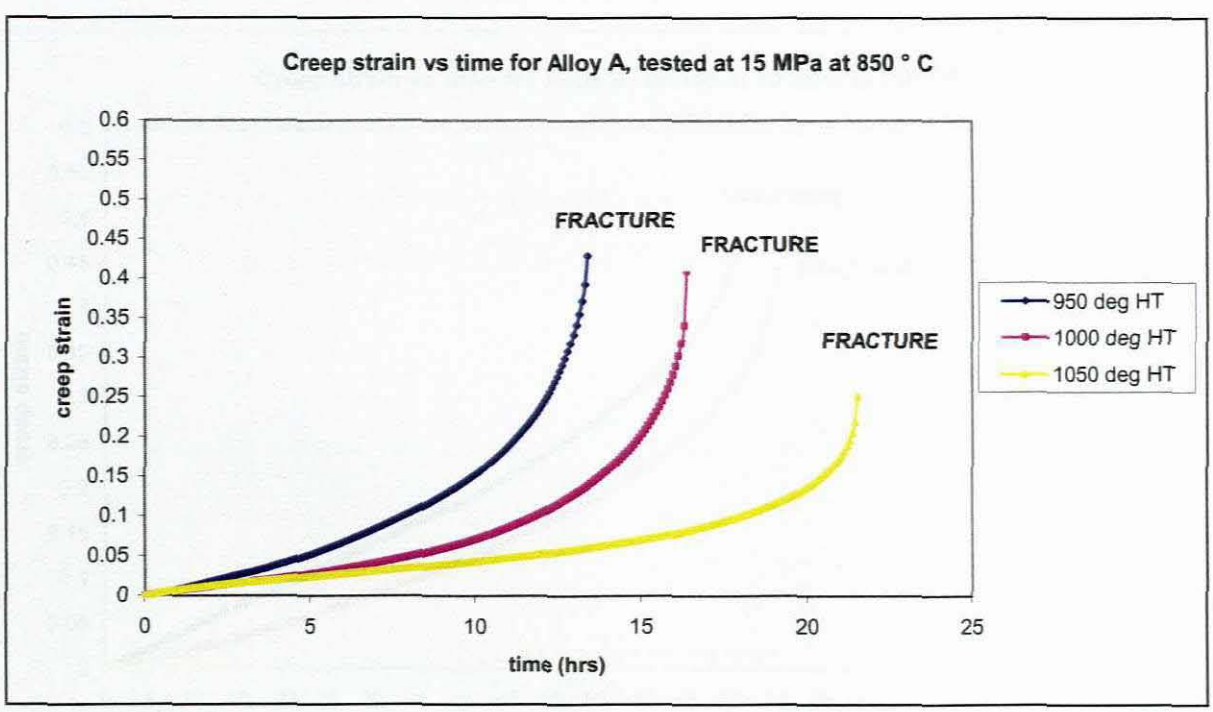

Figure 6.3: Comparison of creep strain of alloy A tested at 15 MPa at three different annealing temperatures.

6.1.2.2 Creep Results: Alloy B

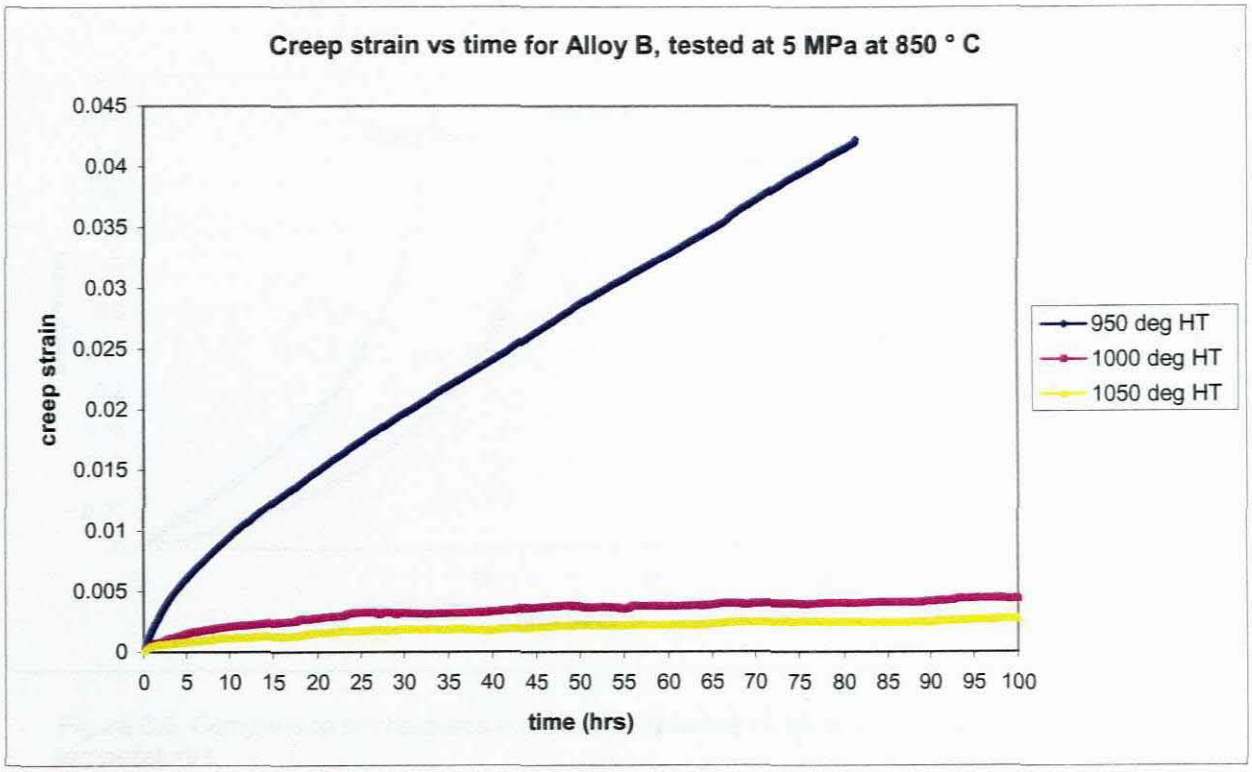

Figure 6.4: Comparison of creep strain of Alloy B tested at 5 MPa at three different temperature annealing.

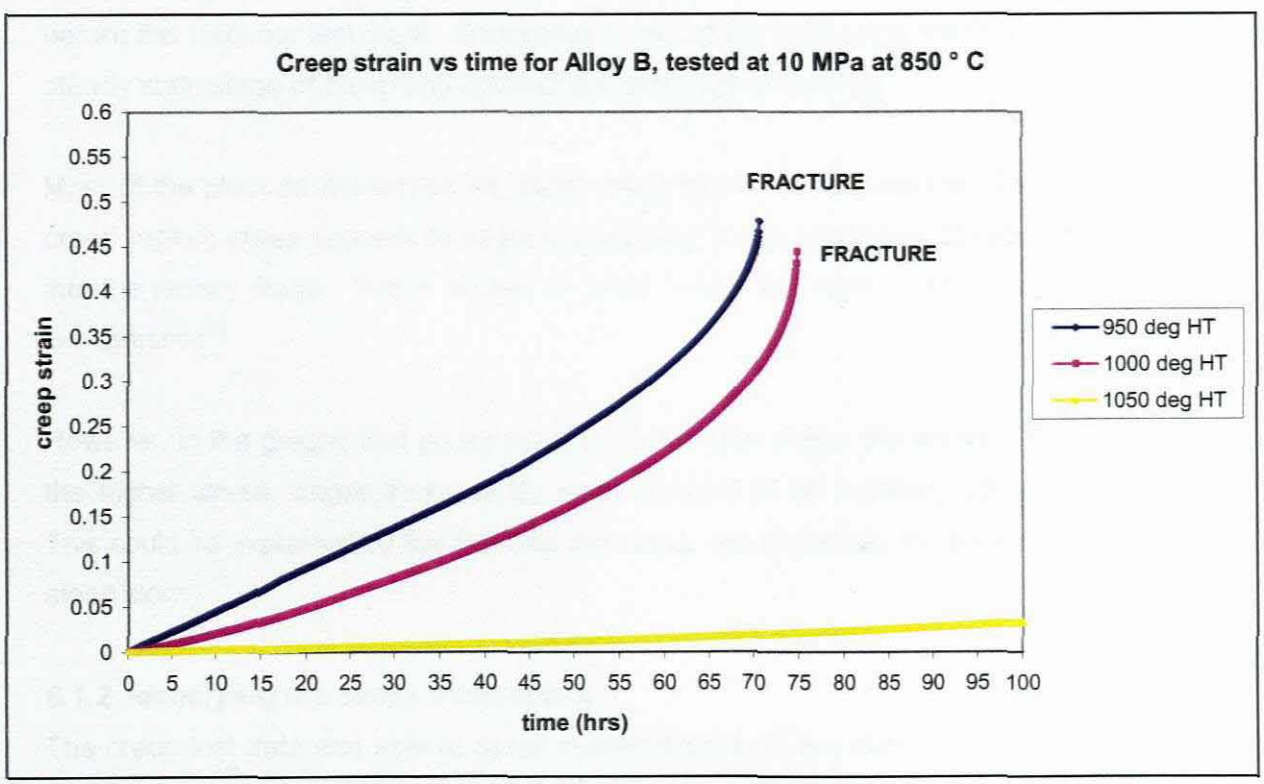

Figure 6.5: Comparison of creep strain of Alloy B tested at 10 MPa at three different temperature annealing.

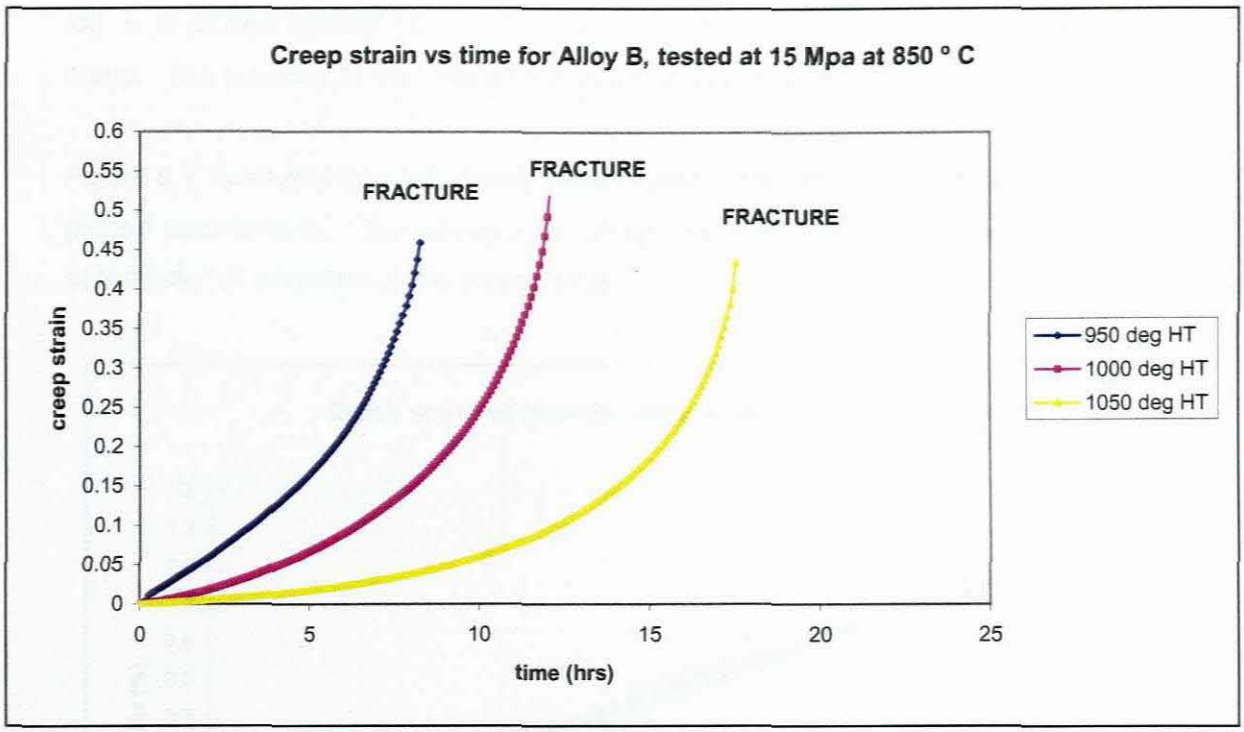

Figure 6.6: Comparison of creep strain of Alloy B tested at 15 MPa at three different annealing temperatures.

As can be seen from the plots of data at a stress of 15 Mpa, all the specimens failed before the 100 hour test mark. Specimens in this stress range spent little time in the steady state stage of creep and entered the tertiary stage quickly.

Most of the plots do not exhibit an 'ideal' creep curve. There appears to be no primary creep region, creep appears to begin immediately in the secondary stage and then goes into the tertiary stage. This is evident of creep data in the case of high temperatures and low stresses[46].

However, in the graphs that do exhibit a primary creep stage, the stage is fairly short. In the higher stress ranges there hardly even appears to be a steady state creep region. This could be explained by the fact that the creep rate is actually increasing continuously, albeit slowly.

6.1.2 Identifying the stress exponent, n

The creep test data was able to assist in identification of the likely creep mechanism that was operative during testing. This was done by deducing the stress exponent, which is related to the steady state creep stage. Norton's law was made use of in identifying the following stress exponents[44]. A straight line relationship is shown in each curve for when

log $\dot{\varepsilon}$ is plotted against log s. Each straight line represents the steady state region of creep. The gradient of the straight line is the stress exponent, n.

Figure 6.7 illustrates how the steady state region is identified from a graph of creep strain plotted against time. This steady state creep rate is estimated by drawing a tangent, AC, at the point of inflection of the creep curve.

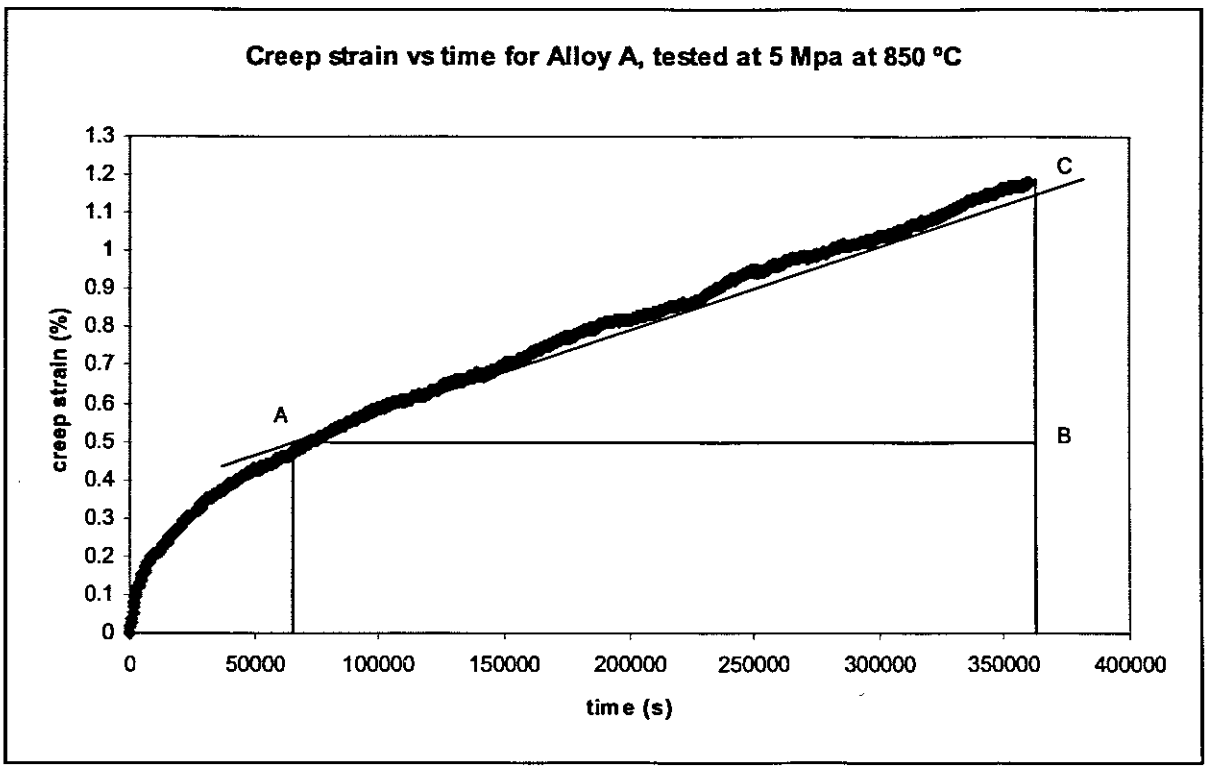

Figure 6.7: Example of a creep curve, illustrating the steady state region

Steady state creep rate:

$$\dot{\varepsilon} = \frac{BC}{AB}$$

$$= \frac{0.71}{295800}$$

$$= 2.4 \text{ x } 10^{-6} \% \text{ s}^{-1}$$

The following graphs illustrate the various stress exponents for alloy A and B at the various annealing temperatures.

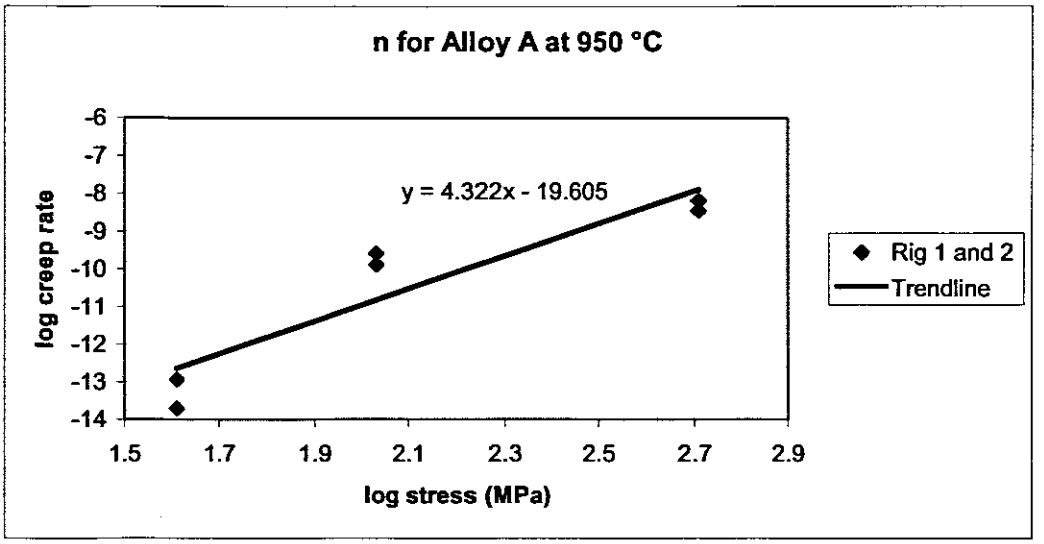

Figure 6.8: Stress exponent for Alloy A at 950 °C

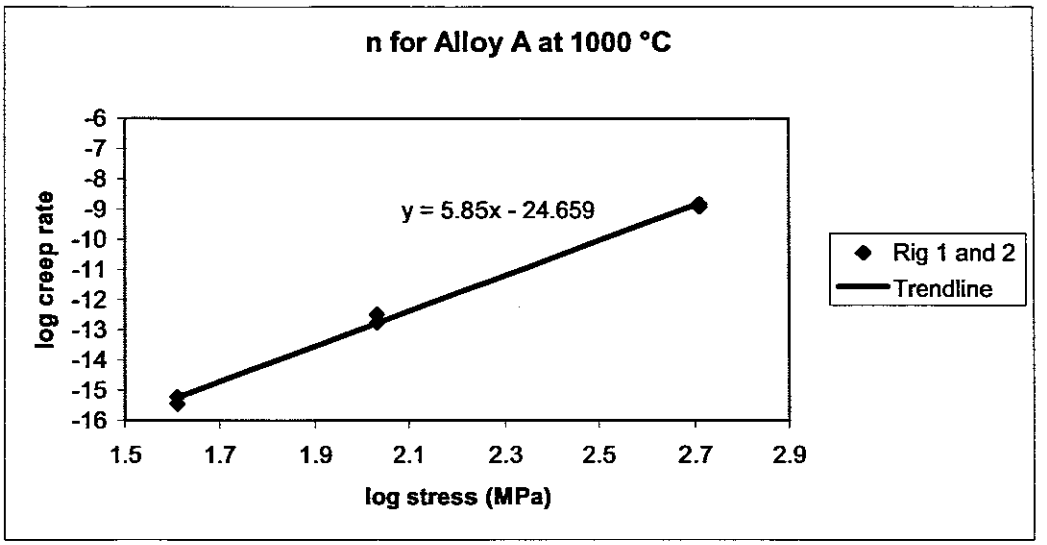

Figure 6.9: Stress exponent for Alloy A at 1000 °C

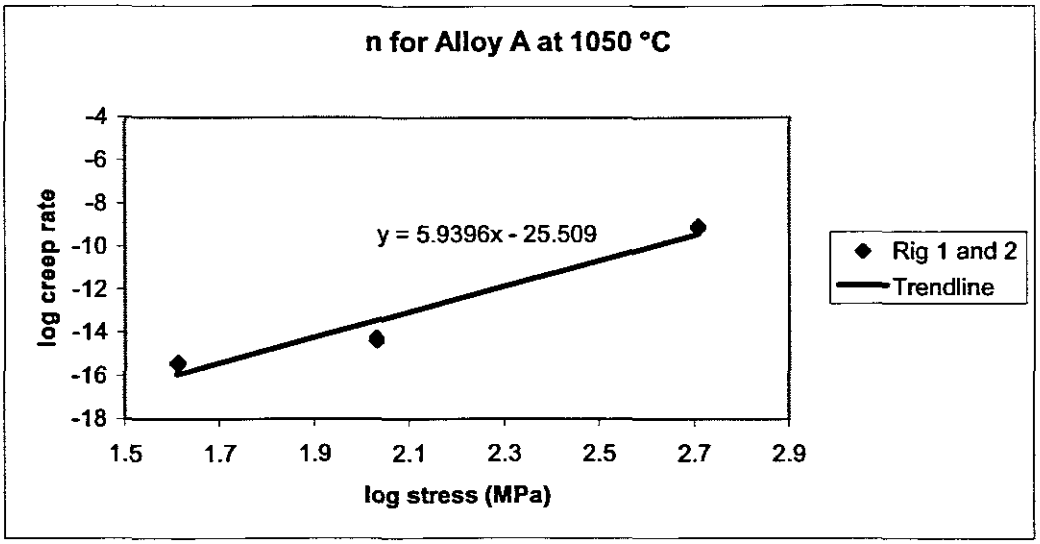

Figure 6.10: Stress exponent for Alloy A at 1050 °C

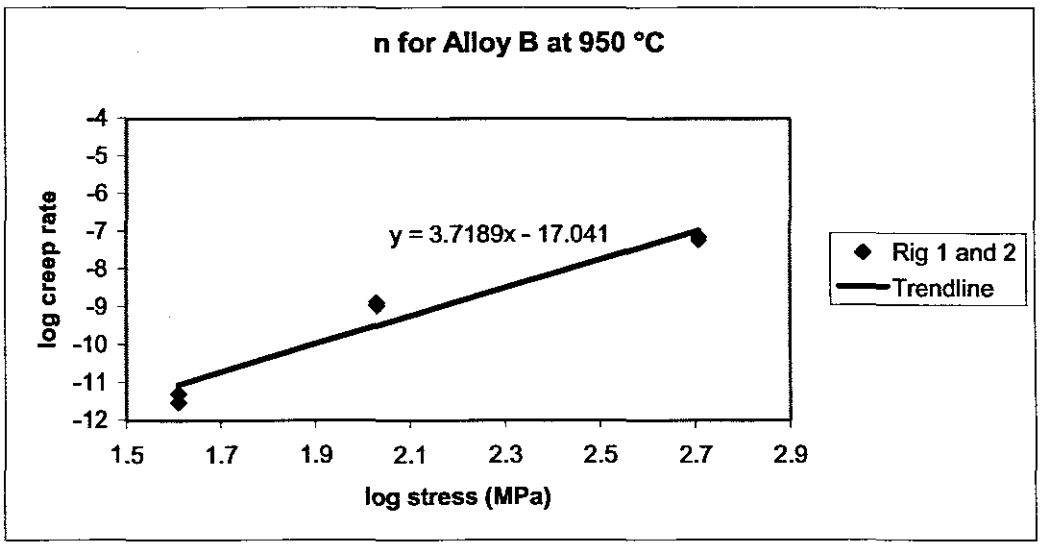

Figure 6.11: Stress exponent for Alloy B at 950 °C

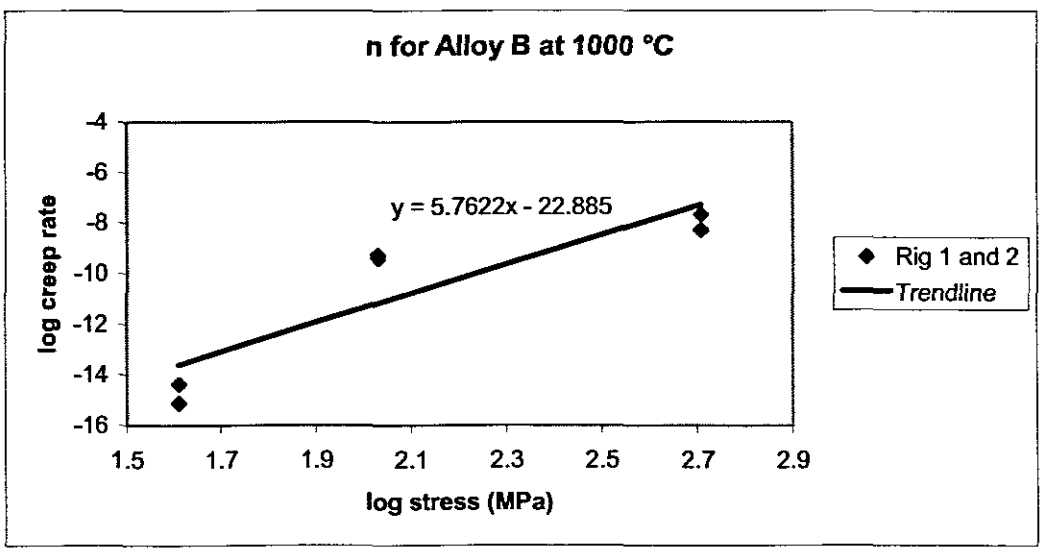

Figure 6.12: Stress exponent for Alloy B at 1000 °C

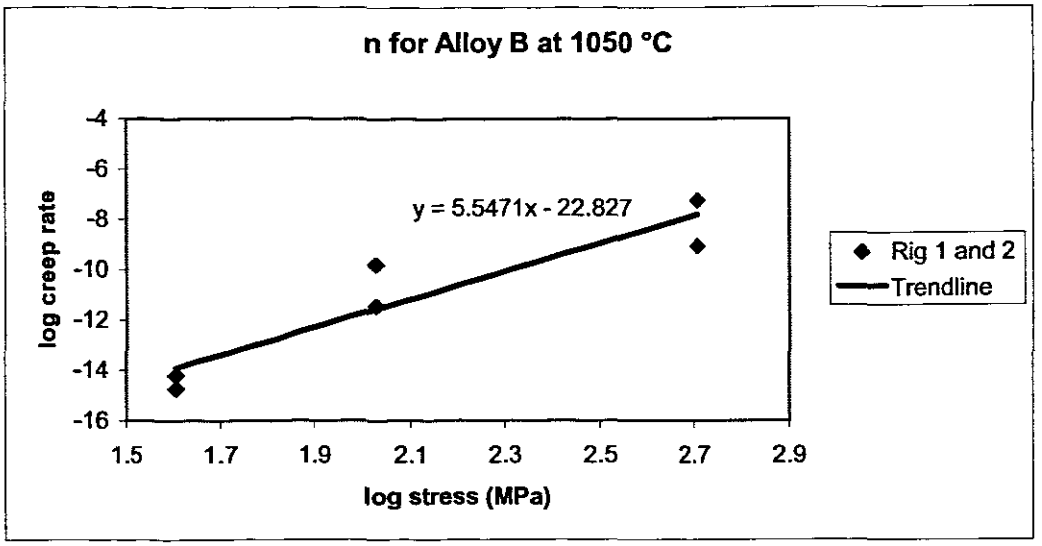

Figure 6.13: Stress exponent for Alloy B at 1050 °C

Table 6.1: Stress exponents of alloy A and B at varying annealing temperatures

Annealing temperature	Stress exponent, n Alloy A	Stress exponent, n Alloy B
950 °C	4.3	3.7
1000 °C	5.9	5.7
1050 °C	5.9	5.5

6.3 Comparison of alloy A versus alloy B

The following graphs aim to demonstrate the difference in displacement of the two alloys due to the various heat treatment temperatures. It is quite evident that alloy A is more creep resistant than alloy B under the chosen parameters. This is contrary to the literature that states that a higher Niobium content results in a more creep resistant alloy. Both alloys appear to become more creep resistant as the temperature of the prior heat treatment increases. Microscopy was done to further investigate this, which is discussed later on in the chapter.

For alloy B there is a noticeable increase in creep resistance between the three heat treatment temperatures. However, for alloy A between 950 °C and 1000 °C there is a fairly significant increase, but between 1000 °C and 1050 °C there is only a slight difference.

Take note that at a stress of 15 MPa the graph shows a displacement at 8 hours. This is due to the fact that under the higher loads the specimens failed way before they reached the 100 hour test mark.

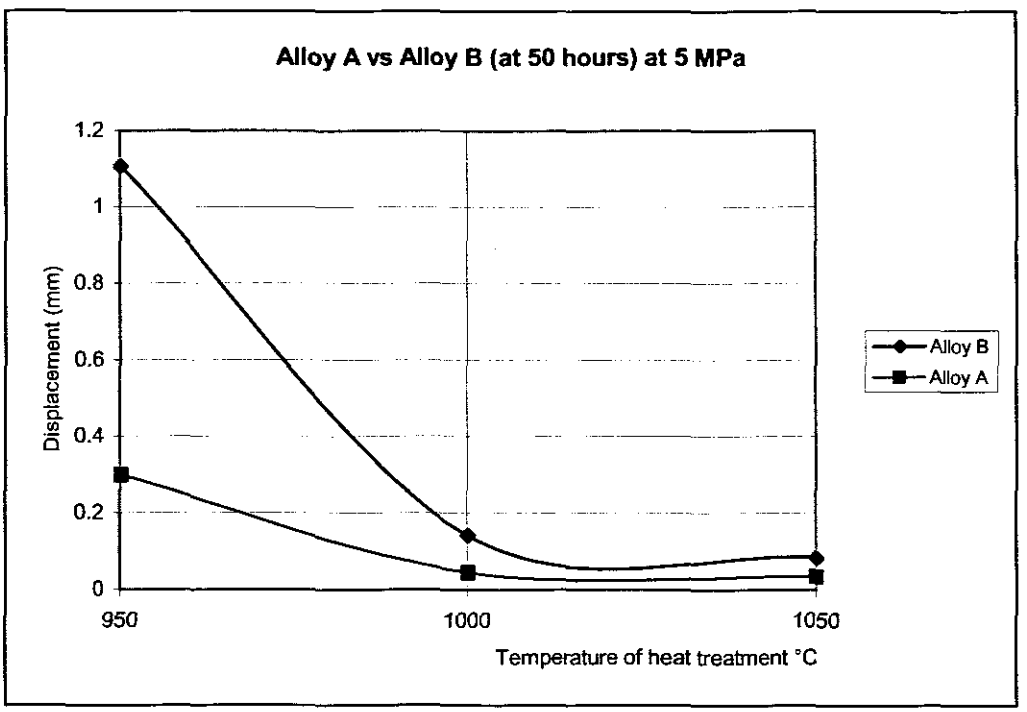

Figure 6.14: Comparison of alloy A and alloy B at 5 MPa

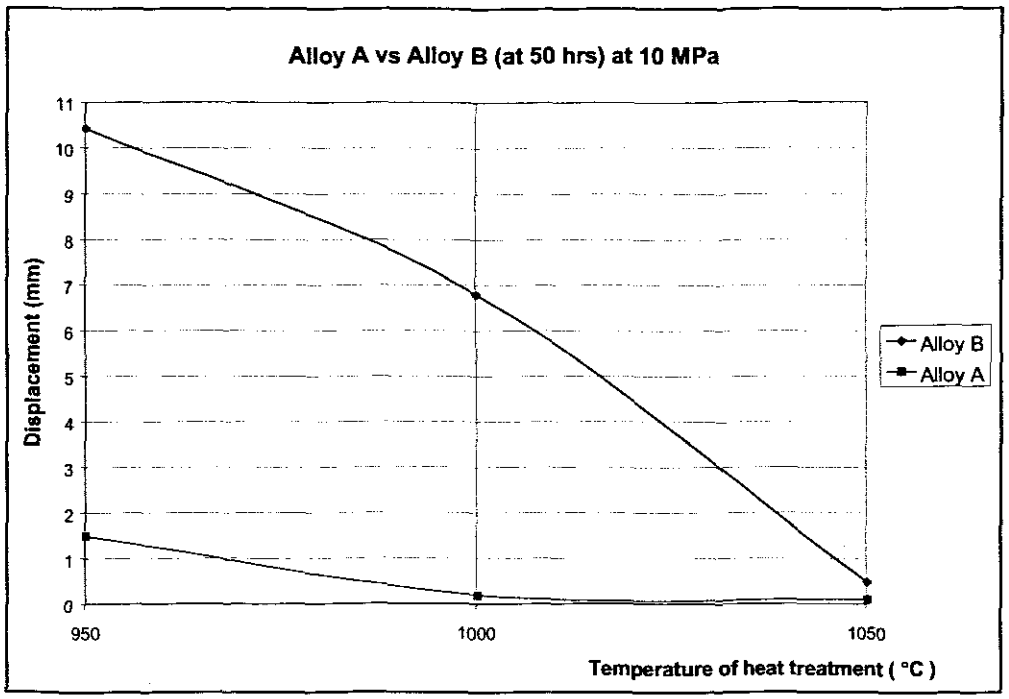

Figure 6.15: Comparison of alloy A and alloy B at 10 MPa

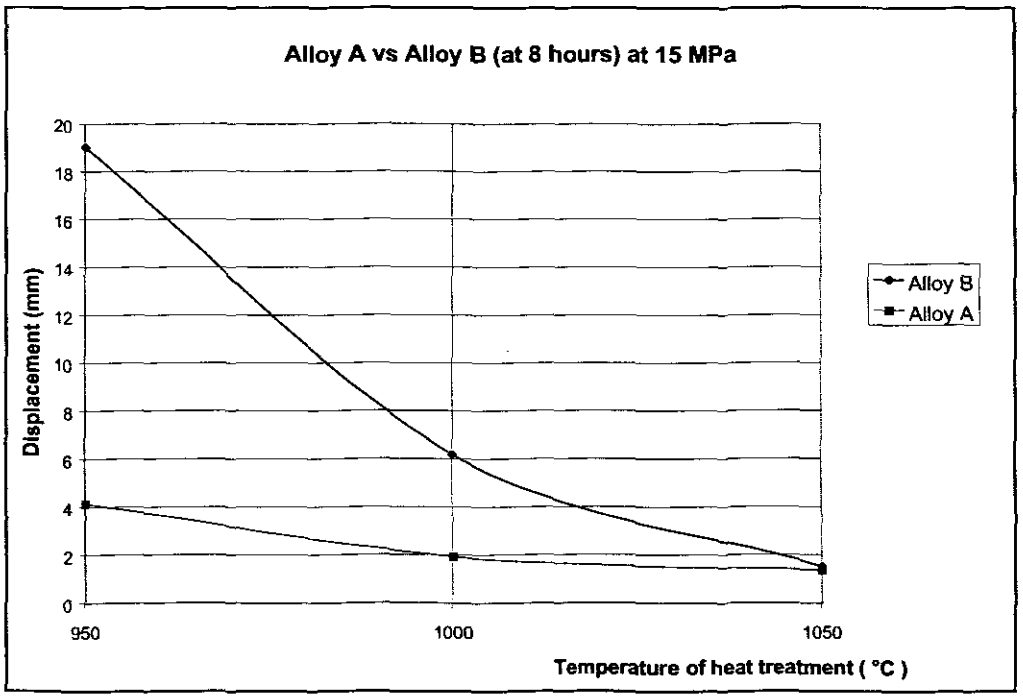

Figure 6.16: Comparison of alloy A and alloy B at 15 MPa

6.4 Microscopy

Microscopy was performed in order to monitor the various microstructures pertaining to each alloy in an effort to aid in describing the creep test results. This was done after heat treatment and again after creep testing. The main purpose for this was to observe how the grain size was effected at the various annealing temperatures.

6.4.1 Prior to creep testing

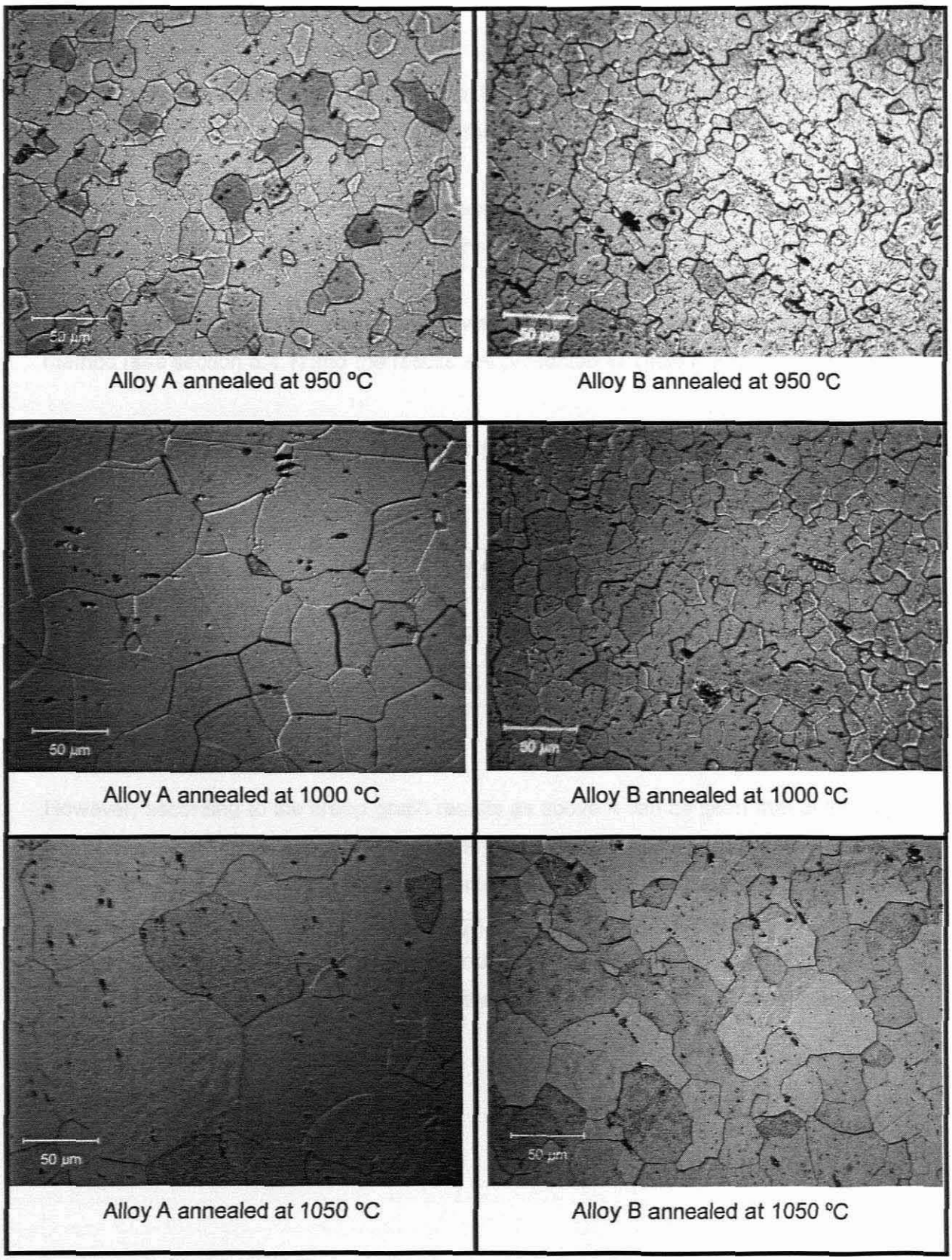

Figure 6.17: Micrographs of alloy A and B at various annealing temperatures, prior to creep testing (*micron marker = 50 µm*)

As can be seen quite clearly according to the above micrographs the dominant difference between the two alloys is the grain size. As the temperature of the heat treatment increased so did the size of the grain size. It is also interesting to note that alloy A has a considerably consistently larger grain size than alloy B. The grain size does have a strong influence on the creep properties of this material.

Other than the grain size difference there appears to be no other differences discernable from the micrographs. All of the micrographs show clearly visible precipitates.

The relevant grain size for each sample was obtained using the mean linear intercept method (see section 5.4.1) and the results are presented in Table 6.2.

Table 6.2: Average grain sizes of alloy A and B including standard deviations of specimens

Annealing temperature	**Average grain size**	
	Alloy A (μm)	**Alloy B (μm)**
950 °C	21 ± 2	18 ± 3
1000 °C	46 ± 5	22 ± 3
1050 °C	52 ± 9	29 ± 4

However, according to the creep graph results as above it can be seen that at the higher heat treatment temperature alloy A and alloy B appear to perform almost the same and both seem to exhibit excellent creep resistance. At this heat treatment the grain sizes are 52 μm and 29 μm respectively. So although the grain size is considerably larger for alloy A than B (almost double) and it has been indicated that the grain size strongly affects the creep resistance, here it could be argued that the Niobium content of alloy B is affecting its creep resistance.

6.4.2 Post creep testing (10 MPa):

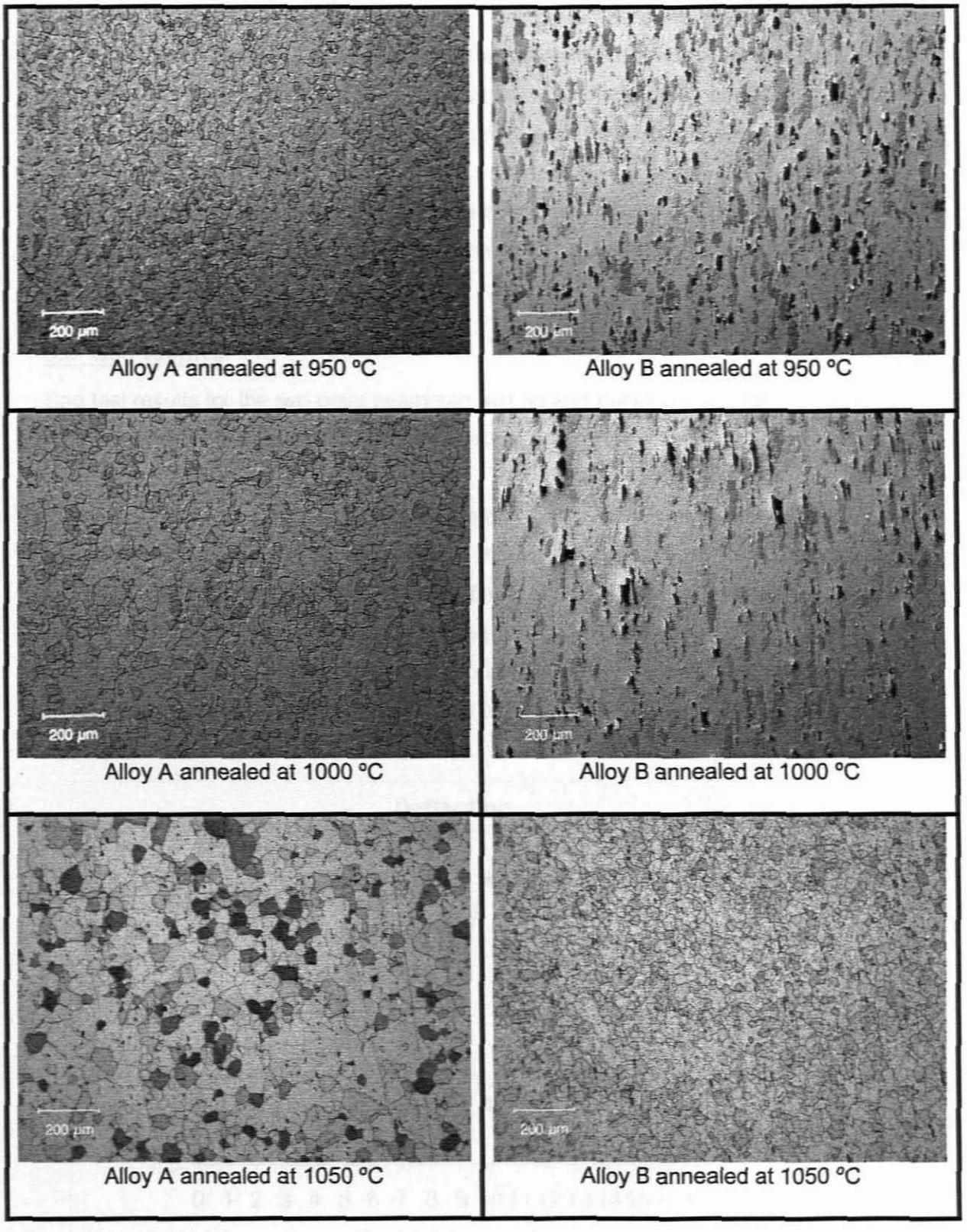

Figure 6.18: Micrographs of alloy A and B at various annealing temperatures post creep testing (micron marker = 200 µm)

All microstructures show images of the gauge length within the area of deformation.

The micrographs of alloy B at 950 °C and 1000 °C show two of the specimens that failed. These micrographs were taken within the necking region close to the fracture surface. The major feature of these micrographs is the existence of voids, which are parallel to the load direction. Creep deformation does create voids, which are generally quite easy to identify in ferritic stainless steels with clear grain boundaries[79].

There appears to be no grain elongation visible in the other micrographs. However, this can be explained by the fact that the percentage strain is fairly low.

6.5 Sag testing

Sag test results for the two-point beam sag test rig and cantilever sag test rig can be seen in figure 6.19. A more detailed version of results are in Appendix D.

Two batches of five specimens and two batches of four specimens were tested each for the cantilever and for the two-point beam method of sag testing. In some cases large discrepancies were noted within the same batch of test. This was especially noted on the results achieved by the two-point beam sag test rig. For the two-point beam method of sag testing average deflection was found to be 3.4 mm. Whilst for the cantilever method of sag testing average deflection was found to be 5 mm.

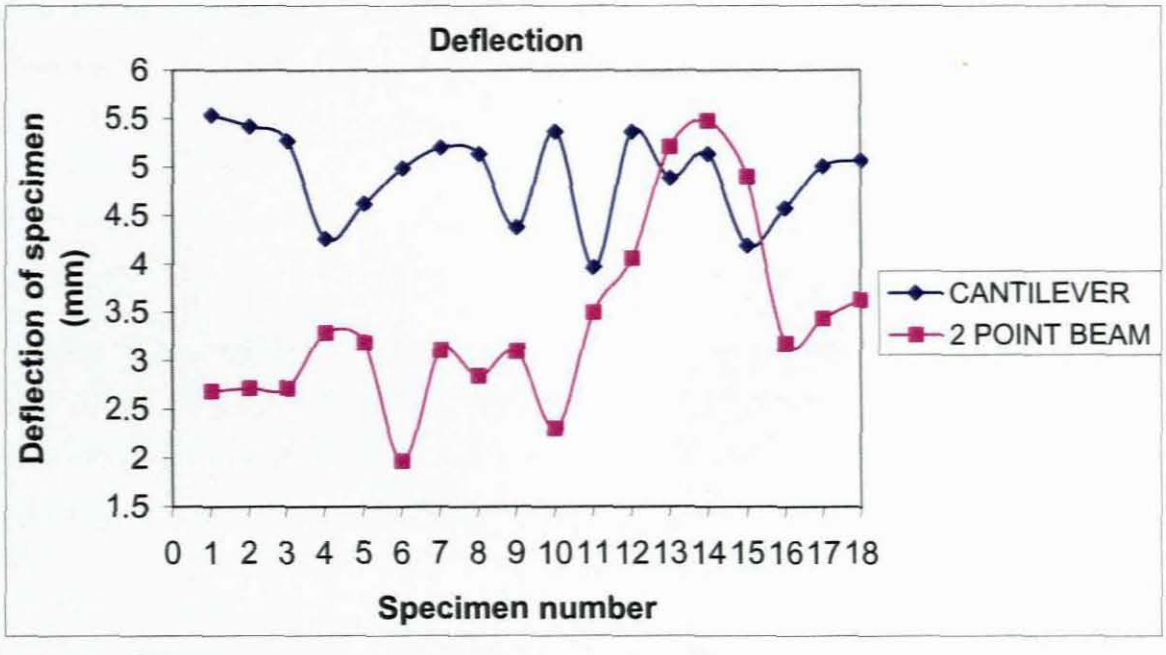

Figure 6.19: Comparison of sag test rig deflection results

From figure 6.19 it can be seen that the results of the cantilever sag test appear to be more consistent. The two-point beam method, however, particularly specimen numbers 12,13,14 and 15 appear to be out of sync with the other results. This could be related to a number of factors, which will be discussed in chapter 7. It does, on the other hand, appear from the above results that the cantilever sag test method produces more consistent and reproducible results.

CHAPTER 7

Discussion

7.1 Creep test data

7.1.1 Interpretations

After various modifications were performed to the creep test rigs, the rigs are now fully functional provided that the user follows careful guidelines during setting up and dismantling of tests.

As discussed in the literature it is possible to obtain stress exponent values from plots of log creep strain rate versus log time. These stress exponents can be used to help to identify the operative creep mechanism (although it is recommended this method be used in conjunction with another method, such as microstructural analysis). But, this stress exponent is related to steady state or secondary creep; it is therefore necessary to firstly identify this stage from results. This can often prove problematic especially at higher stresses where the specimen spends little time in this stage and enters the tertiary stage quite rapidly. This is evident in figures 6.3, 6.5 and 6.6.

It was also often difficult to fully understand the steady state region as all tests were scheduled to last up to 100 hours, unless the specimen fractured before the 100 hour test period expired. For the specimens that proved to be more creep resistant this presented a hindrance, as the creep curve appeared to be incomplete. Two tests, of alloy A at the higher annealing temperatures (1050 °C) were therefore run for a longer period of time (200 hours) in order to obtain a more pronounced creep curve (see figure 6.1). It could therefore be recommended that future tests on the more creep resistant specimens be *run for a period of at least 200 hours in order to account for this.*

It is quite clear from the creep test results that the creep resistance had a trend of increasing as the temperature of the heat treatment was increased. This could be partly due to the fact that excess Niobium is taken into solid solution during high temperature annealing (solid solution strengthening). This excess of Niobium precipitates as very fine particles of Laves phase (Fe_2Nb), which results in an increase in elevated temperature strength[80].

The heat treatment at the highest temperature of 1050 °C appeared to produce optimum results for high temperature creep resistance; this could be related to the formation of Laves phase. Future work could incorporate monitoring how the material performs at an even higher heat treatment temperature such as 1100 °C and 1150 °C. This would be

according to similar work done by Johnson[10], who experimented at heat treatments in the regime of 1040 °C-1150 °C at times of 60-300 seconds.

Although it can be said that Niobium in solid solution increases the high temperature strength of ferritic stainless steel, this may not be the fundamental strengthening mechanism in this situation. Previous research has indicated that although the high temperature strength increases with Niobium content, this is up to a Niobium threshold value[81]. This could account for the reason why alloy A appears to be more creep resistant than alloy B. This is of course beneficial to the producer of the material as less Niobium content needed to achieve the optimum creep resistance equates to a cost saving due to the expense of Niobium[22].

7.2 Microstructural analysis

7.2.1 Observations

Microstructural analysis was performed specifically to monitor the effect the varying temperatures of heat treatment had on the grain size of both alloys. This was done in order to determine how the grain size was affecting the materials creep resistance. As already discussed, an increase in Niobium content is beneficial for heightened creep resistance, as is an increase in average grain size. However, results in this case have proven that the alloy with the higher Niobium content has proved to be less creep resistant than the alloy with the larger grain size. It was therefore necessary to refer to grain size changes in order to explain this apparent difference in creep resistance.

With reference to figure 6.17 alloy B appeared to have very little change in grain size at the varying annealing temperatures, although this could be related to the fact that Niobium in solid solution retards recrystalisation, which would therefore hinder the amount of grain growth[82]. Niobium also has a large effect in decreasing grain size compared with other alloying elements such as Titanium[83], which could be related to the presence of undissolved NbC carbides. Alloy A, on the other hand, showed an increase in grain size as the temperature of the heat treatment was increased (this was especially evident between 950 °C and 1000 °C). This is also evident in the creep test results; the difference in the materials creep resistance for alloy A between 950 °C and 1000 °C is large, whereas the difference in creep resistance between 1000 °C and 1050 °C is rather small (relating to the fairly small difference in grain size increase from 1000 °C and 1050 °C).

It could, however, be argued that the creep comparisons of the two alloys at 1050 °C were actually quite similar. This could indicate that the ideal heat treatment for both alloys is in the vicinity of 1050 °C, although alloy A is still slightly more superior.

So from this we can conclude that for optimum creep resistance under these parameters (of annealing matrix and creep testing parameters) alloy A is superior to alloy B with regards to creep resistance and this can be explained by the alloy's resulting larger grain size, due to heat treatment, despite the high Niobium level in alloy B.

It is evident from the micrographs that there is some level of precipitation. Nevertheless, further research would be necessary in order to identify these precipitates.

7.3 Operative creep mechanisms

There are three possible mechanisms of creep that may occur at high temperatures and low stresses. These mechanisms are diffusion creep, Harper-Dorn creep and grain boundary sliding (dislocation creep)[51]. Dislocation creep processes are considered to be grain size independent whilst diffusion creep processes are grain size dependent[84]. This would lead the results to tend towards saying that diffusion creep is the operative creep mechanism. Yet, this does not correspond to the stress exponents relating to diffusion creep, which should be in the vicinity of unity. Although the high temperatures that the tests are performed at would indicate that diffusion is definitely playing a role in the deformation of the specimen, regardless of the operative creep mechanism.

It can also be reasonably assumed that the operative creep mechanism is not Harper-Dorn creep as this mechanism is grain size independent[85]. This makes for a strong argument against this mechanism being operative as this is clearly not the case with these results. Also Harper-Dorn creep is generally only found in high purity metals such as Aluminium at high temperatures near the melting point (about 650 °C) and low stresses (less than 0.1 MPa). The stress exponents that have been deduced for these creep experiments are in excess of one, whereas Harper-Dorn creep produces a stress exponent of one.

Grain boundary sliding could also be the operative mechanism. However, there is no evidence in the post creep micrographs of grain elongation (Lifshitz sliding). Nevertheless, this could merely be because the strain was just too small to show this. During dislocation creep Rachinger sliding could be operative, this is where the grains slide past one another with no grain elongation, which results in an increased number of grains along the tensile axis of the material. Although to identify this mechanism, more post creep micrographs would need to be studied. An important aspect of this mechanism is that grains retain their relative original shape[51].

In the high stress regime when the stress exponent is greater than 4, creep is known to occur by diffusion-controlled generation and movement of dislocations[84]. This would mean that dislocation processes would govern the creep properties.

Peterseim and Sauthoff in their research made a similar note. Their creep test results on a ferritic stainless steel with 20 % Cr and 0.61 % Nb found that there was a strong stress dependence of the creep rate, which indicates that the observed creep rate was controlled by dislocation creep[86].

As the resulting stress exponents yielded from the present creep experiments are in the vicinity of 4~6 it can be stated that dislocation creep is the predominant creep mechanism, with dislocation climb probably being the leading mechanism.

Owing to the fact that it is quite evident that the grain size has a large effect on the materials creep resistance, it is felt necessary that future work should incorporate growing the grain size of alloy B in order to match that of alloy A (in order to produce a uniform grain size across specimens). This will allow the alloys to be compared more directly and will also give a clearer understanding of the effect Niobium content has on the creep resistance.

On examining the stress exponents it appears that dislocation creep is present, although the grain size effect indicates that diffusion creep is present. Due to this discrepancy it is not possible to conclusively state what creep mechanism is operative.

7.4 Sag testing

Part of this project was to introduce a different method of sag testing to the one presently accepted by industry. To do this it was necessary to run tests using the two-point beam method sag test rig and using the same testing parameters run identical tests using the newly designed rig, the cantilever sag test rig.

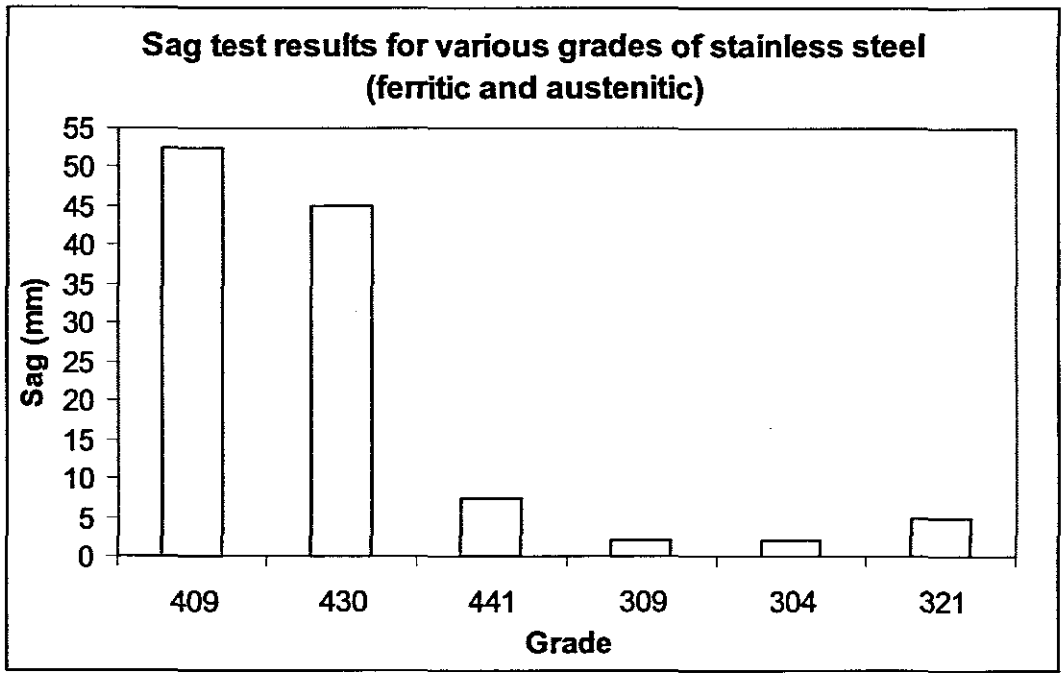

Figure 7.1: Sag test results of grades of stainless steel[81]

According to research done by Barteri[81] et al the average value of sag deflection obtained for 441 at a temperature of 900 °C over a period of 100 hours was 7.5 mm. However, there is no clear indication of the prior heat treatment of these specimens. Perhaps more comparable are the results achieved in recent research done by M Dollman[43] who obtained values of sag ranging from approximately 1.3 mm to 8.7 mm. The respective annealing temperatures of the specimens were 950°C, 1000°C and 1050°C. The deflection of specimens annealed at 1000°C was approximately 3.7 mm. However, Dollmans work also included the difference between alloy A and alloy B (as done in the case of this project, but for creep testing). The average deflection of alloy A over the annealing range ranged from 1.2 mm to 3.2 mm. On the other hand, for alloy B this changed to a range of 4.6 mm to 8.7 mm. This information, although not useful for the sag testing section of this project, does still confirm the creep test results that showed alloy A being superior in creep or sag resistance to alloy B. The values of sag obtained in this investigation (using the two-point beam method, as Dollman) where in the range of 3.4 mm. This would place this data within a similar range to that of Dollman.

7.4.1 Interpretations

The level of accuracy of data obtained was consistent for the cantilever sag test rig. However, paying attention to figure 6.19 for the two-point beam method, data was not consistent. This could be related to various factors such as friction between the specimen and the supports. This could then be worsened by the formation of oxide scale on both the specimen and ceramic rods on which the specimen is supported during the test and is allowed to slide on during its deflection or sag. The surface roughness of the ceramic rods was also checked for continuity, which could also relate to the haphazard results as these rods are taken off the rig after testing and may be arranged in a random manner for each consequent test.

By analysing the results it was hoped that a comparison of the two testing methods could be made, in order to identify the most accurate method. It was further anticipated that the results achieved by the cantilever sag test rig would prove to be more reproducible and therefore more reliable than those attained by the two-point beam sag test rig, owing to the possible friction problem.

From the calculations as seen in Appendix C a correcting factor of 3.33 was calculated for the deflection of the cantilever, meaning that the deflection on the cantilever specimens was expected to be 3.33 times that of the two-point beam. It must be stressed, however, that the calculations implemented are based on normal bending theory of beams with the applicable restrictions.

The deflections of the specimens tested on the cantilever sag test rig did not correspond with the correction factor. This correction factor was therefore found to be invalid.

A direct link between the results of the benchmark testing method and the cantilever testing method cannot be deduced. It can be stated though, that the cantilever sag test rig produced more consistent results as already discussed, indicating that reproducibility would be better. This could be due to the fact that friction between the rig and the specimen as it is sagging is eliminated in this method of testing.

7.4.2 Statistical analysis

The difference between the results of the two-point beam and the cantilever sag test rig is, however significant.

7.4.2.1 Two-point Beam

A descriptive statistical analysis was run on the results to develop an understanding of the distribution of the data achieved. Deflection ranges of the specimens are presented on the x-axis of the histogram while the y-axis indicates the amount of specimens falling into the ranges depicted by the x-axis. The standard deviation of the results was found and a histogram was established. With the aid of the histogram the normal distribution of the data is shown, which is seen as a red bell shaped curve in this case. A distribution of data along the bell shaped line would indicate consistent data. The blue fields on the histogram point out the actual data achieved through testing.

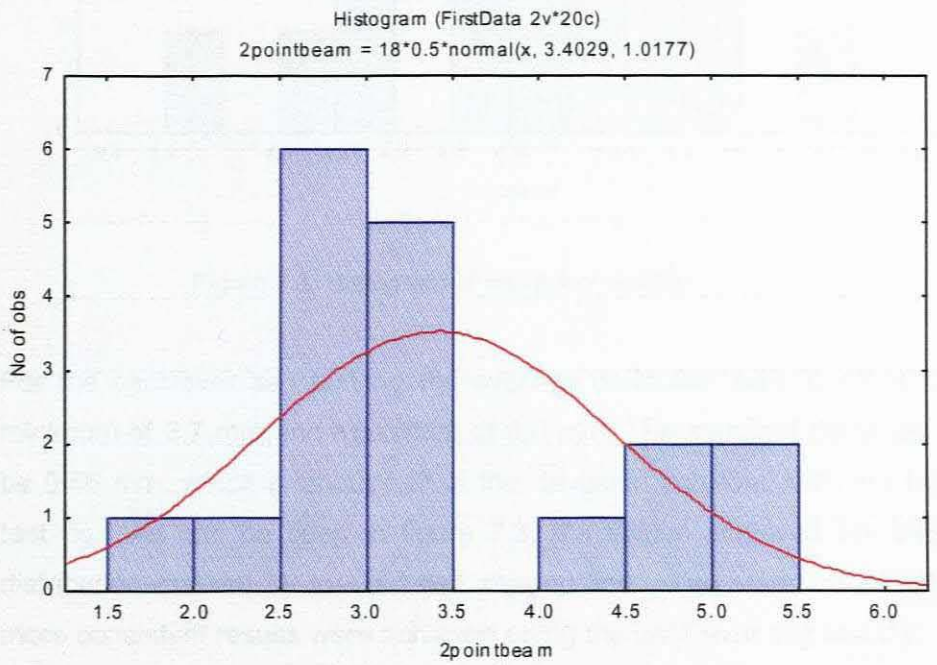

Figure 7.2: Histogram of two-point beam results

For the two-point beam sag test rig the average deflection was found to be 3.4 mm, the minimum 2.0 mm and the maximum 5.5 mm. The standard deviation was calculated to be 1.0 mm. The data is wide spread and does not follow the normal distribution line very accurately.

7.4.2.2 Cantilever

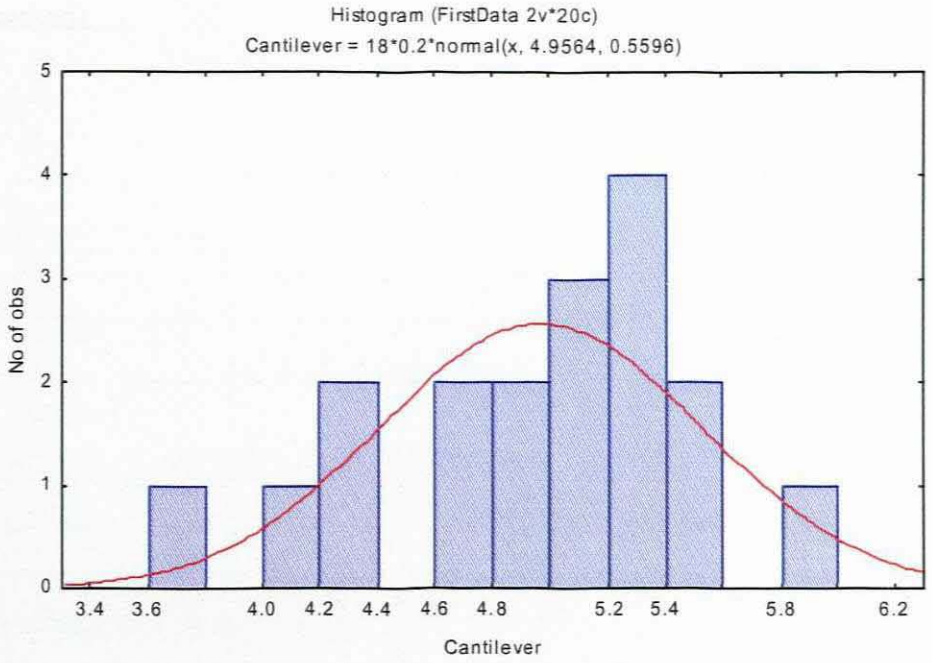

Figure 7.3: Histogram of cantilever results

For the cantilever sag test rig the average deflection was found to be 5.0 mm with a minimum of 3.7 mm and maximum of 6.0 mm. The standard deviation was calculated to be 0.56 mm, which is about half of the deviation achieved with the two-point beam sag test rig. As can be seen in figure 7.3, the values achieved are closer to the normal distribution marked by the red bell shaped line. The standard deviation indicates that more consistent results were achieved using the cantilever sag test rig.

7.4.3 Analysis of ceramic rods

In order to obtain a fair understanding of the fluctuating results that were achieved by the two-point beam method, it was attempted to measure the surface roughness of the ceramic rods. It was deduced that the surface roughness of the tubes could be related to the friction co-efficient between the specimens and the ceramic rods and therefore a noticeable variation in friction values would be observed.

Surface roughness was measured at three positions along the length of the ceramic rods, while four equally spaced readings were taken around the circumference. This was done using a Taylor-Hobson Surtronic 3P profilometer.

Results of the surface roughness for both rods 1 and 2 were found to be almost the same. It was therefore concluded that the roughness of the rods had no impact on the fluctuating

results of displacement that were obtained during sag testing (using the two-point beam method).

CHAPTER 8

Conclusions

8.1 Constant load creep test rigs

Two constant load creep test rigs were fully commissioned for use as a testing facility for constant load creep testing of stainless steel 441.

Initially the rigs were not suitable for the testing procedure and various modifications were necessary. The rigs are now able to log load and extension as a function of time, whilst also logging the temperature of the specimen itself. All of these readings can be monitored throughout the test.

Due to the difficulty involved in the setting up of creep tests and the nature of the tests themselves it is strongly recommended that users carefully follow the guidelines for creep test set up and end procedures (Appendix F and G). Users should also refer to the calibration procedures for the sensors (Appendix E).

8.2 Salt bath furnace

It was necessary that a high temperature salt bath furnace be acquired, as it was crucial that heat treatments be undertaken in a controlled environment. This furnace was designed, manufactured and is now commissioned to heat treat steels in the temperature range of 750 °C to 1050 °C.

8.3 Heat treatment

The annealing parameters chosen (as per previous research) were used as a measure to determine the effect that annealing time and temperature had on the creep resistance of the material. It was deduced that the higher the temperature of the heat treatment (to the highest level reached within the parameters of this project) the more creep resistant the material became. It was necessary to determine therefore whether it was the amount of Niobium in solution (dislocation creep) that was affecting this factor or the grain size (diffusion creep).

8.4 Creep test results

Creep curves of log of creep strain rate versus log of stress were produced for the two alloys at various annealing temperatures, with the specimen under various loads. From observing the steady state stage of these creep curves it was possible to deduce stress exponents which could aid in the identification of the mechanism of creep that is operative during service operation of a catalytic converter housing.

Once stress exponents were identified microscopy was used to further aid in the identification of the operative creep mechanism.

Although stress exponents have been identified, it is not felt that one can conclusively say what type of creep mechanism is in fact active. More creep testing and post creep microscopy is felt to be necessary to be more conclusive in this matter. As the resulting stress exponents yielded from the creep experiments are in the vicinity of 4~6 it does appear that dislocation creep is the predominant creep mechanism, with dislocation climb seeming to be the leading mechanism.

It was found that alloy A showed superior creep resistance to alloy B. Although this was contradictory to the literature, which states that, the higher Niobium content results in a higher creep resistance. On the other hand, Alloy B has the higher Niobium content, although alloy A has on average a larger grain size than that of alloy B. It could therefore be assumed that the mechanism of creep leans towards that of diffusion creep, as diffusion would be related to the grain size. Dislocation creep would be affected by the amount of Niobium in solution, which would therefore indicate that alloy B would be the superior alloy with regards to creep resistance. This research has shown that the effect of Niobium in solution appears to be inferior to the effect that grain size has on creep resistance in relation to these two alloys. In closing the effect of the grain size overcame the effect of the Niobium content.

In concluding it can be said that alloy A is superior to alloy B with regards creep resistance over the annealing range. Alloy A exhibited the highest level of creep resistance at an annealing temperature of 1050 °C (for a 200 second period).

8.5 Sag testing

A new form of sag testing was investigated in order to improve on the industry accepted method of sag testing, namely the two-point beam method. Tests were run using the two-point beam sag test rig and the newly designed and manufactured cantilever sag test rig. Results were compared and an attempt was made to correlate the two. A direct link between the results of the benchmark testing and the cantilever method could not be deduced. However, it can be stated that the cantilever test rig produced more consistent results as already discussed, indicating that reproducibility using this method would be greater than that of the two-point beam method.

In concluding it can be stated that according to data produced from the two methods of sag testing, the cantilever sag test rig would be an improved alternative method to the two-point beam method. The results produced via this method are repeatable whereas for the two-point beam method they were not. It is believed that by making use of the cantilever method that the problem due to friction has been eliminated, rendering more accurate results.

CHAPTER 9

Recommendations

9.1 Constant Load Creep test rigs

9.1.1 Circulating pump for cooling coil

The present cooling system has proved adequate, but there are large masses of water wastage. It is deemed necessary to introduce a system whereby the water could be recirculated, although the water would have to be kept cool, so as to keep the effect of the cooling system.

9.1.2 Furnaces

The inside of the furnace where the specimen and extensometer system is housed has very little tolerance between the extensometer system and the inside of the furnace. Problems have incurred when the furnace is moved over the specimen and the extensometer systems hits up against the brittle ceramic interior of the furnace. This problem is especially evident when one of the temperature monitoring thermocouples of the furnace dislodges from its position within the furnace wall. The thermocouple stands proud of the furnace and the extensometer train hits up against it. This is a major problem especially when tests are running at low loads, as the entire train can rest up against the thermocouple preventing the extensometer from moving and so influencing the displacement result of the specimen.

Due to the effort required in moving the furnaces up and down a recommendation can be made whereby pneumatics could be introduced to assist with this process.

If the furnaces were to ever be replaced it would be recommend that the furnace be split in half and then open up sideways, this could eliminate the problem that is encountered with the weight of the furnaces. Also it could ease the problem of specimen monitoring thermocouple attachment, which has proved in itself to be a difficult process. With the change of the furnace arrangement there could be a stationary mounting that has the thermocouples already in the correct place (for a particular length of guage length of specimen). This would alleviate the problem of the specimen monitoring thermocouples becoming loose from their positions during testing.

9.2 Creep testing

9.2.1 Creep tests

Creep tests could be run for longer periods of time; as often the test is stopped (at 100 hours) just as the steady state creep stage is being approached. A longer test period would aid in easier classification of this steady state stage.

9.2.2 Identifying the stress exponent, n

It is necessary that more microscopy be done post creep testing. This could help in aiding the identification of the creep mechanism during creep.

9.3 Identification of precipitates

It can be recommended that an analysis of the precipitates be performed, as in accordance with the literature NbC caribides and Laves phase should be present in some amounts. This would also indicate the effect these precipitates have, if any, on the creep strength of the material.

9.4 Sag testing

9.4.1 Sag test rigs

Presently the cantilever sag test rig is constructed from 10 mm 316 stainless steel plate, due to the thickness of material the rig is particularly heavy and is not very practical for lifting, especially considering the rig is placed inside of the furnace when it is at temperature. It would therefore be recommended that future cantilever sag test rigs be manufactured using a thinner plate, perhaps 8 mm plate.

9.5 Material

Alloy A has proved to be superior to alloy B with regards to creep resistance. This variance appears to be associated to grain size; it is therefore recommended that the grain size of alloy B could be grown to match that of alloy A (at an optimum heat treatment, possibly at 1050 °C). An investigation could be done by adjusting the annealing times of alloy B in order to increase its grain size to match that of alloy A. This would result in a uniform grain size across specimens. Further investigation would then reveal ultimately whether or not alloy A was in fact superior to alloy B with regards creep resistance. This process will, however, have to be carefully monitored so as to gauge the change in the amount of uncombined Niobium that would go into the solution of alloy B.

9.6 Heat treatment

Future work could incorporate monitoring how the material performs at an even higher heat treatment temperature such as 1100 °C and 1150 °C. This would be according to similar work done by Johnson[10]. Johnson claimed that the optimum heat treatment temperature to promote optimum creep resistance for ferritic stainless steel is 1040 °C, which appears to be related to a Laves phase formation.

1 Douthett, J.A. 1995. Automotive Engineering. Designing Stainless Exhaust Systems. *Automotive Engineering,* November.

2 Edsall, W. D. 1988. Stainless steel for automotive exhaust systems. *Chromium Review,* (9):1-4, December.

3 Hau, M., Garcia, C. I., Tither, G and DeArdo, A. J. 1996. Dual Stabilised Ferritic Stainless Steels for Demanding Applications such as Automotive Exhaust Systems. *Proceedings of ISS 38th Mechanical Working and Processing Conference,* Cleveland, Ohio, October: 453-457.

4 Davies, J. R (ed). 1994. Stainless Steels. ASM speciality handbook. Materials Park OH. ASM International.

5 Lagier, J., Rombeaux, P., Ragot, J and Vaugeois, P. 1993. Ferritic stainless steels in exhaust systems. *Innovation stainless steel.* Florence, Italy, 11-14 October: 159-164

6 Columbus Stainless Steel (PTY) Ltd. Technical data sheet, SX 441. September 2002.

7 Keown S. R and Pickering F. B. 1984. Niobium in stainless steels. *Niobium: Proceedings of the International* Symposium: 1113-1141.

8 Miyazaki, A., Gunzi, M and Yoshioka, K. 1994. High Formability R429EX and Heat-Resistant R444EX Stainless Steels for Automotive Exhaust Manifold. *Kawasaki Steel Technical Report.* No 31: 21-28, November.

9 Fujita, N., Ohmura, K., Kikuchi, M., Suzuki T., Funaki, S. and Hiroshige, I. 1996. Effect of Nb on high temperature properties for ferritic stainless steel. *Scripta Materialia,* 35 (6):705-710, March.

10 Johnson, J.N. 1981. An influence of Columbium on 870°C creep properties of 18% chromium ferritic stainless steels. *Proceedings of International Congress and Exposition, Society of Automotive Engineers, Inc.* Cobo Hall, Detroit, Michigan, 23-27 February 1981:810035.

11 Douthett, J.A. 1981. Oxidation Resistant 12 % Cr Automotive Stainless Steel. *Proceedings of International Congress and Exposition, Society of Automotive Engineers, Inc.* Cobo Hall, Detroit, Michigan, 23-27 February 1981:810036.

12 SASSDA (Southern Africa Stainless Steel development Association). Stainless Steel Buyers Guide 2004/2005.

13 Anon. 2001. History of Stainless Steel. Metal Strategies Technologies.

14 Colombier, L and Hochmann, J. 1967. Stainless and heat resisting steels. London. Edward Arnold (Publishers) Ltd.

15 Stainless Center:
http://www.stainlesscenter.com/data/history.htm. (24 June 2002)

16 Sedriks, A. J. 1979. Corrosion of stainless steels. New York. Wiley.

17 Wikipedia
http://en.wikipedia.org/wiki/Niobium. (30 January 2003)

18 Columbus Stainless

http://www.columbus.co.za/aboutus/aboutusmain.htm. (24 June 2002)

19 AK steel product data bulletin. 2000. 441 Stainless Steel.

20 Fujita. T. 1986. Advanced High-Chromium Ferritic Steels for High temperatures. *Metal Progress*: 33-40.

21 Nirosta and Thermax data sheet: Stainless Steels for automobile exhaust systems. 2002.

22 Barteri, M, Mecozzi, M. G, Fortunati, S. 1999. Low cost weldable ferritic stainless steel for hot end of automotive exhaust gas systems. *Proceedings of the 1999 conference, Stainless Steel: Science and Market*, Sardinia, Italy, 6-9 June 1999: 75-84.

23 Hill, J.B. 1993. Meeting North American demands for stainless steel exhaust systems. *Steel Times International*: 35-38, July.

24 Otto, C. Arwin Meritor. Correspondence via e-mail. 4 September2002.

25 University of York
http://www.uyseg.org/catalysis/catalytic/ccat1.htm. (24 September 2002)

26 Gosling, M. 2002. Plan for cleaner fuel hailed as boost for health, environment. Cape Times: 14 November.

27 How Stuff Works
http://www.howstuffworks.com/catalytic-converter.htm. (13 July 2002)

28 Murray and Roberts
http://www.murrob.com. (24 September 2002)

29 DieselNet
http://www.dieselnet.com/news/9906corning.html. (24 September 2002)

30 Chandler, H. 1998. Metallurgy for the non-metallurgist. Ohio. Materials Park.

31 Nabarro, F. R. N and de Villiers, H. L. 1995. The physics of creep. London. Taylor and Francis Ltd.

32 Tanaka, H., Murata, M., Abe, F and Irie, H. 2001. Microstructural evolution and change in hardness in type 304 H stainless steel during long-term creep. *Materials Science and Engineering*. A319-321: 788-791, 2001.

33 Honeycombe, R. W. K. 1984. The plastic deformation of metals 2nd ed. London. Edward Arnold Publishers Ltd.

34 Dowling, N. E. 1999. Mechanical behaviour of materials 2nd ed. New Jersey. Prentice Hall international.

35 Poirier, J. P. 1985. Creep of crystals. New York. Cambridge University Press.

36 Drotsky, J. G. 1995. Strength of Materials for Technicians. Johannesburg. Butterworth Publishers (Pty) Ltd.

37 Rhoads, J. L. Basic Explanation of creep processes. Dept of Nuclear Engineering university of California Berkeley . NE report NE 161.

38 Baillie, C, and Vanasupa, L. 2003. Navigating the materials world. London. Academic Press.

39 University of Arkansas
http://www.Uark.edu/~pjansma/structure_ppt/3. (29 February 2004)

40 University of Cambridge
http://www.poco.phy.cam.ac.uk/teaching/A_Donald. (29 February 2004)

41 Christian-Albrechts University
http://www.tf.uni-kiel.de/matwis/amat/def_en/kap_5/backbone/r5_3_1.html. (3 January 2003)

42 Stouffer, D. C and Dame L. T. 1996. Inelastic Deformation of metals: models, mechanical properties and metallurgy. Canada. John Wiley and sons.

43 Dollman, M. 2003. The Influence of microstructure on the creep properties of 441 ferritic stainless steel. Unpublished MSc dissertation, University of Cape Town, Cape Town.

44 Evans R. W and Wilshire, B. 1993. Introduction to creep. London. The institute of materials.1993.

45 United States naval Academy
http://web.usna.navy.mil/~schubbe/EM214%20(CH%206%20(creep))%20web_files/v3_document.htm (31 October 2002)

46 Cadek, J. 1988. Creep in Metallic Materials. New York. Elsevier.

47 Nabarro, F. R. N. 2002. Creep at very low rates. *Metallurgical and Materials transactions*,33 A: 213-218, February.

48 Rensselaer Polytechnic Institute
http://www.rpi.edu/~nosedc/nano/page7.html. Visited on 22/03/2003

49 Coble, R. L. 1963. A model for boundary diffusion controlled creep in polycrystalline materials. *Journal of Applied Physics*, 34 (6): 1679-1682, June.

50 Langdon, T G. 2000. Identifying creep mechanisms at low stresses. *Materials Science and Engineering* A 283: 266-273.

51 Harper J and Dorn J. E. 1957. Viscous creep of Aluminium near its melting temperature. *Acta Metallurgica*, 5: 654-660, November.

52 Nabarro, F. R. N. The mechanism of Harper-Dorn Creep. 1989. *Acta Metallurgica*, 37 (8): 2217-2222, 1989.

53 Nabarro, F. R. N. 2000. Harper-Dorn creep - A legend attenuated. *Phys Stat Sol.* (a)182, 627-629, September.

54 Zhang, W. J and Deevi, S. C. 2002. The controlling creep processes in TiAl alloys at low and high stresses. *Intermetallics,* 10: 603-611.

55 Groisbock, F. 1992. Creep behaviour of a heat resistant ferritic Chromium steels in terms of stress exponents. *Journal of materials science*, 27: 4373-4380.

56 Ruano, O. A, Sherby, O. D, Wadsworth, J and Wolfenstine, J. 1998. Diffusional creep and diffusion-controlled dislocation creep and their relation to denuded zones in Mg-ZrH_2 materials. *Scripta Materialia,* 38 (8):1307-1314, 1998.

57 Evans R. W and Wilshire, B. 1985. Creep of metals and alloys. London. The Institute of metals.

58 Kurtz, R. J., Ermi, A. M and Matsui, H. 2001. An update on biaxial thermal creep of Vanadium alloys. *Fusion Materials Semiannual Progress Report,*: 7, December.

59 Ajaja, O. 1986. A dislocation network model of recovery-controlled creep. *Journal of Materials Science,* 21: 3351-3356.

60 Langdon, T. G. 2002. Creep at low stresses: An evaluation of diffusion creep and Harper-Dorn creep as viable creep mechanisms. *Metallurgical and materials transactions*, 33A: 249-259, February.

61 Ruano, O. A., Sherby, O. D., Wadsworth, J and Wolfenstine, J. 1996. Rebuttal to "In defense of diffusional creep". *Materials Science and Engineering.* A211: 66-71, 1996.

62 Wilshire, B. 2002. Observations, Theories and Predications of High - Temperature Creep Behaviour. *Metallurgical and Materials Transactions*, 33A: 241-247, February.

63 Blum, W and Maier, W. Harper-Dorn creep - A Myth. *Phys Stat. Sol.* (a) 171: 467-474, October 1998.

64 Bhandarkar, M. D., Shanthidas Bhat, M., Zackay, V. F and Parker, E. R. 1975. Structure and elevated temperature properties of carbon-free ferritic alloys strengthened by a Laves phase. *Metallurgical Transactions,* 6A: 1281-1289, June.

65 Keown, S. R and Pickering, F. B. 1992. Effect of Niobium caribide on the creep rupture properties of austenitic stainless steels. *The metals society.* London.

66 Fujita, N., Bhadeshia, H. K. D. H and Kikuchi, M. 2004. Precipitation sequence in Niobium-alloyed ferritic stainless steel. *Modeling and simulation in materials science and engineering*, 12: 273-284.

67 Murata, Y., Koyama, T., Morinaga, M., Miyazaki, T. 2002. Prediction of the Laves Phase Morphology in Fe-Cr-W-C Quaternary steels with the aid of system free energy concept. *The iron and steel institute*, 42 (12): 1423-1429, 2002.

68 Fujita, N., Ohmura, K and Yamamoto, A. 2003. Changes of microstructure and high temperature properties during high temperature service of Niobium added ferritic stainless steels. *Materials science and Engineering*, 351 (1-2): 272-281, 25 June.

69 Anon. 1996. Metal Testing. Colliers Encyclopaedia, CD-ROM, 02-28.

70 Pomeroy, C. D. 1978. Creep of engineering materials. London. Mechanical Engineering Publications.

71 Anon. 1984. Mechanical Testing. ASM Metals Handbook, 10th ed. Volume 8. Materials Park OH. ASM International.

72 ASTM E 139-00. 1990. Standard Practice for Conducting Creep, Creep Rupture and Stress Rupture Tests of Metallic Materials. American Society for Testing Materials.

73 Samuel, K. G., Mannan, S. L and Rodriguez, P. 1995. A substructure characterizing parameter in creep. *Journal of Materials Science,* 30: 1521-1528.

74 Haynes International
http://www.haynesintl.com (3 August 2002)

75 Houghton Durferrit. 1999. Durferrit A5/ GS 750. Safety Data Sheet (93/112/EEC).

76 Houghton Durferrit. 2000. Cyanide-free annealing baths. Technical information.

77 Muller, B. 2002. Evaluation of the creep properties in a dual stabilised ferritic stainless steel. Unpublished MSc dissertation, University of Cape Town, Cape Town.

78 ASTM E 112-88. 1988. Standard Test Methods for Determining Average grain size. American Society for Testing Materials.

79 Yalin, M., Bamberger, M and Rosen, A. 1995. Microstructural changes during creep of a high Chromium Steel. *Metallurgical and Materials Transactions,* 26A, February.

80 Allegheny Ludlam Technical Data blue sheet. 2002. 441 Stainless steel.

81 Barteri, M., Fazio, F and Fortunati. 1999. Stainless steels in car exhaust gas systems. *La Metallurgia Italiana,* 5: 31-36, May.

82 Lee, K. J. 1999. Recrystallisation and precipitation interaction in Nb-containing steels. *Scripta Materialia,* 40 (7): 837-843.

83 Fujiwara, M., Uchida, H and Ohta, S. 1995. Effect of Niobium content on creep strength of cold-worked 15Cr-15Ni-2.5Mo austenitic steel. *Journal of Materials Science Letters* 1: 297-301.

84 Wilshire, B and Palmer, C. J. 2002. Grain size effects during the creep of copper. *Scripta Materialia,* 46: 484-488.

85 Kloc, L and Fiala, J. 1999. On creep behaviour of several metallic materials at low stresses and elevated temperatures. *Chem. Papers.* 53 (3): 155-164.

86 Peterseim, J and Sauthoff, G. 1986. The effect of fine precipitate particles on the creep behaviour of ferritic model steels - Part 2 - Analysis of creep results. *Steel Research 57.* Number 1: 19-23, 1986.

Appendix A

Table 1:Load check

RIG 1

Mass	Reading (on box)	Box should read	Accuracy
0.477kg	4.4/4.5kg	4.477kg	98.28%
0.760kg	4.7/4.8kg	4.769kg	98.55%
1.055kg	4.9/5kg	5.055kg	96.93%
2.583kg	6.4kg	6.583kg	97.22%
4.939kg	8.5/8.6kg	8.939kg	95.09%
5.708kg	9/9.1kg	9.708kg	92.71%
7.522kg	10.4/10.5kg	11.522kg	90.26%
9.588kg	12.6/12.7kg	13.588kg	92.73%
12.058kg	14.3/14.4kg	16.058kg	89.05%

Zero point at 4kg
Lever arm resting firmly against frame,
Counter weight brought forward
Weight hung directly from pull rod

RIG 2

Mass	Reading (on box)	Box should read	Accuracy
0.477kg	0.5kg	0.477kg	95.40%
0.760kg	0.8/0.9kg	0.760kg	95.00%
1.055kg	1.1kg	1.055kg	95.91%
2.583kg	2.5/2.6kg	2.583kg	96.79%
4.939kg	4.8kg	4.939kg	97.19%
5.708kg	5.5/5.6kg	5.708kg	96.36%
7.522kg	7.2/7.3kg	7.522kg	95.72%
9.588kg	9.2/9.3kg	9.588kg	95.95%
12.058kg	11.5/11.6kg	12.058kg	95.37%

Zero point at 0kg
Lever arm resting firmly against frame,
Counter weight brought forward
Weight hung directly from pull rod

RIG 1

Mass	Reading on box	Box should read	Lever ratio
0.796kg	9.3kg	9.4	= 0.769 X 3
		=(7.1+2.307)	2.307kg
	(-4)	5.4kg	
1.055kg	10.1/10.2kg	10.265kg	= 10.55 x 3
		=(7.1+3.165)	3.165kg
	(-4)	6.265kg	
2.47kg	13/13.1kg	14.51kg	= 2.407 x 3
		=(7.1+7.41)	7.41kg
	(-4)	10.51kg	
4.939kg	20.5/20.6kg	21.917kg	= 4.939 x 3
		=(7.1+14.817)	14.817kg
	(-4)	17.917kg	

Zero load with specimen in place
Box reading 7.1/7.2kg with 0kg in WP
=3.2kg (weight of pull rod etc + 4kg zero)
Lever in horizontal position
Pin touching brace

RIG 2

Mass	Reading on box	Box should read	Lever ratio
0.769kg	5.2/5.3kg	5.507kg	= 0.769 X 3
		=(3.2+2.307)	2.307kg
1.055kg	6kg	6.3kg	= 10.55 x 3
		=(3.2+3.165)	3.165kg
2.470kg	10.4kg	10.61kg	= 2.407 x 3
		=(3.2+7.41)	7.41kg
4.939kg	16.7/16.8kg	18.017kg	= 4.939 x 3
		=(3.2+14.817)	14.817kg

Zero load with specimen in place
Box reading 3.2/3.3kg with 0kg in WP
=3.2kg (weight of pull rod etc)
Pin touching brace

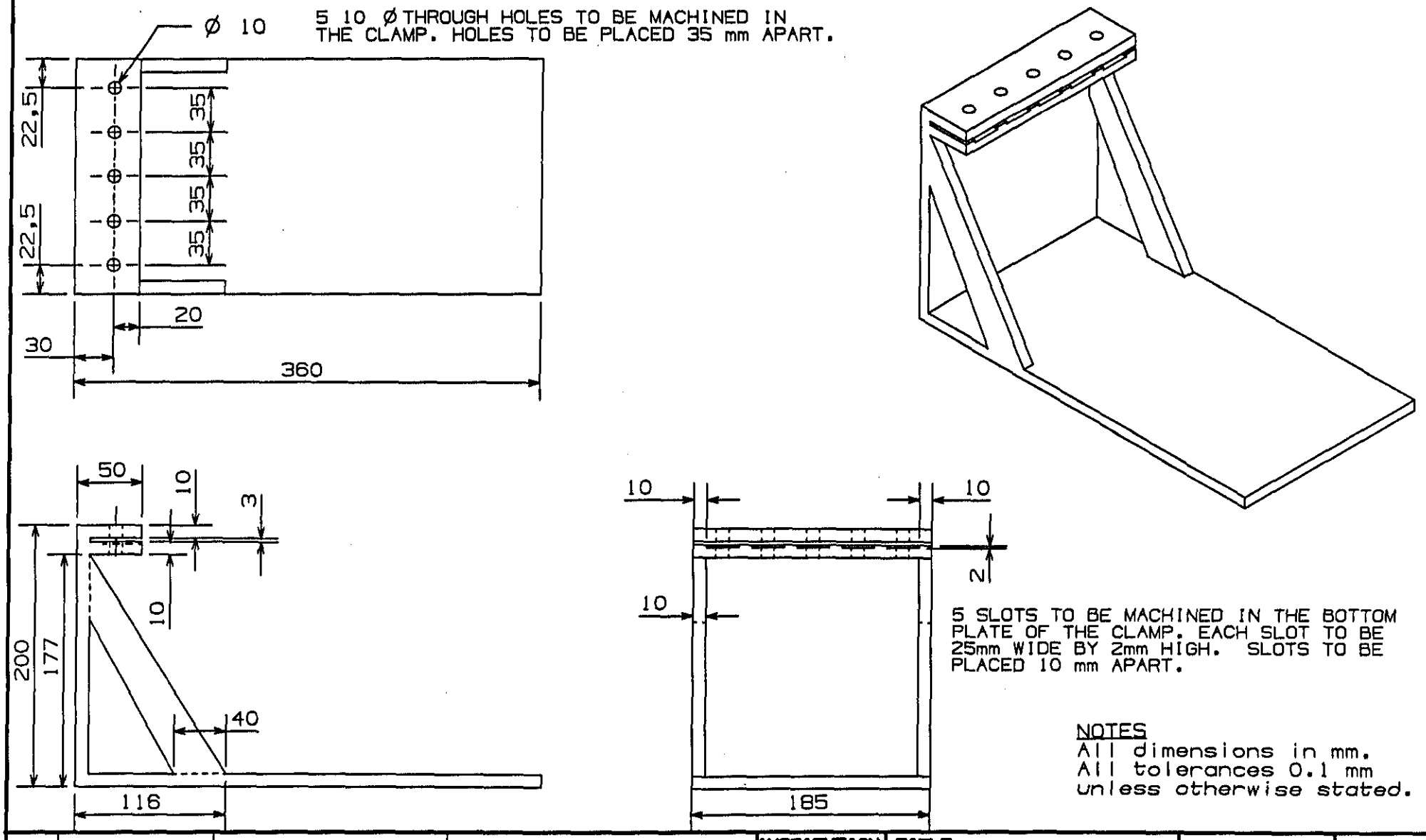

				INSTITUTION	TITLE SAG TEST RIG	REVISION 2	SCALE NTS
1		RIG	316 S/S 10 mm PLATE	DRAWN	DEPT	DRAWING No. CT001	DATE FEB 2003
ITEM	PART No.	MATERIAL	DESCRIPTION				

Appendix C

Sag testing Calculations

The industrial benchmark two-point beam test was taken as a reference. Strips of material used are 25.4 mm wide with a length of 304.8 mm. A 12.7 mm (1/2 inch) 90° locating bend is placed at one end. The span that deflects is therefore 290.6 mm. The maximum bending stress in the two-point beam can be calculated using bending theory. An equivalent length for the cantilever was calculated on the basis that the same bending stress should be reached in the cantilever and the two-point beam. The bending theory used in the calculations makes the following assumptions:

- The load to which the beam is subjected is applied gradually
- The beam is initially straight, although this is not necessarily true
- The deflection is small

The weight acting on the beams was taken to be a uniformly distributed load.

Two point beam:

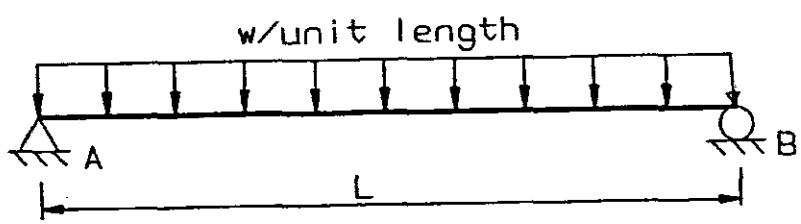

Maximum Bending Moment

$$BM_{max} = \frac{wl^2}{8}$$

where: w is the uniformly distributed load per meter

l is the length of the beam

Cantilever:

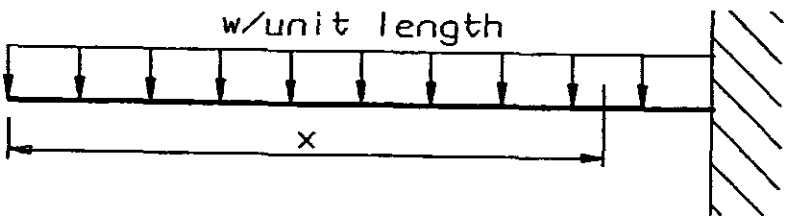

Maximum Bending Moment

$$BM_{max} = \frac{wl^2}{2}$$

where: w is the uniformly distributed load per meter

l is the length of the beam

The maximum bending stress can be calculated from the following formula:

$$\sigma = \frac{My}{I}$$

where: M is the maximum bending moment

y is the distance from the neutral axis

I is the second moment of area ($I = bd^3/12$)

For the same maximum bending stress in two-point beam and cantilever:

$$BM_{two-point\ beam} = BM_{cantilever}$$

$$\frac{wl^2}{8} = \frac{wl^2}{2}$$

Due to the fact that the material is the same in both cases,

$\therefore$ $W_{two\ pointbeam} = W_{cantilever}$

$\therefore$

$$\frac{l^2}{8} = \frac{l^2}{2}$$

where: $l_{two\ point\ beam}$ = 290.6 mm

$$\frac{290.6^2}{8} = \frac{l^2}{2}$$

$l = 145.3mm$ equivalent length for the cantilever resulting in same maximum bending moment as in two-point beam

Maximum deflection of the two point beam under own weight:

$$y = \frac{5wl^4}{384EI}$$

where: w is its own weight

l is the length over which the weight is acting

E is the modulus of elasticity (E = 200 GPa)

I is the second moment of area = $7.143 \times 10^{-12} m^4$

$$w = \rho \times vol \times g$$
$$= 7800 \times 0.2906 \times 0.0254 \times 0.0015 \times 9.81$$
$$= 0.8472kg$$

$$y = \frac{5 \times 0.8472 \times 0.2906^4}{384 \times 200 \times 10^6 \times 7.143 \times 10^{-12}}$$
$$y = 0.055mm$$

Maximum deflection of the cantilever under its own weight:

$$y = \frac{wl^4}{8EI}$$

where: w is its own weight

l is the length over which the weight is acting

E is the modulus of elasticity (E = 200 GPa)

I is the second moment of area = $7.143 \times 10^{-12} m^4$

$$w = \rho \times vol \times g$$
$$= 7800 \times 0.1453 \times 0.0254 \times 0.0015 \times 9.81$$
$$= 0.4236kg$$

$$y = \frac{0.4236 \times 0.1453^4}{8 \times 200 \times 10^6 \times 7.143 \times 10^{-12}}$$

$$y = 0.01652mm$$

correcting factor = $\frac{y_{twopo\,int\,beam}}{y_{cantilever}} = \frac{0.05506}{0.01652} = 3.33$

The bending stress is found to be:

$$\sigma = \frac{My}{I}$$

$$= \frac{0.0307x0.00075}{7.143x10^{-12}}$$

$$= 3.2234MPa$$

Appendix D

Two point beam sag test results

All specimens were annealed at 1000 °C for 200 seconds, excepting for the final three specimens on the table, which were in the cold rolled condition.

Table 1: Two point beam sag test rig results

Specimen	Test Start		Test End		Condition	Total Sag after Test
	Date	Time	Date	Time		mm
1	08-Jul	12:20	12-Jul	16:20	Annealed	2.69
2	08-Jul	12:20	12-Jul	16:20	Annealed	2.72
3	08-Jul	12:20	12-Jul	16:20	Annealed	2.72
4	08-Jul	12:20	12-Jul	16:20	Annealed	3.29
5	08-Jul	12:20	12-Jul	16:20	Annealed	3.19
						Average = 2.92 mm
1	15-Jul	13:00	19-Jul	17:00	Annealed	1.97
2	15-Jul	13:00	19-Jul	17:00	Annealed	3.11
3	15-Jul	13:00	19-Jul	17:00	Annealed	2.85
4	15-Jul	13:00	19-Jul	17:00	Annealed	3.10
5	15-Jul	13:00	19-Jul	17:00	Annealed	2.31
						Average = 2.67 mm
1	25-Sep	13:00	27-Sep	19:00	Annealed	3.50
2	25-Sep	13:00	27-Sep	19:00	Annealed	4.06
3	25-Sep	13:00	27-Sep	19:00	Annealed	5.21
4	25-Sep	13:00	27-Sep	19:00	Annealed	5.48
						Average = 4.56 mm
1	21-Oct	11:00	25-Oct	15:00	Annealed	4.90
2	21-Oct	11:00	25-Oct	15:00	Annealed	3.18
3	21-Oct	11:00	25-Oct	15:00	Annealed	3.44
4	21-Oct	11:00	25-Oct	15:00	Annealed	3.63
						Average = 3.79 mm
1	05-Oct	11:00	09-Oct	15:00	Cold-rolled	37.16
2	05-Oct	11:00	09-Oct	15:00	Cold-rolled	39.77
3	05-Oct	11:00	09-Oct	15:00	Cold-rolled	36.10
						Average = 37.68 mm

Cantilever sag test rig results

All specimens were annealed at 1000 °C for 200 seconds, excepting for the final three specimens on the table which were in the cold rolled condition.

Table 2: Cantilever sag test rig results

Specimen	Test Start		Test End		Condition	Total Sag after Test
	Date	Time	Date	Time		mm
1	27-Aug	11:00	31-Aug	15:00	Annealed	6.54
2	27-Aug	11:00	31-Aug	15:00	Annealed	5.42
3	27-Aug	11:00	31-Aug	15:00	Annealed	5.27
4	27-Aug	11:00	31-Aug	15:00	Annealed	4.26
5	27-Aug	11:00	31-Aug	15:00	Annealed	4.62
						Average = 5.22 mm
1	02-Sep	13:00	06-Sep	17:00	Annealed	4.99
2	02-Sep	13:00	06-Sep	17:00	Annealed	5.20
3	02-Sep	13:00	06-Sep	17:00	Annealed	5.94
4	02-Sep	13:00	06-Sep	17:00	Annealed	4.38
5	02-Sep	13:00	06-Sep	17:00	Annealed	5.37
						Average = 5.18 mm
1	09-Sep	11:15	13-Sep	15:15	Annealed	3.67
2	09-Sep	11:15	13-Sep	15:15	Annealed	5.37
3	09-Sep	11:15	13-Sep	15:15	Annealed	4.89
4	09-Sep	11:15	13-Sep	15:15	Annealed	5.14
						Average = 4.77 mm
1	16-Sep	10:45	20-Sep	14:45	Annealed	4.19
2	16-Sep	10:45	20-Sep	14:45	Annealed	4.58
3	16-Sep	10:45	20-Sep	14:45	Annealed	5.01
4	16-Sep	10:45	20-Sep	14:45	Annealed	5.07
						Average = 4.71 mm
1	21-Sep	11:00	25-Sep	15:00	Cold-rolled	43.2
2	21-Sep	11:00	25-Sep	15:00	Cold-rolled	44.4
3	21-Sep	11:00	25-Sep	15:00	Cold-rolled	40.3
						Average = 42.63 mm

Appendix E

Constant Load Creep test rig calibration procedure

Software

Running the software

From the desktop click on CreepRigNew to enter the data logging programme.

The minimum sample rate in the software for the creep rigs is 2 seconds, although several minute rates can also be accommodated.

The number of samples (edit box) sets the effective test duration.

The displacement values (LVDT values) are autozeroed automatically on the start of logging the data. This feature can be disabled by clicking the AZ checkboxes to the off state before running the test. Also Rig 1 and / or Rig 2 may be disabled by clicking the enable checkboxes to the off state before running.

The last configuration may be loaded by clicking the **"Load Config"** button. The current configuration may be saved by clicking on the **"Save Config"** button.

Before a test is performed, the measurement sensors must be calibrated. Each sensor should be calibrated.

Calibration:

It is firstly necessary to click on the **calibrate** button to enter the calibration page. The calibration for each sensor is done in the following manner:

Thermocouples

Click on the offset radio button and the TC row radio button. Calibrate the offset of the TC's by changing the **"Offset Value"** in the edit box of the software. Note that about 40μV equates to about 1°C for a type K thermocouple. Click on the **"Save"** button to save the calibrations to memory.

LVDT's

Calibrate the LVDT's by fixing the initial mounting position of the LVDT. Click on the **offset** column radio button and the LVDT row radio button. Then depress the spring (not right to the bottom). Using a Vernier measure the distance that the LVDT has been allowed to displace, note this measurement (a value of about 33 mm is sufficient). Make sure this displacement has been secured. This will then become the zero mm point. Then click on the **"Execute Current Chan Cal"** button. The offset value is automatically calculated. Note that the offset value may be manually entered by changing the **"Offset Value"** in the edit box of the software.

After offset calibration is performed, click on the **scale** column radio button. Allow the LVDT to displace, using a Vernier measure the distance that the LVDT has displaced (53 mm for this particular LVDT is acceptable). Enter 53 in the **"Scale Cal Val"** edit box of the calibration page Then click on the **"Execute Current Chan Cal"** button. The scale value is automatically calculated. Click on the **"Save"** button to save the calibrations to memory.

Load Cells:

Calibrate the load cells by removing all mass from the weight pan. Attach specimen into setup (technically there is now no load on the specimen) click on the **offset** radio button and the **Load Cell** row radio button (of the load cell which is to be calibrated). Make sure that the counterweight on the lever is brought forward enough to allow the lever to rest firmly against the frame. Click on the **"Execute Current Chan Cal"** button. The offset value is automatically calculated (which should be reading close to zero kg). Click on the **"Save"** button. Note that the offset value may be manually entered by changing the **"Offset Value"** in the edit box of the software.

After offset calibration is performed, click on the **scale** radio button. Attach a calibrated mass piece to the specimen (+-10 kg is acceptable). Enter the calibration mass value in the **"Scale Cal Val"** edit box. Then click on the **"Execute Current Chan Cal"** button. The scale value is automatically calculated. Click on the **"Save"** button to save the calibrations to memory.

Remember that the load cell is accurate up to 100 grams, this is why the load cell reading may vary slightly.

To exit the calibration page click on the **"EXIT"** button.

Appendix F

Constant Load Creep test rig set-up procedure

The basic procedure to follow in setting up a creep test using the rigs is as follows:

1. Ensure counter weight on lever is brought forward so as to bring the lever forward to touch the front end of the frame.
2. Insert sample into grips.
3. Ensure that the reading for the load cell is as close to zero as possible. If not satisfactory it may be necessary to recalibrate the load cell.
4. Attach extensometer clamps to sample gauge length. Ensure that clamps are secure to prevent slippage during testing.
5. Attach lower pull rod and pin.
6. Adjust the counter weight on the lever until the lever is horizontal. A spirit level should be used to be certain the lever is horizontal. Allow the load cell to stabilise.
7. Adjust screw jack such that the lower pull rods are hanging completely free from the lower pull rod assembly.
8. Adjust lever to horizontal position.
9. Add the plates for LVDT placement.
10. Attach LVDT.
11. Attach monitoring thermocouples onto the specimen; one as close to the top of the gauge length as possible and one as close to the bottom of the gauge length as possible. Ensure that the thermocouples are securely attached to lower pull rod.
12. Adjust lever to horizontal.
13. Gently lower the furnace over the sample making sure that nothing clashes with the brittle furnace tube.
14. Check that the load train is hanging completely free from the furnace and other components.
15. Insert ceramic brick inserts into the top open end of the furnace.
16. Turn on tap for cooling water (for load cells, max operating temperature for load cells is 60 °C).
17. Switch on furnace and set all three zones of the furnace to the desired testing temperature.

18. When the set temperature has been reached on the furnace temperature controllers, check that the temperature distribution shown by the monitoring thermocouples is within acceptable limits. Allow the furnaces to settle at the desired temperature for +- one hour.
19. Using the screw jack, slowly adjust the lower pull rod assembly downwards until the top brace of the lower pull rod assembly is just touching the pin through the lower hot pull rod.
20. Gently load the required weight onto the weight pan. Remember to take into account the correct lever ratio when calculating the required weight pan load. Be certain to allow the load cell to stabilize.
21. Ensure all the information entered into the data acquisition system is correct and start logging.

Appendix G

Constant Load Creep test end procedure

The basic procedure to follow when a creep test, using these rigs, is finished is as follows:

1. Ensure that furnaces have reached room temperature before attempting to dismantle a test. If not the furnaces have not cooled down sufficiently this could lead to burning or ruining of the load cells from over exposure to heat.
2. Remove ceramic brick inserts from top open end of furnace.
3. Carefully remove weight from weight pan, it is recommended that the weight pan is held steady whilst doing this.
4. Push up furnace.
5. Move counter weight on lever forward so as to free pin from brace. Move forward enough so as to position lever securely against frame.
6. Remove LVDT.
7. Remove thermocouples.
8. Remove LVDT plates.
9. Remove lower pin.
10. Remove lower pull rod (watch out for movement of the lever).
11. Undo bolts on extensometer and remove from notches on specimen.
12. Let extensometer drop to upper brace (it may be necessary to remove bolts on both sides of top of extensometer).
13. Remove upper pin and specimen.
14. Using Windows Explorer search in CreepdataNew for logged data.
15. Open the file into Excel.